AIR FORCE INSTITUTE OF TECHNOLOGY

AIR UNIVERSITY
UNITED STATES AIR FORCE

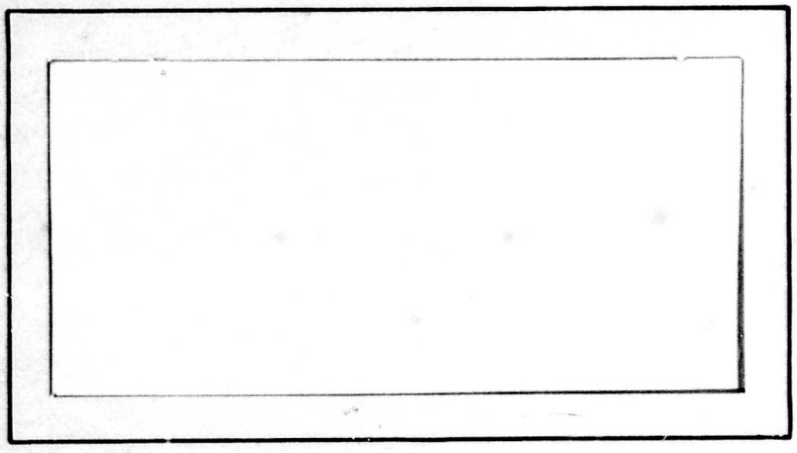

SCHOOL OF ENGINEERING

WRIGHT-PATTERSON AIR FORCE BASE, OHIO

GE/EE/67S-7

INVESTIGATION OF THE PRIMATE VESTIBULAR SYSTEM FUNCTION THROUGH ANALYSIS OF THE VESTIBULO-OCULAR REFLEX RESPONSE TO VARIOUS INPUT STIMULI

by

Marvin H. Chasen
Captain USAF
GE-67S

James W. Guthrie
1st Lt. USAF
GE-67S

AFLC-WPAFB-FEB 68 49

INVESTIGATION OF THE PRIMATE VESTIBULAR SYSTEM FUNCTION THROUGH ANALYSIS OF THE VESTIBULO-OCULAR REFLEX RESPONSE TO VARIOUS INPUT STIMULI

THESIS

Presented to the Faculty of the School of Engineering
of the Air Force Institute of Technology
Air University
in Partial Fulfillment of the
Requirements for the Degree of
Master of Science

by

Marvin H. Chasen, B.E.E.
Captain USAF

and

James W. Guthrie, B.S.E.E.
1st Lt. USAF

Graduate Electrical Engineering
December 1967

Preface

This is a report of an investigation of a portion of the primate vestibular system (otolith organs) by measurement of the vestibulo-ocular reflex of eyeball counterroll in Rhesus monkeys. As a complete analysis is beyond the scope of this investigation, many of the conclusions reached and the recommendations presented are aimed at providing a starting point for further investigations. Toward this end, care is given to provide as much data as possible so that duplication of effort will be avoided.

The authors wish to gratefully acknowledge the assistance rendered by Mr. R. Talmadge of the Flight Dynamics Laboratory, Sonic Fatigue Facility; and Mr. R. Riccardi of the Directorate of Computations. We are greatly indebted to Captain John W. Hahn, DVM, for his direct support in performing the necessary surgery required to prepare the subjects, and to the Veterinary Medicine Division of the Aeromedical Research Laboratories for supporting this investigation by providing the subjects tested. Finally, we wish to thank Dr. Clyde R. Replogle, our sponsor and faculty thesis advisor, whose knowledge of physiology and engineering time and again saved the day.

Marvin H. Chasen

James W. Guthrie

BLANK PAGE

Contents

List of Figures

Abstract

An indirect measurement of dynamic responses of the primate vestibular system was obtained through the measurement of eyeball counterroll from six Rhesus monkeys. A control system was developed to provide three types of input stimuli. These stimuli consisted of constant speed rotations, pendular oscillations, and Gaussian random noise. The experimental data was analyzed by use of correlation functions, power spectral density functions, and probability densities.

Results show that angular acceleration and the acceleration resulting from centripetal force affect the counterroll response. Gaussian noise position inputs failed to produce counterroll distributions that are Gaussian. However, because of the two acceleration inputs, this evidence is not sufficient to conclude that the system is nonlinear. Suppression of response to random inputs was observed, indicating that suppression does not necessarily result from anticipation of the input as was suggested by previous investigators.

BLANK PAGE

INVESTIGATION OF THE PRIMATE VESTIBULAR SYSTEM FUNCTION THROUGH ANALYSIS OF THE VESTIBULO-OCULAR REFLEX RESPONSE TO VARIOUS INPUT STIMULI

I. Introduction

The ability of man to perform in the environment of space flight has been the subject of a great deal of research. Maintenance of equilibrium under conditions of reduced and zero gravity has received particular attention. A sensory organ through which man maintains equilibrium is the vestibular apparatus. The vestibular apparatus consists of the semicircular canals and the otolith organs, the utricle and saccule. This thesis is a report on an investigation of the function of the otolith organs in primates.

Previous research has shown that eyeball counterroll is an external manifestation of the vestibular system response. Counterroll is defined as an involuntary conjugate rolling movement of the eyes around their line of sight and in a direction opposite to a lateral inclination of the head with respect to gravity (Ref 9:1). In this study the responses of the otolith organs are investigated by the measurement of counterroll.

History

In 1962, Dr. Earl F. Miller (Ref 9) developed a photographic technique for measuring counterroll which is accurate to within five minutes of arc. Using the technique, he obtained data on human subjects under static test conditions. With this data Dr. Miller proposed a theory to describe the function of the otolith organs. In 1964, R. J. Flaherty and G. K. Pritchard (Ref 4), using Dr. Miller's photographic technique, developed equipment to obtain dynamic counterrolling data from human subjects while rotating them at constant speeds about an axis parallel to their line of sight. In 1965,

V. L. Hartzler and P. A. Roccaforte (Ref 6) continued the dynamic experiments and proposed a mathematical model to describe vestibular function through the use of Fourier curve fitting techniques. A shortcoming of Dr. Miller's technique was the excessive time required to reduce the photographic data and interpret the results. In 1966, C. S. Lessard and J. R. Gnuse (Ref 8) developed a direct readout method for measuring counterroll responses. They obtained counterroll data from Rhesus monkeys with a contact lens-resolver system while rotating the monkeys at constant speeds about an axis parallel to their line of sight. Their subjects were monkeys rather than humans because of the measuring technique used (Ref 8:20-24). The data obtained was similar to human dynamic responses except transient phenomena could be readily observed by the direct readout method, which were not reported by the previous investigators.

A discussion of the hypothesis of Dr. Miller describing otolith organ function and a summary of the results obtained by the previous investigators is presented in Appendix A.

Present Study

Previous investigations of dynamic counterroll responses have been restricted to one type of input stimuli (constant speed rotations). The result of this restriction is a limited view of a system which is adaptive and possibly nonlinear. The purpose of this study is to investigate dynamic counterroll responses obtained from constant speed rotations as well as two additional types of input stimuli: variable amplitude pendular oscillations and narrow band Gaussian random noise.

The investigation is divided into three parts:

(1) development of equipment to provide the desired input stimuli

(2) collection of data from a group of subjects

(3) analysis of the experimental data.

The equipment which was developed is discussed in Section III, and the

analysis techniques employed are given in Section V. Section VI is a discussion of the results and conclusions from the investigation.

II. Description of the Vestibular System

The vestibular system is the nonaccoustical part of the inner ear (Fig. 2-1). The semicircular canals and the otolith organs make up the vestibular components (Fig. 2-2). The function of the semicircular canals is to provide angular acceleration information to the central nervous system in response to angular movements of the head. The otolith organs consist of the utricles and saccules which are apparently stimulated by gravity and rectilinear acceleration. The operation of the semicircular canals is better understood than the operation of the otolith organs. Since the otolith organs are the prime concern in this study, their description is presented here, and their relation to the semicircular canals in overall vestibular operation is discussed in Section VII.

Utricle

The utricle is one of two sacs of the membranous labyrinth located in the bony vestibule of the inner ear. The utricle communicates with the semicircular ducts by five openings on the posterior wall and with the sacculus and endolymphatic duct by an opening on the anterior wall. On its inner surface is an area of sensory epithelium, the macula utriculi, containing cells which respond to movement of otoliths due to changes in position (Ref 13).

Saccule

The saccule is the smaller of two sacs comprising the portion of the membranous labyrinth occupying the vestibule of the inner ear. It communicates with the utricle, cochlear duct, and the endolymphatic duct. In its wall is the macula sacculi, a sensory area (Ref 13).

Otolith Organ Response

The maculae of the utricle and saccule consist of supporting cells that provide lodgings for hair cells bearing hair tufts that are embedded in a gelatinous mass. On the surface of this mass are embedded otoconia

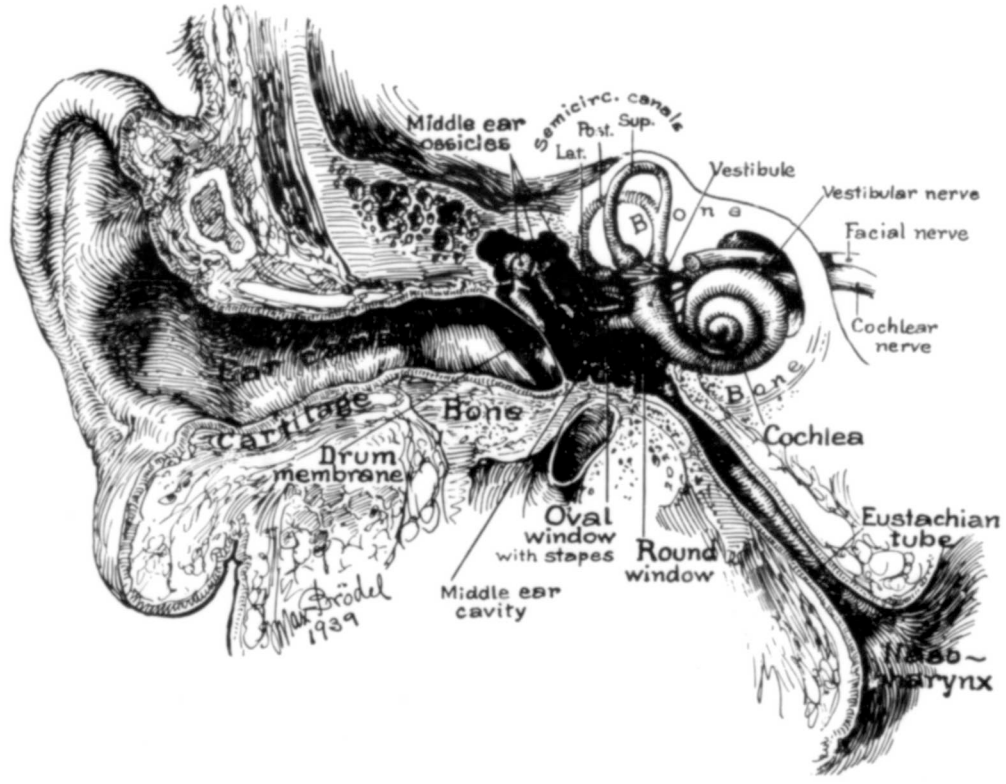

A Frontal Cross-Section of the Vestibular System
(From the Aerospace Medical Research Laboratory, WPAFB)
Fig. 2-1

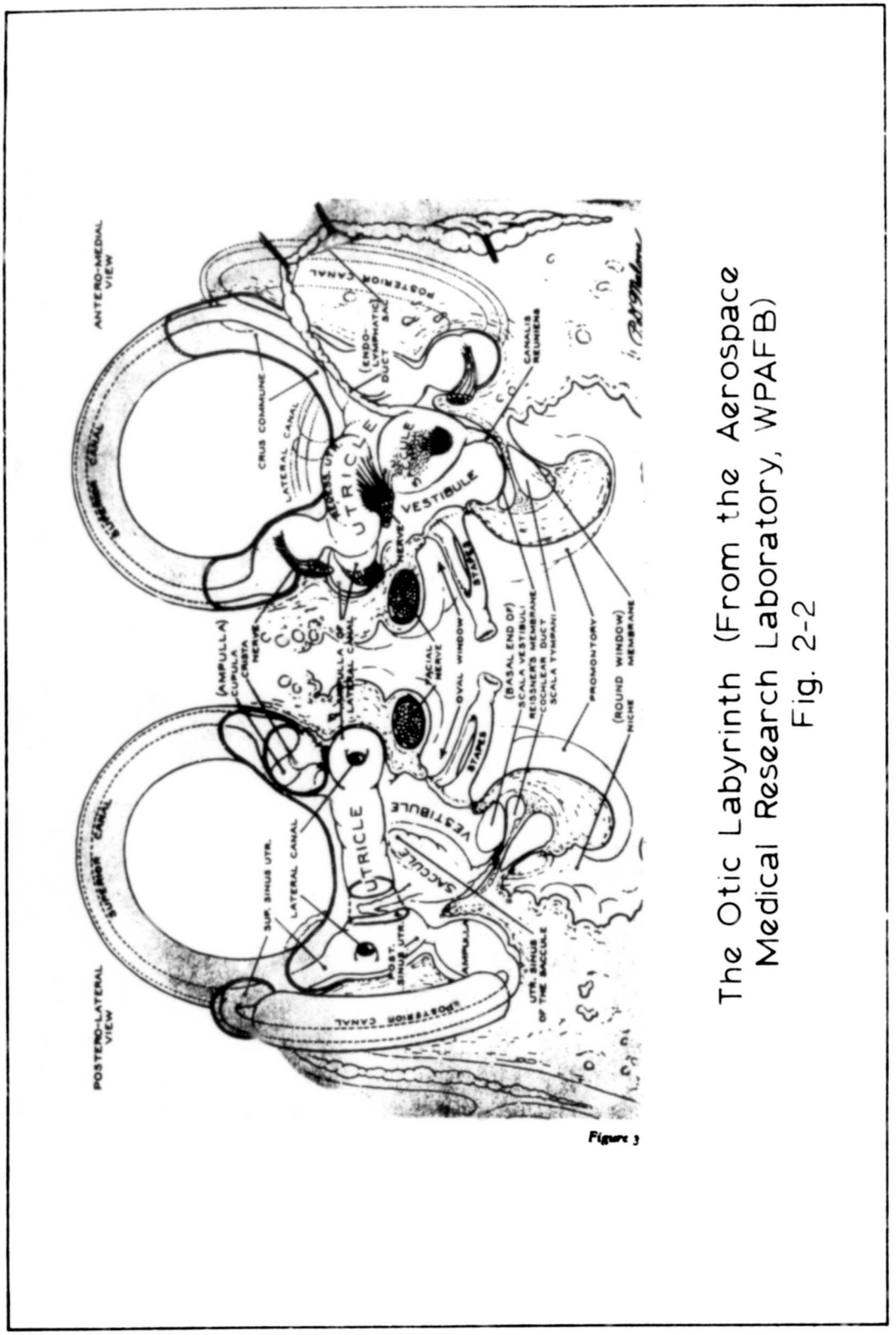

Figure 3

The Otic Labyrinth (From the Aerospace Medical Research Laboratory, WPAFB)
Fig. 2-2

(otoliths), small grains which consist mainly of calcium carbonate (Ref 10:66). Figure 2-3 is a cross section of the macula of the otolith organs.

When the head is erect, the otoconia rest on the hair cells producing a resting discharge frequency that is transmitted via nerve fibers to the central nervous system. When the head is tilted, the hair cells deflect due to the higher specific gravity of the otoconia with respect to the surface upon which they rest. This deflection changes the discharge frequency of the fibers, which is then coded for transmission through the central nervous system. A detailed discussion of the probable central nervous system centers to which this information is transmitted can be found in most physiology texts (Ref 12).

O—Otoconia
G—Gelatinous Layer
HT-Hair Tufts
H—Hair Cells
S—Supporting Cells
BM-Basilar Membrane
N—Nerve Fibers

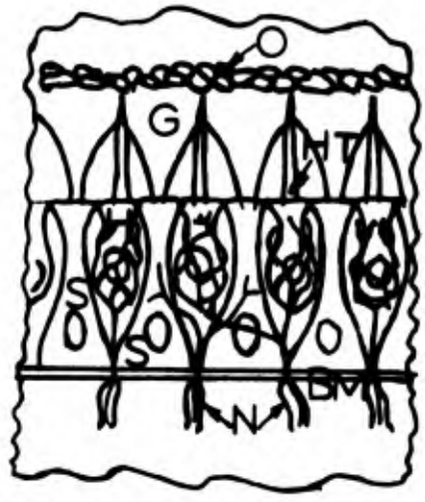

Structure (Schematic) of a Macula
(From Ref 10)
Fig. 2-3

The counterroll of the eye is a reflex of the vestibulo-ocular system which keeps the image on the retina stabilized when motion of the head from the vertical occurs. It is theorized that the change in the otolith activity is reflected back as a tonus change in the extraocular muscles, resulting in a

rotation of the eyes about their lines of sight opposite to the rotation of the head. A topographical mapping of the location of the otolith organs with respect to the head in an erect position is given in Appendix A.

III. Equipment

The equipment required for this study consists of two systems. First, a rotation system was needed which was capable of rotating a Rhesus monkey in a vertical plane about an axis parallel to his line of sight. The rotation system was to provide the following types of inputs:

(1) constant angular velocity rotation

(2) low-frequency oscillatory movements of various amplitudes about the vertical

(3) random movements about the vertical.

Second, an instrumentation system was required which would simultaneously measure the rotary movements of the subject's eye, the subject's position with respect to the gravity vector, and the subject's angular velocity. Also, the instrumentation system was to record these measurements in a form such that the data could be analyzed on a digital computer. A photograph of the equipment is shown in Figure 3-1 and a detailed equipment list is given in Appendix B.

Rotation System

The rotation system consists of two main components:

(1) the support and chair assembly

(2) the drive assembly.

The Support and Chair Assembly. C. S. Lessard and J. R. Gnuse (Ref 8) were responsible for the design and construction of the support and chair assembly. The assembly provided a platform on which a Rhesus monkey could be tightly secured and rotated in a vertical plane about an axis parallel to the line of sight and midway between the eyes of the subject. The assembly is a two-point suspension device. Two separate box-like stands on a 4 ft by 9 ft platform support bearings from which a frame and chair are suspended. The stands and the platform are constructed of 3/4 in. plywood and the frame is constructed from 1/4 in. by 1-1/2 in. aluminum angle. Adjustable counter-

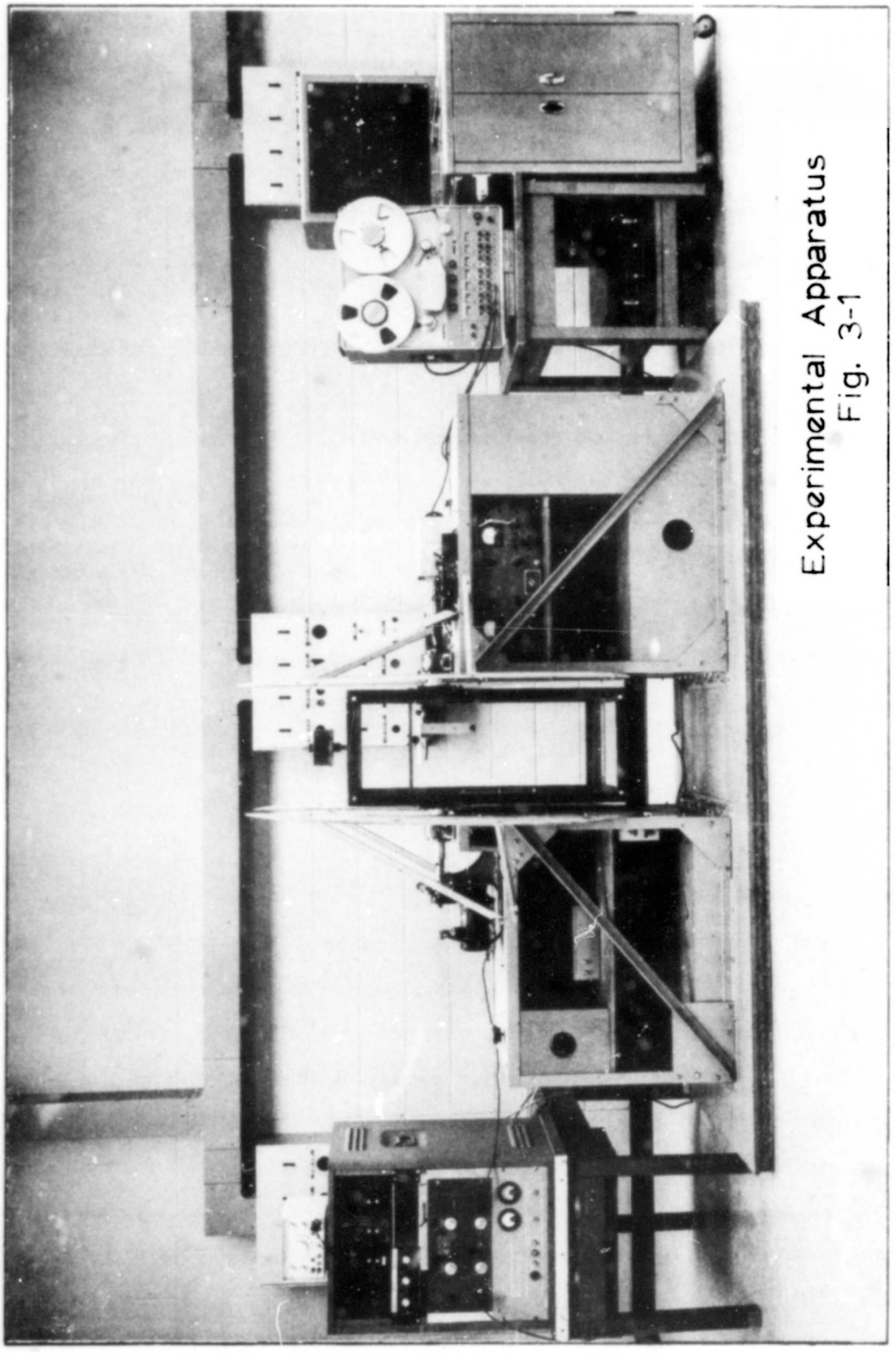

Experimental Apparatus
Fig. 3-1

balance weights provide a means to balance the chair and subject so that the center of mass is on the axis of rotation. The form-fitted chair (Fig. 3-2) is molded from fiberglass and is lined with felt cloth. The subject is secured in the chair by a hinged face and chest plate, a Velcro waist band, a hip and thigh strap, boots, and armlength gloves. The chair is secured to the frame with four 1/4 in. bolts. A more detailed description of the support and chair assembly can be found in Reference 8.

The Drive Assembly. To provide the desired types of rotary movements, a feedback control system was designed which could function either as a velocity or position control system. If constant velocity rotation was desired, the system was used to control velocity; and if oscillatory or random movements about the vertical were desired, the system was used to control position. A block diagram of the drive assembly is shown in Fig. 3-3. The drive assembly consists of an error signal amplifier, A1, a silicon-controlled rectifier motor-drive amplifier, A2, a 1/2 hp d-c motor, speed reduction gearing, a d-c tachometer, and a position feedback circuit. A detailed circuit diagram of the drive assembly is given in Appendix C.

A schematic diagram of the position feedback circuit is shown in Fig. 3-4. The circuit consists of a one-turn, 30 kilohm, linear potentiometer, and two 3 volt batteries. The linearity of the potentiometer is 0.15%. The position feedback signal is taken between the potentiometer wiper and the connection between the two batteries. With the rotating chair in a vertical position, the potentiometer wiper is in the center of the resistance element; thus, the position feedback signal is equal to zero. As the rotating chair turns clockwise (direction of rotation is defined as viewed by the subject), the potentiometer wiper moves toward the positive potential end of the resistance element, and the position feedback signal is a positive voltage. When the rotating chair reaches 180°, the position feedback signal is equal to 3 volts. Positive angles are defined as rotation in the clockwise direction. Likewise, when the rotating chair is rotated counterclockwise, the position feedback signal is a negative

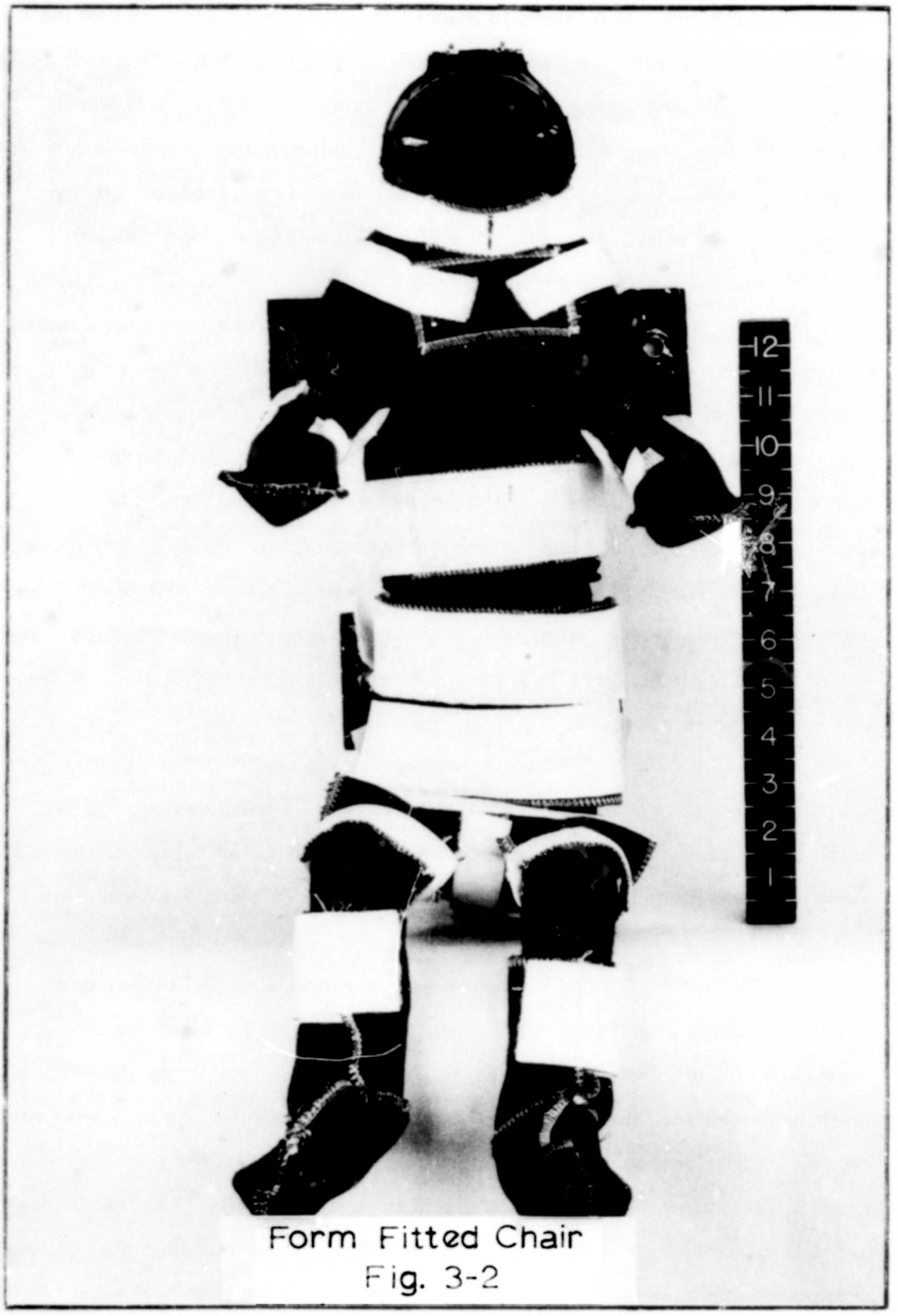

Form Fitted Chair
Fig. 3-2

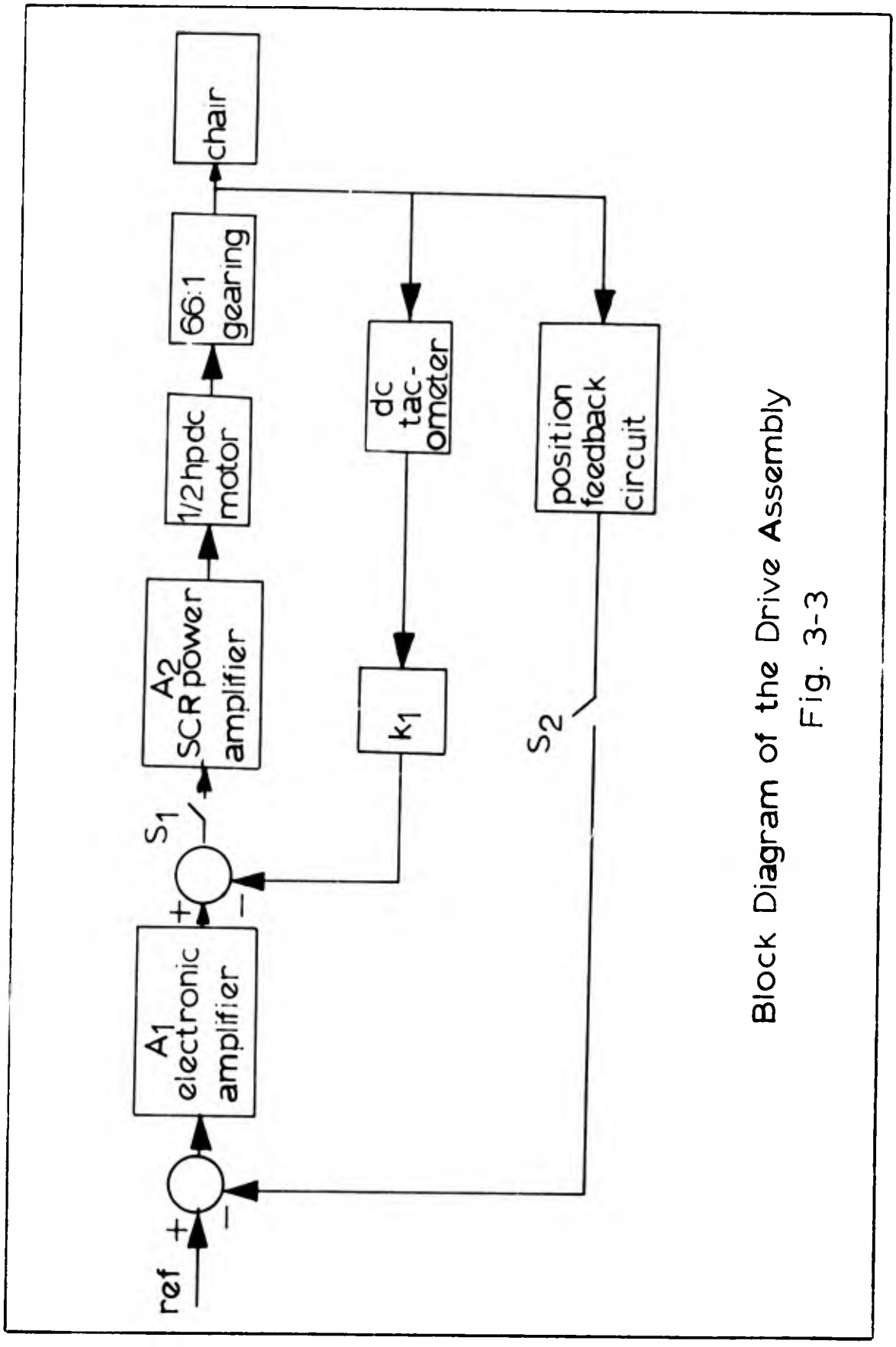

Block Diagram of the Drive Assembly
Fig. 3-3

voltage. The relation between the position feedback signal and the rotating chair position is given by the equation:

$$Vo = \frac{\theta c}{60} \qquad (1\text{-}1)$$

where V_o = position feedback signal in volts

θ_c = position of rotating chair with respect to the vertical in degrees.

To preserve the linearity of the position feedback control system and for the above equation to hold, it is essential that the position feedback circuit operate into a high impedance to prevent loading the potentiometer. This requirement was satisfied by the use of the error-signal amplifier.

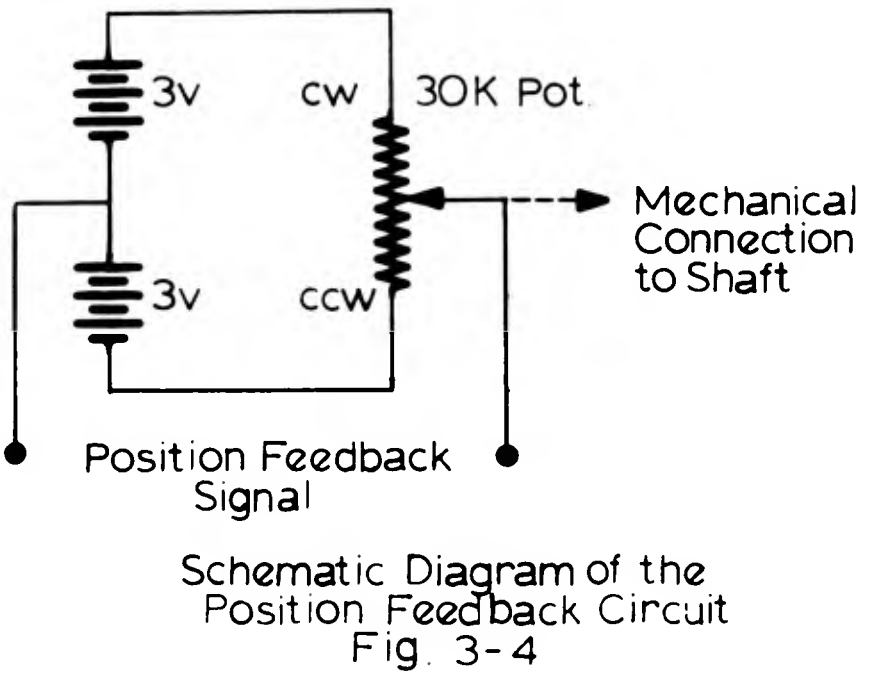

Schematic Diagram of the
Position Feedback Circuit
Fig. 3-4

The error-signal amplifier, A1, is a variable gain, direct-coupled, differential amplifier. The rated input impedance of the amplifier is 11 megohms which satisfies the no loading requirement of the position feedback circuit. In addition to providing a high input impedance, the error-signal amplifier provides a voltage amplification of the position error signal, thus decreasing the steady state error in position. When operating the con-

trol system in the position-control mode, A1 is adjusted to provide a voltage gain of 20. When operating in the velocity-control mode, the amplifier provides a high input impedance for the command signal. In this mode of operation it is not essential to amplify the command signal; therefore, the voltage gain of A1 is decreased to 10.

The silicon controlled rectifier power amplifier, A2, is used to increase the power level of the output of the error signal amplifier to a level sufficient to drive the motor. This amplifier was designed and constructed as a part of this project. The amplifier is a half-wave phase control circuit. The power input to the circuit is 400 hz a-c. The output from the amplifier is rectified 400 hz a-c. The d-c average and the polarity of the output is dependent on the signal input to the amplifier. The voltage gain of the amplifier is 20, and the power gain is 40 db. A schematic diagram and a complete description of the circuit operation are given in Appendix D.

The motor which is used to drive the rotating chair is a 1/2 hp d-c machine connected for armature control. The field is separately excited with a fixed d-c source of 28 volts. Complete specifications of the motor are given in Appendix B. The motor shaft is connected to the rotating chair through a speed-reduction gear assembly. The main-drive-gear is coupled to the rotating chair by means of a universal joint.

The switch S2 in Fig. 3-3 is the control selection switch. With S2 in the closed position, the control system is in the position-control mode with feedback compensation provided by the tachometer feedback loop. When operating in this mode, a command input is compared with the output from the position feedback potentiometer circuit. The difference between the command signal and the position feedback signal is amplified by A1. The output from A1 and the tachometer feedback are compared and their difference is amplified by A2. The output from A2 supplies power to the motor, which drives the chair through the reduction gear assembly. The chair continues to turn until the position is reached at which the position feedback voltage equals the command

input. Positive command signals rotate the chair clockwise and negative signals rotate the chair counterclockwise. A plot of chair position versus command input voltage is given in Fig. 3-5.

Since the position-control system was to be used to provide oscillatory and random movements about the vertical, the frequency response of the system is an important design criterion. The bandwidth of the system is 2.76 radians per second. The bandwidth, as it is used here, is defined as the range of frequencies from $\omega = 0$ up to the frequency at which the system gain was 3 db below the gain at $\omega = 0$. A bode plot for the position control system is given in Fig. 3-6. A low frequency sine wave generator was used as a command input to provide the oscillatory movements of the chair.

As was previously mentioned, it was desired to provide random movements about the vertical to the rotating chair. In particular, it was desired to rotate the chair between 180° and -180° from the vertical (0°) such that the amplitudes of rotation would be distributed normally. This type of rotation was obtained by providing a command input of zero mean, band-limited Gaussian noise to the position control system. The output from a low-frequency Gaussian noise generator filtered by a bandpass filter yielded this command input. Fig. 3-7 illustrates the probability density function of the noise generator output after being filtered by the bandpass filter. The lower and upper cutoff frequencies of the bandpass filter were 0.002 hz and 10 hz respectively. Fig. 3-8 is the probability density function of the rotating chair position with band-limited Gaussian noise as a command input to the position control system. Both of these curves were obtained by analysis on the Amplitude Probability Density Analyzer located at the Sonic Fatigue Facility of the Flight Dynamics Laboratory, Wright-Patterson Air Force Base, Ohio. The curve in Fig. 3-8 was tested for normality by the Kolmogorov-Smirnov test and was accepted as being normal. A description of this test and the results obtained are presented in Appendix E.

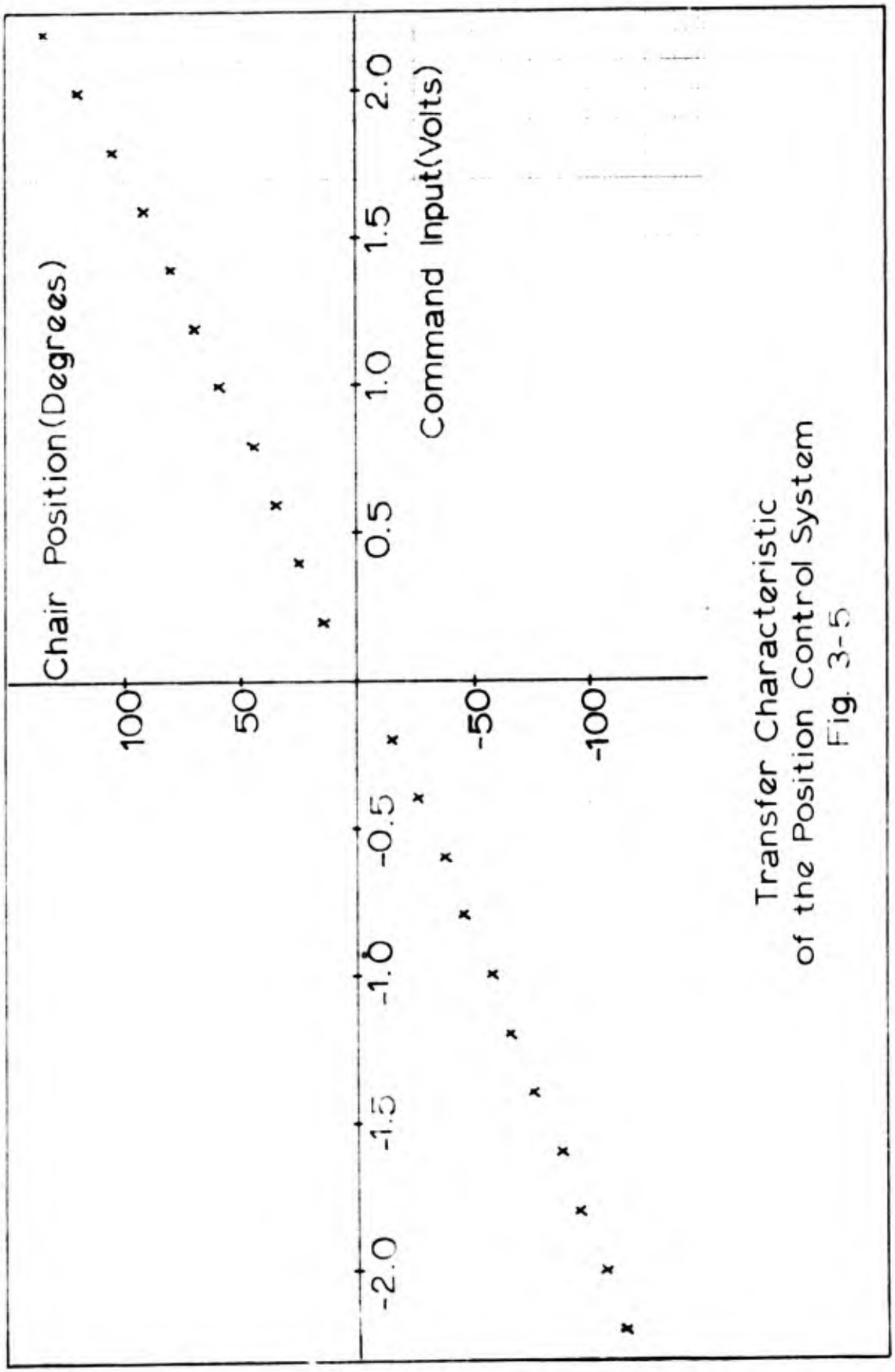

Transfer Characteristic
of the Position Control System
Fig. 3-5

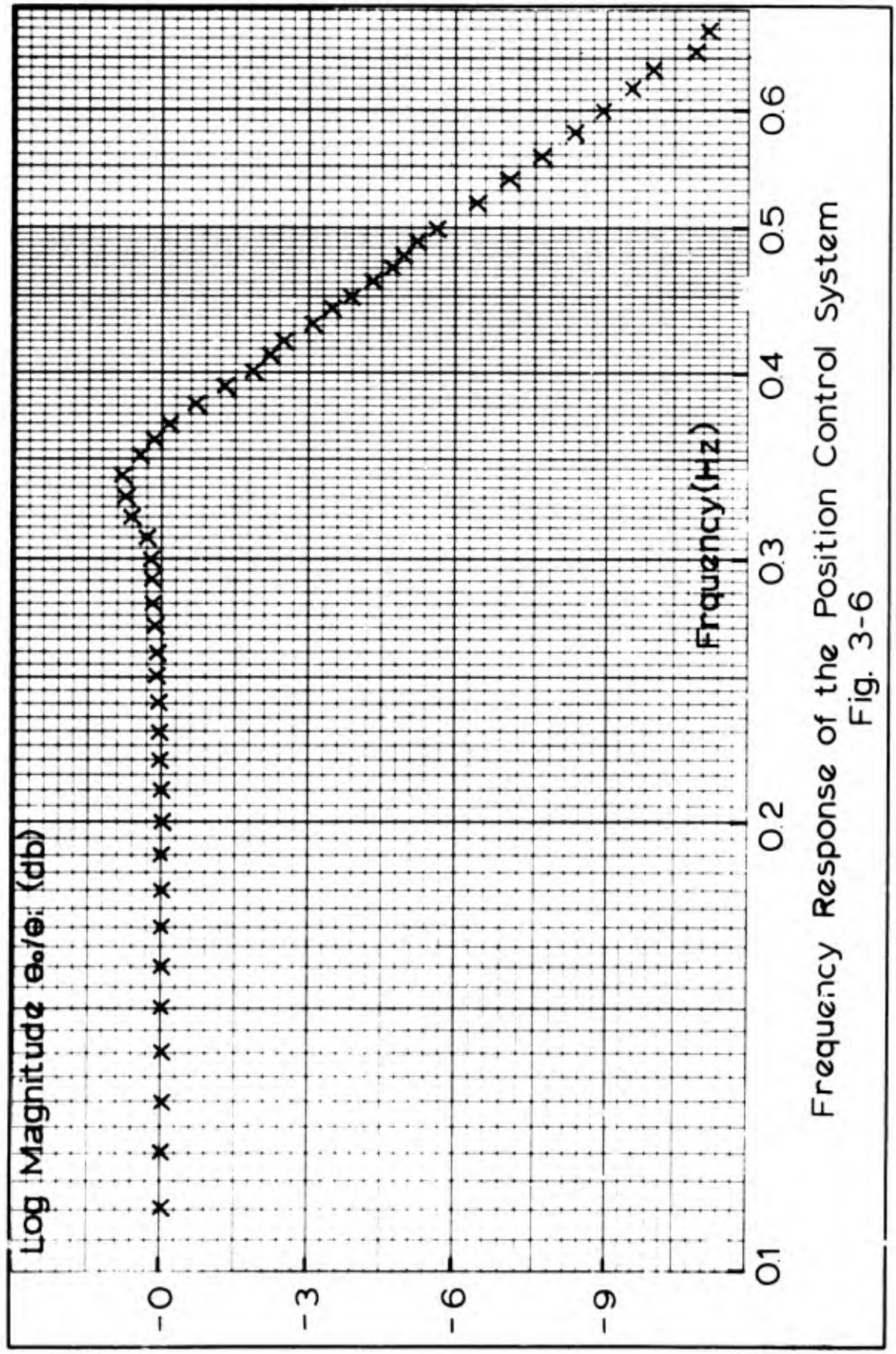

Frequency Response of the Position Control System
Fig. 3-6

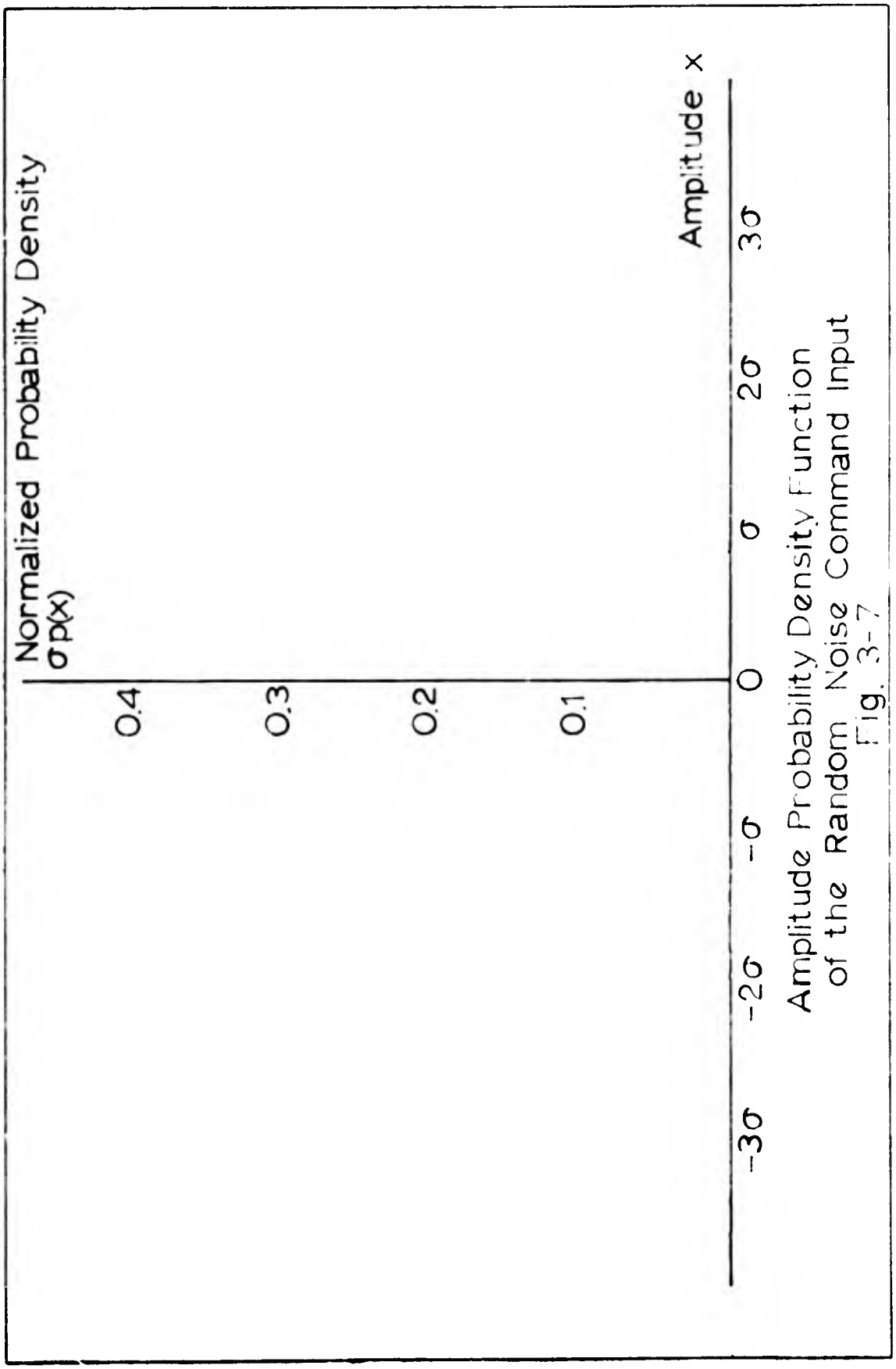

Amplitude Probability Density Function
of the Random Noise Command Input
Fig. 3-7

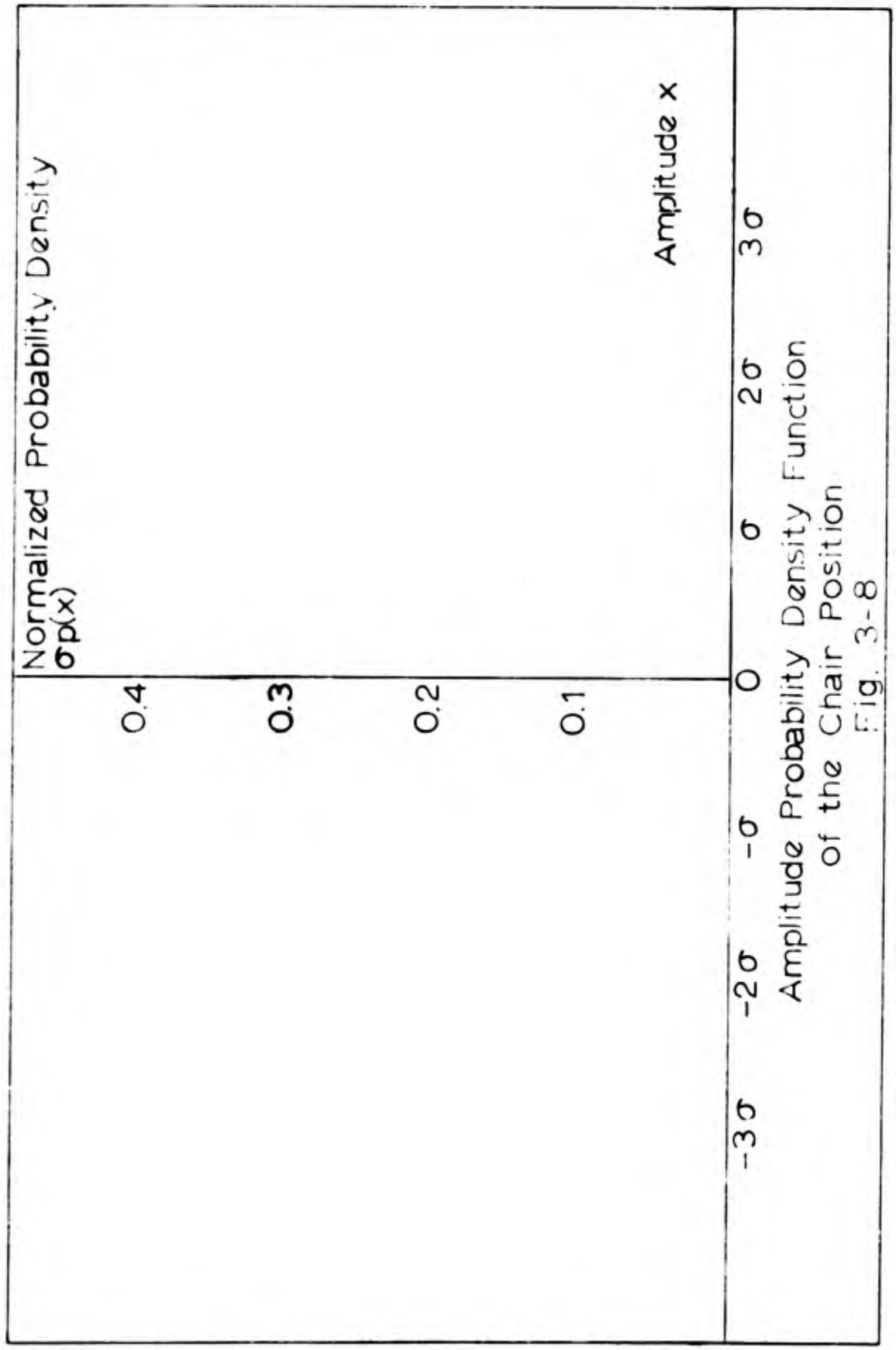

Amplitude Probability Density Function
of the Chair Position
Fig. 3-8

With the switch S2 in the open position, the control system is in the velocity-control mode. In this mode of operation, the system operates as a standard tachometer-feedback speed-control system. This type of operation was used for constant speed rotation of the chair.

Instrumentation System

As was previously stated, there were three quantities which were to be simultaneously measured and recorded:

(1) rotary movements of the subject's eye (counterroll)

(2) subject's position with respect to the vertical

(3) subject's angular velocity.

Measurement of Subject's Rotary Eye Movements. A method of directly measuring the rotary movements of the subject's eye was adopted for this study. It was mentioned in Section I that a direct measurement technique was developed in a previous investigation of counterrolling. In principle, the technique used in this study is similar to that used by Lessard and Gnuse (Ref 8) in their investigation; however, the implementation of the technique was changed.

The counterroll measurements were made with a linear transformer mechanically coupled to the subject's eye by a contact lens assembly. The contact lens assembly shown in Fig. 3-9, consists of a plastic contact lens and a shaft for coupling the contact lens to the linear transformer. The contact lens was sutured to the subject's eye with 6-0 silk suture thread. A 0.019 in. diameter hole was drilled at 45° intervals around the perimeter of the contact lens. This provided a means to suture the lens to the subject's eye. A 3/16 in. aluminum cylinder 3/8 in. long was attached to the contact lens with Eastman 910 adhesive. This aluminum cylinder was fastened to a 3/16 in. inside-diameter, flexible, polyethylene tube, 2-1/4 in. in length, by means of a set-screw coupling which was attached to the polyethylene tube with Eastman 910 adhesive. The opposite end of the polyethylene tube was attached to the linear transformer with another set-screw coupling.

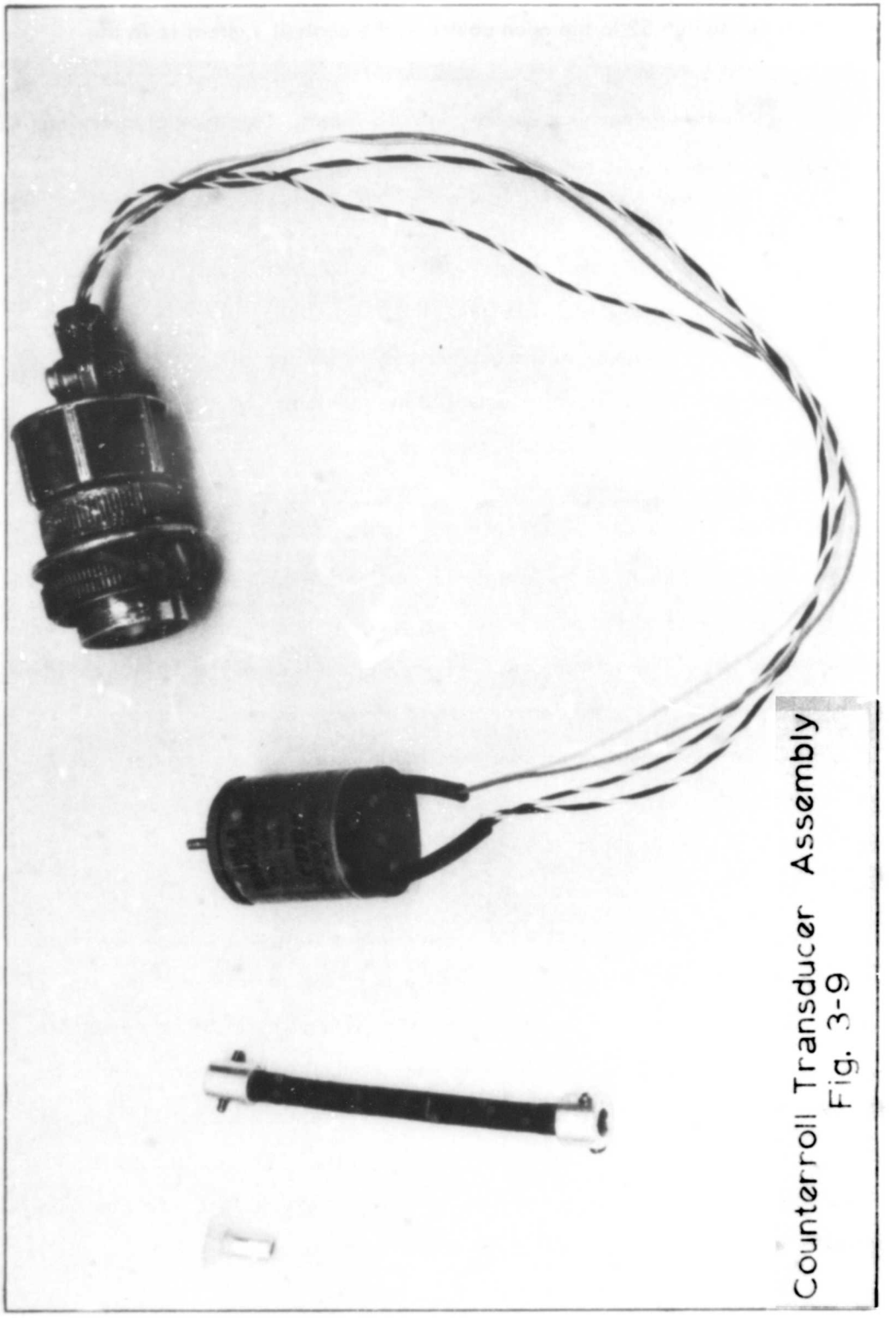

Counterroll Transducer Assembly
Fig. 3-9

The linear transformer is used to convert the mechanical position of the subject's eye into a voltage. The input to the device is a 26 volt, single phase, 400 hz voltage. The device provides a 400 hz output voltage which is a linear function of the shaft position over a 70° range. The output voltage varies from 0 to 26 volts in phase with the input voltage for shaft positions of 0° to 35° and 0 to 26 volts, 180° out of phase with the input for shaft positions of 0° to -35°. Therefore, by adding the output and a bias voltage of 26 volts 400 hz, in phase with the input, to the transformer, the total output was made to vary linearly from 0 to 52 volts for shaft positions from -35° to +35°. This a-c output voltage is then full-wave rectified and filtered to provide a d-c voltage which is a linear function of the subject's rotary eye movements. A d-c bias voltage is added to the rectified transformer output so that the resulting d-c output can be set to zero without the need for critical alignment of the linear transformer zero and the reference position of the subject's eye. A schematic diagram of the rotary eye movement detection circuit is shown in Fig. 3-10. The calibration curve of the circuit is given in Fig. 3-11.

Measurement of the Subject's Position With Respect to the Vertical. The subject's position was measured by means of the circuit shown in Fig. 3-12. A linear, one turn, 30 kilohm potentiometer was used in the circuit. Two 1 kilohm fixed resistors in series were connected in parallel with the potentiometer. This was done so that the output voltage could be taken between the potentiometer wiper and the connection between the two fixed resistors, thus providing positive output voltages for rotations in the clockwise direction and negative output voltage for rotations in the counterclockwise direction. The potentiometer was adjusted so that the output voltage was zero when the rotating chair was in the vertical position. A plot of output voltage versus chair position is given in Fig. 3-13.

Measurement of Subject's Angular Velocity. The subject's angular velocity was measured by means of a 4.5 volts per 100 rpm d-c tachometer which was directly connected to the drive shaft of the rotating chair. Calibra-

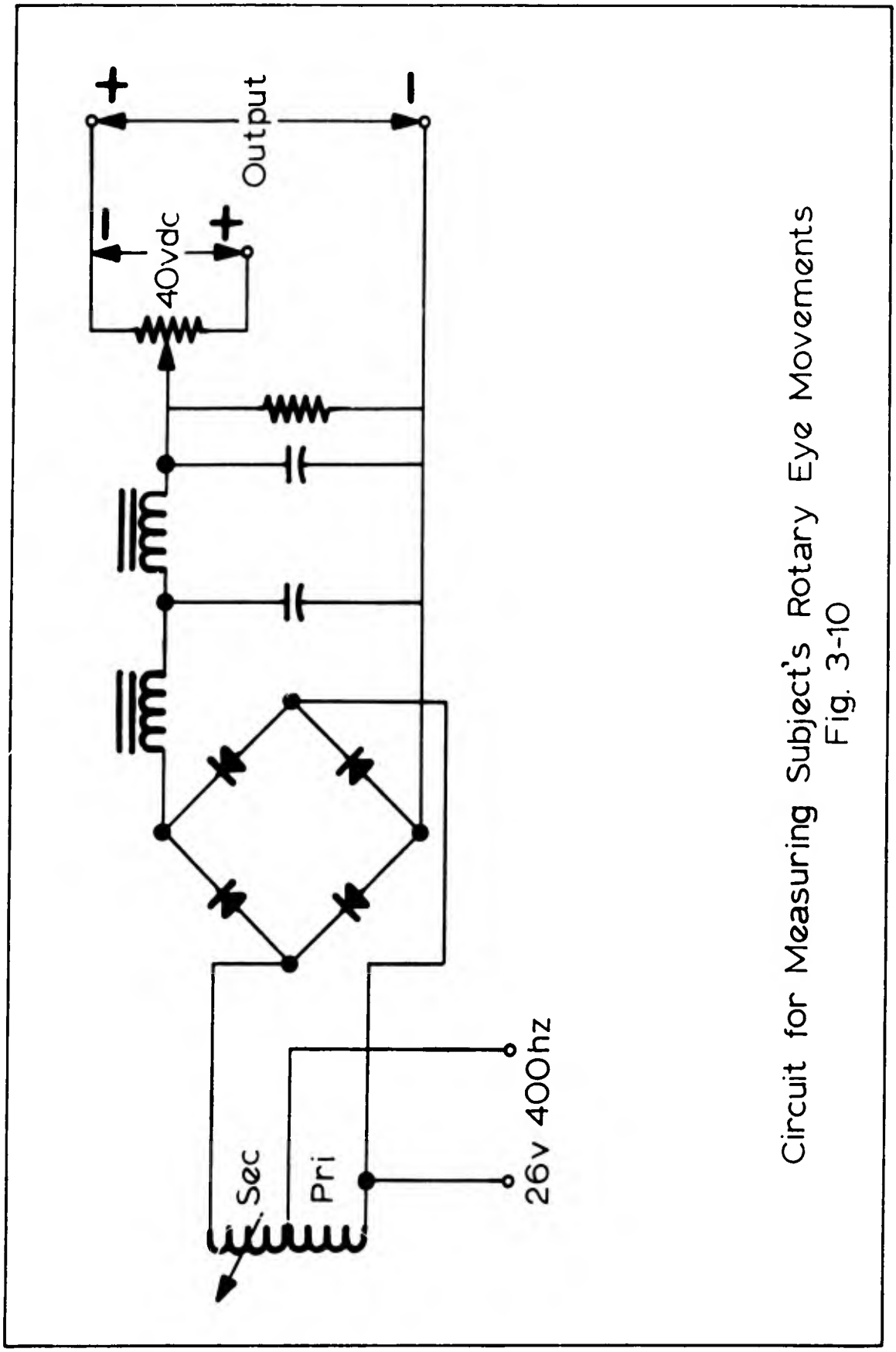

Circuit for Measuring Subject's Rotary Eye Movements
Fig. 3-10

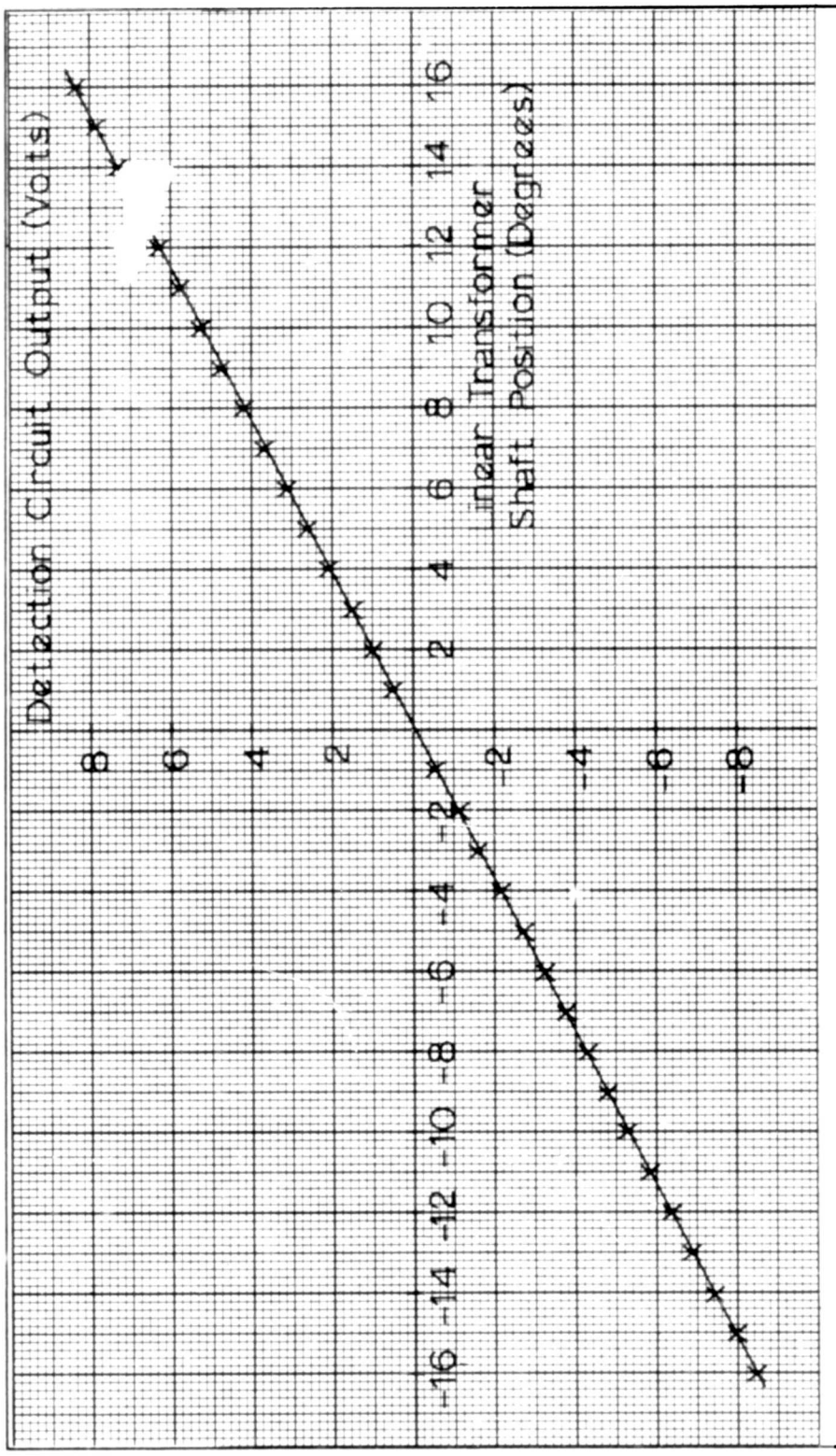

Calibration Curve of the Counterroll Detection Circuit
Fig. 3-11

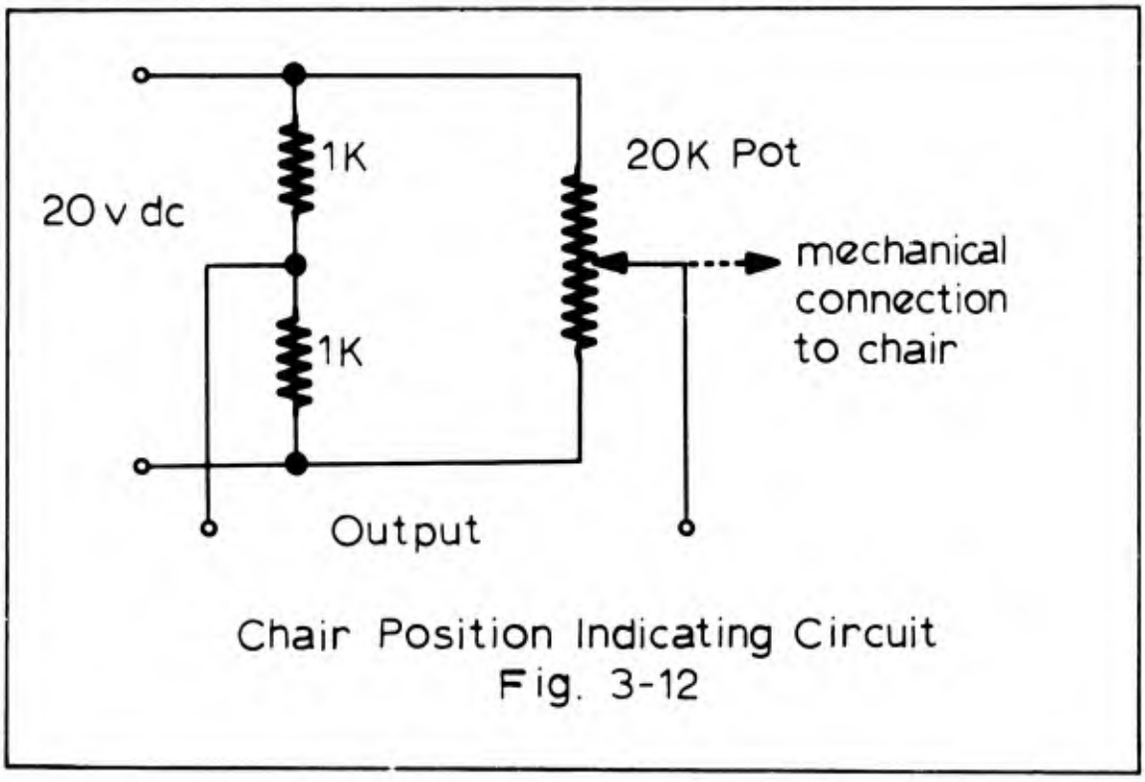

Chair Position Indicating Circuit
Fig. 3-12

tion of the tachometer is given in Fig. 3-14.

Recording the Measurements. The data were recorded on an Ampex Model SP-300 magnetic tape recorder reproducer. A PDP-1 analog to digital converter was used to digitize the analog data for analysis on the 7094 digital computer.

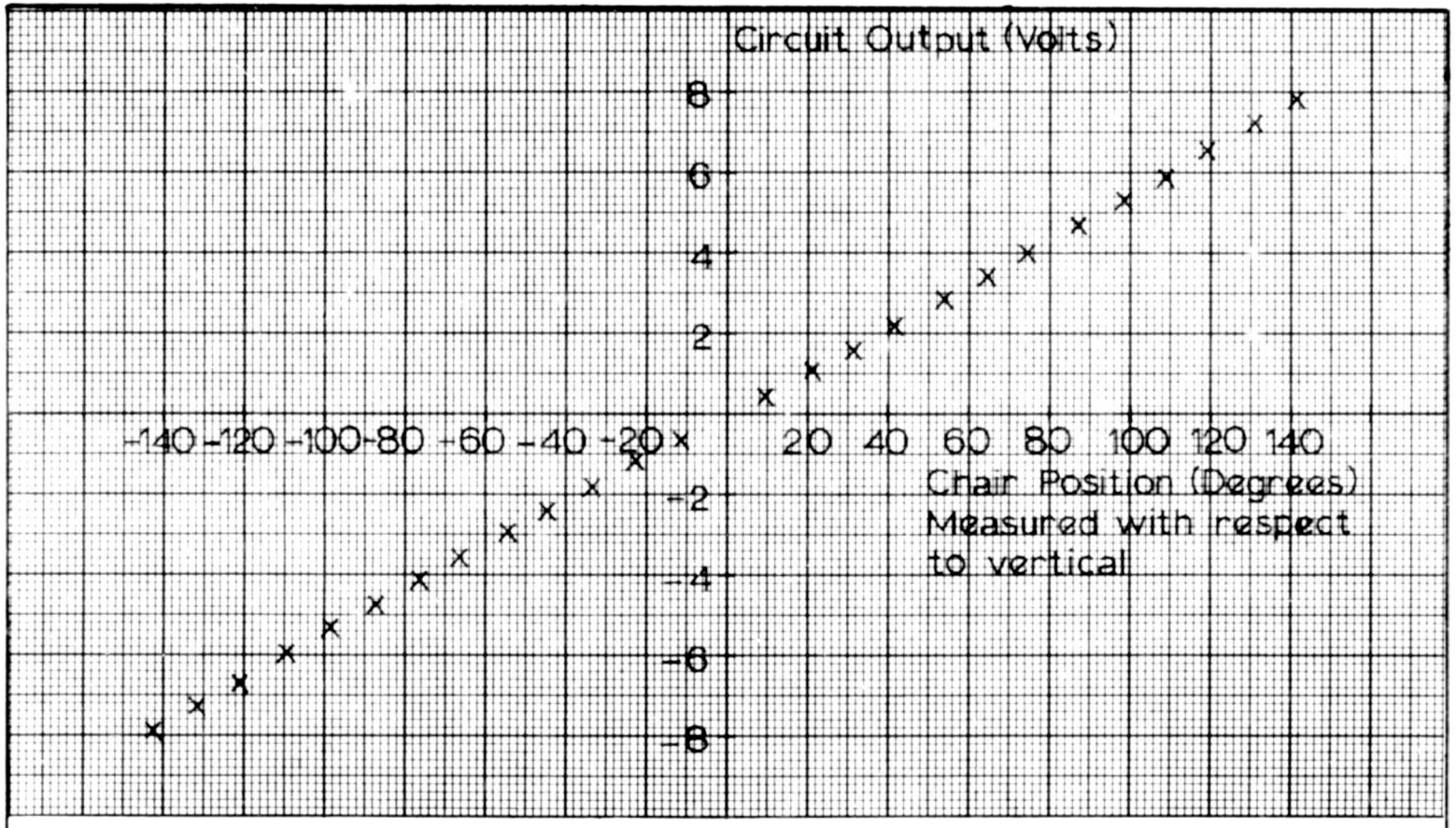

Calibration Curve of the Chair Position Indicating Circuit
Fig. 3-13

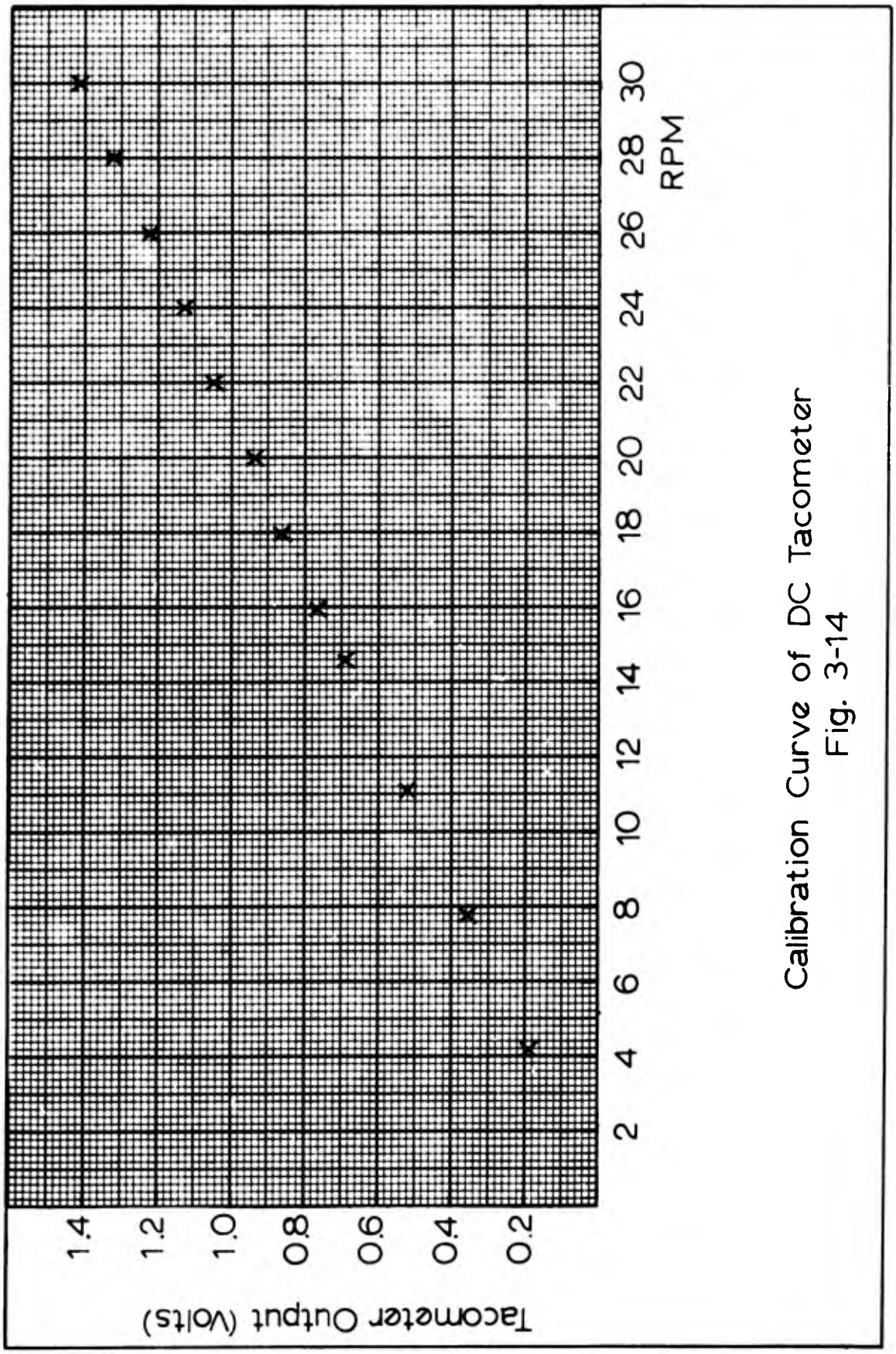

Calibration Curve of DC Tacometer
Fig. 3-14

IV. Experimental Procedure

The experimental procedure consists of two parts, the pre-test and the test run.

Pre-Test

The pre-test procedure consists of animal preparation and equipment preparation.

Animal Preparation. Twelve hours prior to testing, the subject is taken off feed to prevent vomiting resulting from anesthesia or motion sickness. Approximately one hour before testing, the subject is prepared in the following manner:

(1) Metafane (methoxyfluorane), a volatile anesthetic, is administered to effect. This anesthetic will allow the subject to fully recover consciousness within fifteen minutes.

(2) The hair is clipped from the area around the brow and eyes.

(3) Two horizontal mattress stitches are sutured, using 000 silk suture, through the skin of the eyelid next to the tarsal border and through the skin one-half inch above the brow. This will prevent the subject from closing his eye and clamping down on the contact lens to be sutured to his eye (Fig. 4-1).

(4) Opthaine (proparacaine hydrochloride), a local anesthetic for the eye, and chloramphenicol, an antibiotic, are administered to the eye in preparation for suturing a contact lens to the sclera of the eye. Saline solution is constantly administered to the eye to keep it in a moist state since the eyelid has been sutured to the brow. This is done to prevent damage to the cornea caused by drying of the eye. Saline, as well as additional anesthetic, is administered to the eye at periodic intervals during both the test runs and the post test period.

(5) Using 6-0 silk suture, a plastic contact lens is sutured to the sclera of the left eye (Fig. 4-1). The lens has eight 0.019 in. diameter holes, located

Surgical Preparation
Fig. 4-1

around the outer edge of the lens, through which the suture silk is passed.

Normally four sutures, located at right angles, are made; although, up to eight can be made if necessary.

Equipment Preparation. One hour before testing, all equipment and instrumentation are energized except the motor-drive electronics. This is done to stabilize the equipment to avoid errors in operation due to temperature changes and drift. Ten minutes before the test run, the restraining chair is bolted to the frame assembly and statically balanced. The linear transformer shaft is then locked in position and the contact lens is inserted into the polyethylene shaft that couples the lens to the linear transformer.

Test-Run

The test run is divided into four parts:

(1) Gaussian noise position input

(2) pendular motion position input

(3) static test

(4) constant angular velocity rotation.

Gaussian Noise Position Input. A five minute test is made with random noise as a reference input and the control system in the position control mode. The counterroll, shaft position, and shaft velocity are simultaneously recorded on magnetic tape and the dynagraph recorder.

Pendular Motion Position Input. A series of seven one-minute tests are made with two volt peak-to-peak sine waves applied to the input of the control system. The first test is performed with the input frequency equal to 0.2 hz. The frequency of the input is increased by 0.05 hz for each successive test. The control system is in the position control mode for these tests.

Static Test. The chair assembly is slowly rotated by hand 180° clockwise and 180° counterclockwise in 20° increments. Approximately one minute is allowed for each increment.

Constant Angular Velocity Rotation. Constant velocity rotation is obtained by applying d-c voltage to the input with the control system in the velocity control mode. Velocities of 5, 10, 20, and 30 rpm are imparted to the chair assembly in each direction of rotation.

V. Analysis of Data

Past investigations of the vestibulo-ocular reflex of counterrolling have resulted in data which cannot be accurately described by explicit mathematical expressions (Ref 5, 8). Therefore, in the present investigation the experimental data are analyzed with the ultimate aim being to provide a statistical model of the system.

Three main types of statistical functions are used to describe the properties of the experimental data obtained in this investigation:

(1) probability density functions

(2) correlation functions

(3) power spectral density functions.

These functions were calculated from the raw data on an IBM 7094 computer using the Systems Analysis Translator Program developed at Wright-Patterson Air Force Base (Ref 7, 14). The analog data obtained from the experiments were digitized at a sampling rate of 10 samples per second. The sampling rate was selected in accordance with Shannon's sampling Theorem to recover the highest frequency of interest in the data. The relationship between the sampling rate and the highest frequency of interest is given by

$$h = 2\,HF \tag{5-1}$$

h = sampling rate

HF = highest frequency of interest.

A choice of 5 hz was made for HF. In analyzing the experimental data the assumption is made that the process representing the counterroll response is both wide-sense stationary and ergodic.

Examples of control decks to provide the necessary instructions to the Systems Analysis Translator Program for calculation of correlation functions, power spectral density functions, and probability density functions are given in Appendix F.

Probability Density Function

The first order distribution function, F(x;t), of a stochastic process, x(t), is defined by:

$$F(x;t) = P\{x(t) \leq x\} \qquad \text{(Ref 11)} \qquad (5\text{-}2)$$

= probability of the event $\{x(t) \leq x\}$

The probability density function is defined as the derivative of F(x;t) with respect to x as follows:

$$p(x;t) = \frac{\partial F(x;t)}{\partial x} \qquad \text{(Ref 11)} \qquad (5\text{-}3)$$

Correlation Functions

The autocorrelation function, $R(\tau)$, of a stationary process, x(t), is defined as the joint moment of the random variable x(t) and $x(t+\tau)$ as follows:

$$R(\tau) = E\{x(t)x(t+\tau)\} \qquad \text{(Ref 11).} \qquad (5\text{-}4)$$

For an ergodic process the autocorrelation function may be obtained from the time average

$$\overline{R(\tau)} = \frac{1}{2T}\int_{-T}^{T} x(t)x(t+\tau)dt \qquad \text{(Ref 2).} \qquad (5\text{-}5)$$

The bar over $R(\tau)$ indicates that it is a random variable. The mean of $\overline{R(\tau)}$ is an estimate of the autocorrelation function of x(t), and as T approaches infinity $\overline{R(\tau)}$ approaches $R(\tau)$.

The cross-correlation function $Rxy(\tau)$ of two stationary processes x(t) and y(t) is defined as:

$$R_{xy}(\tau) = E\{x(t)y(t+\tau)\} \qquad \text{(Ref 11).} \qquad (5\text{-}6)$$

For ergodic processes the function can be obtained from the time average

$$\overline{R_{xy}(\tau)} = \frac{1}{2T}\int_{-T}^{T} x(t)y(t+\tau)\,dt \qquad \text{(Ref 2).} \qquad (5\text{-}7)$$

As with the autocorrelation estimate, the random variable $\overline{Rxy(\tau)}$ approaches $Rxy(\tau)$ as T approaches infinity.

Power Spectral Density Functions

The power spectral density function is used to describe the frequency composition of experimental data. The power spectral density, $G_x(f)$, is defined as the Fourier transform of the autocorrelation function as follows:

$$G_X(f) = \int_{-\infty}^{\infty} R_X(\tau) e^{-j\omega\tau} d\tau \qquad \text{(Ref 2)} \qquad (5\text{-}8)$$

$$= \int_{-\infty}^{\infty} R_X(\tau)\cos\omega\tau\, d\tau - j\int_{-\infty}^{\infty} R_X(\tau)\sin\omega\tau\, d\tau . \qquad (5\text{-}9)$$

and since $R_x(\tau)$ is an even function (Ref 2), equation (5-9) reduces to:

$$G_X(f) = 2\int_{0}^{\infty} R_X(\tau)\cos\omega\tau\, d\tau . \qquad (5\text{-}10)$$

The principle application of the power spectral density is to determine the frequency composition of experimental data which yields important information about the physical system involved. For example, if the function x(t) with power spectral density $G_x(f)$ is the input to a linear system with frequency response function H(f), the power spectral density of the output from the system, $G_y(f)$, is given by:

$$G_Y(f) = |H(f)|^2 G_X(f) \qquad \text{(Ref 2).} \qquad (5\text{-}11)$$

The Fourier transform of the cross-correlation function yields the cross-spectral density function. The cross-spectral density is defined as:

$$G_{XY}(f) = \int_{-\infty}^{\infty} R_{XY}(\tau) e^{-j\omega\tau} d\tau \qquad \text{(Ref 2).} \qquad (5\text{-}12)$$

When the cross-correlation function $Rxy(\tau)$ is computed on a digital computer using equation (5-7), the resulting cross-correlation is defined for only positive values of τ. The Fourier transform has limits from minus infinity to infinity. This means that the cross-correlation function must be integrated over non-zero minus τ values to compute the cross-spectral density. It can be shown that:

$$R_{xy}(-\tau) = R_{yx}(\tau) \qquad \text{(Ref 2).} \qquad (5\text{-}13)$$

Therefore, since the computer will calculate the transform for only positive τ, the power spectrum can be developed as:

$$G_{xy}(f) = \Phi_{xy}(f) + \Phi^{*}_{yx}(f) \qquad \text{(Ref 2)} \qquad (5\text{-}14)$$

$\Phi_{xy}(f)$ = Fourier transform of $R_{xy}(\tau)$ for positive

$\Phi^{*}_{yx}(f)$ = complex conjugate of the Fourier transform of $R_{yx}(\tau)$ for positive

$G_{xy}(f)$ = cross-spectral density.

A principle application of the cross-spectral density is to determine the frequency response function of linear systems. If an input $x(t)$ with a power spectrum $G_x(f)$ is applied to a linear system with a frequency response function $H(f)$, the cross-spectrum between the input and output will be:

$$G_{xy}(f) = H(f)G_x(f) \qquad \text{(Ref 2).} \qquad (5\text{-}15)$$

Therefore, $H(f)$ is given by:

$$H(f) = \frac{G_{xy}(f)}{G_x(f)} . \qquad (5\text{-}16)$$

VI. Results and Conclusions

Counterrolling experiments were performed on six Rhesus monkeys. The responses from all the subjects had like shapes but varied in amplitude and phase shift. Variations were observed in the responses obtained from the same subject in separate tests as well as response from different subjects. In the following discussion no emphasis is placed on a specific monkey. Representative responses for the different tests are given rather than the results from every subject.

Static Tests

The static-test data exhibit bias drifts which completely mask the counterroll response. The term "bias drifts" was defined by previous investigators to mean drifts in the base line or reference level. A time record of a static test is given in Figure 6-1 which shows the continual bias drifts observed. Since these bias drifts are present, no analysis was performed on the static-test data.

Constant Angular Velocity Tests

A series of constant angular velocity tests were performed on each subject. In these tests, each subject's counterroll response was recorded for various rates of rotation in the frontal plane. The subjects were rotated both clockwise and counterclockwise with rotational rates of 5, 10, 20, and 30 rpm. These tests provided a means to check the measurement technique by comparing the data with responses measured by previous investigators.

Results. All of the subjects showed the characteristic response reported by previous investigators for constant velocity angular rotations. Figures 6-2 and 6-3 are time records of counterroll for rotations of 5 rpm counterclockwise and 30 rpm clockwise.

The following characteristics were observed in the response of all the subjects:

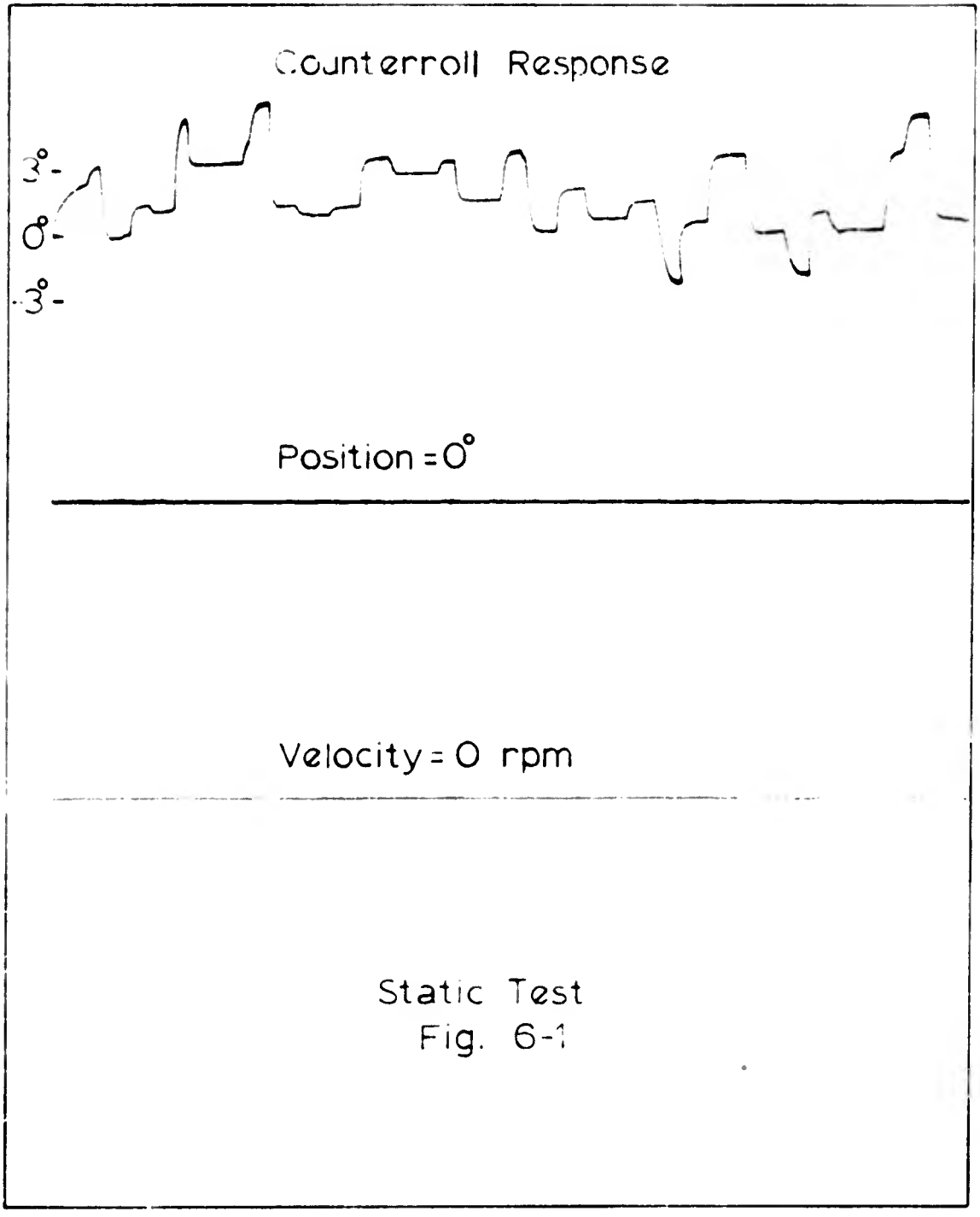

Static Test
Fig. 6-1

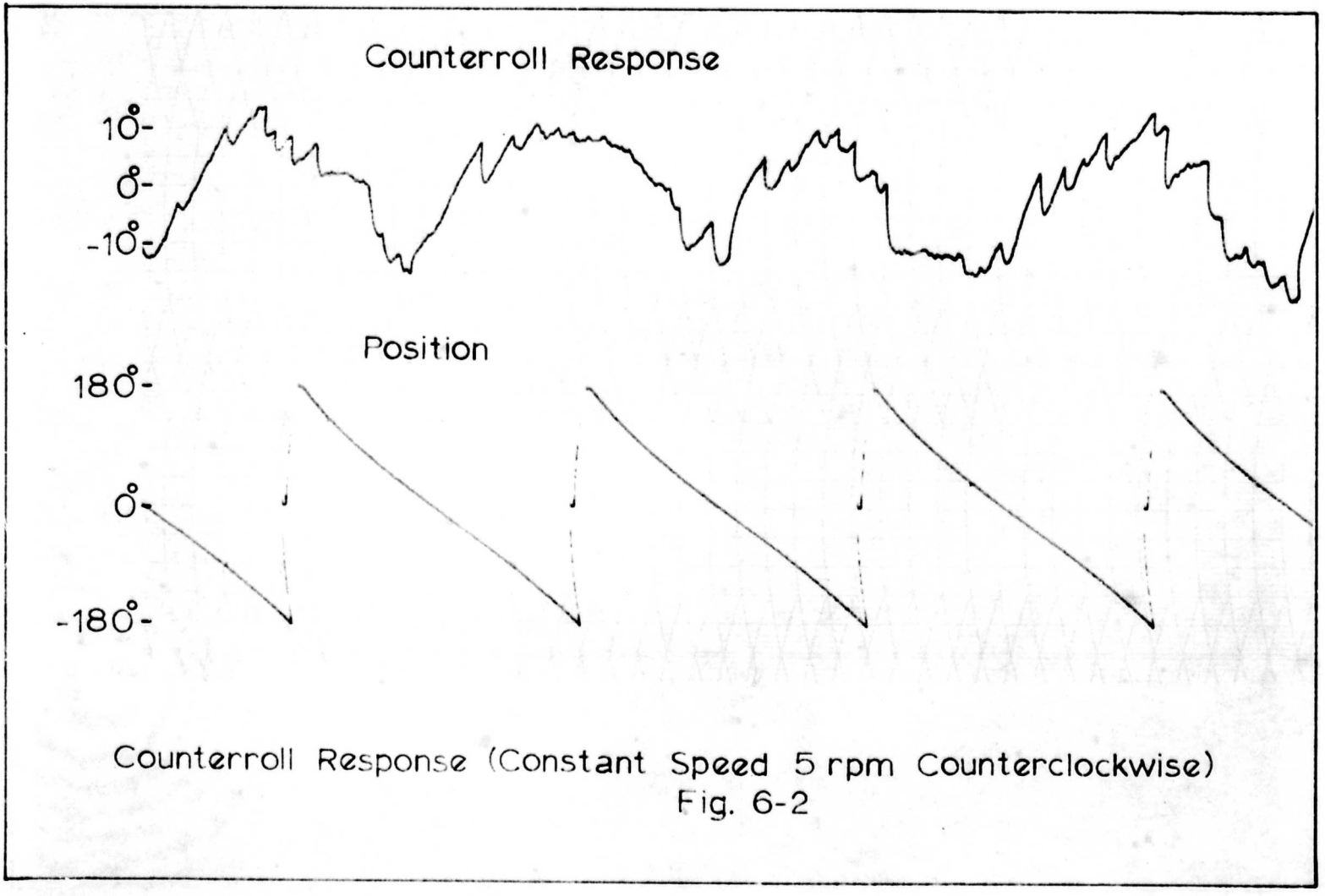

Counterroll Response (Constant Speed 5 rpm Counterclockwise)
Fig. 6-2

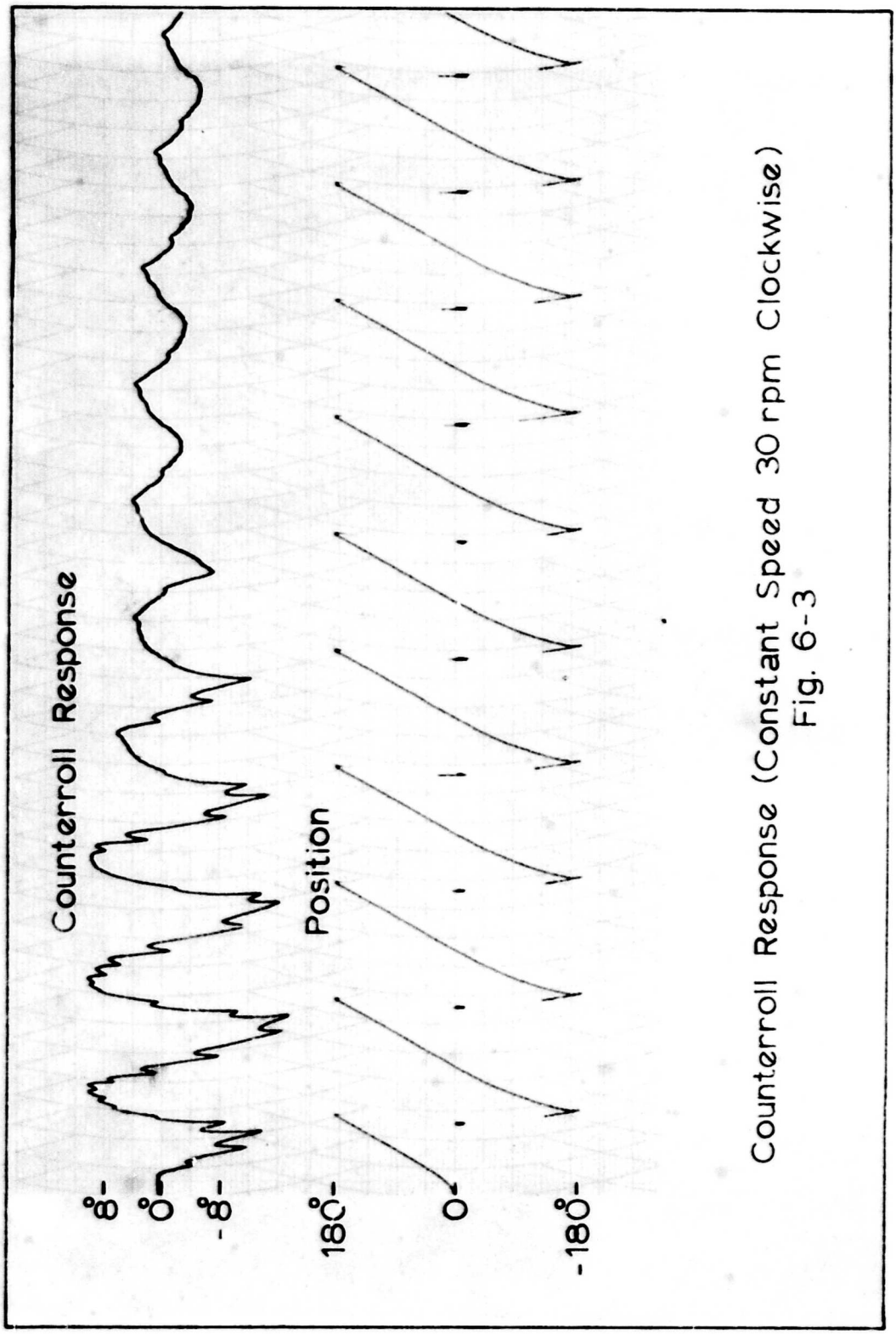

Counterroll Response (Constant Speed 30 rpm Clockwise)
Fig. 6-3

1. The peak-to-peak amplitude of the response decreased for increasing rates of rotation. This result is illustrated by Figures 6-4 and 6-5 which are plots of two cycles of counterroll versus position for clockwise rotations of 5 and 30 rpm. The corresponding plots for counterclockwise rotations are given in Figures 6-6 and 6-7. The counterroll responses obtained in the 10 rpm and 20 rpm tests are consistent with this result.

2. As the angular velocity was increased, the response tended to become more sinusoidal in shape; that is, the random fluctuations in the response decreased as the angular velocity increased.

3. There was an increasing positive phase shift with increasing rates of clockwise rotation and an increasing negative phase shift with increasing rates of counterclockwise rotation. Figures 6-4 and 6-5 illustrate this result for clockwise rotations, and Figures 6-6 and 6-7 illustrate this result for counterclockwise rotations.

4. Suppression of the counterroll response from all but one subject was observed in the constant angular velocity tests. No explanation for the one exception is known.

5. The power spectral densities of the counterroll responses to constant angular velocity rotations have their peak value at the frequency of the sinusoidal gravity input. Power spectra of responses to rotations of 5 and 30 rpm are shown in Figures 6-8 and 6-9. These power spectra also show that the response has components which occur at the harmonics of the gravity input frequency.

6. The peak-to-peak counterroll was observed to be large for the first few revolutions of the rotating chair, and then it decayed to an approximately constant value. The time record shown in Figure 6-2 illustrates this result.

Discussion of Results. The decrease in the peak-to-peak counterroll response with increasing rates of rotation is consistent with Dr. Miller's theory on otolith organ operation (Ref 9). According to Dr. Miller, the otolith organs sense a rotation from the vertical only when the maculae of

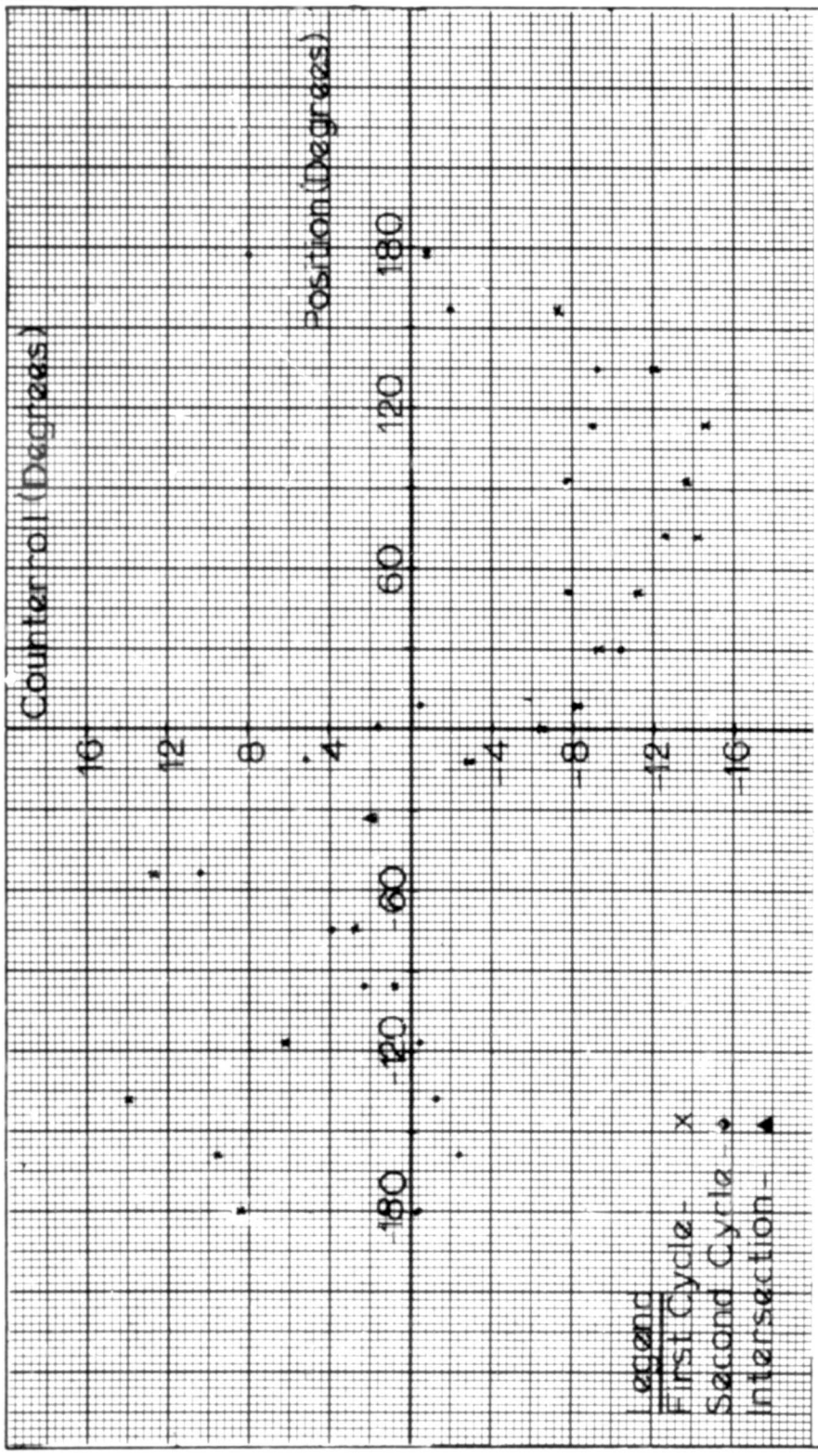

Counterroll versus Position (Constant Speed 5 rpm Clockwise)
Fig. 6-4

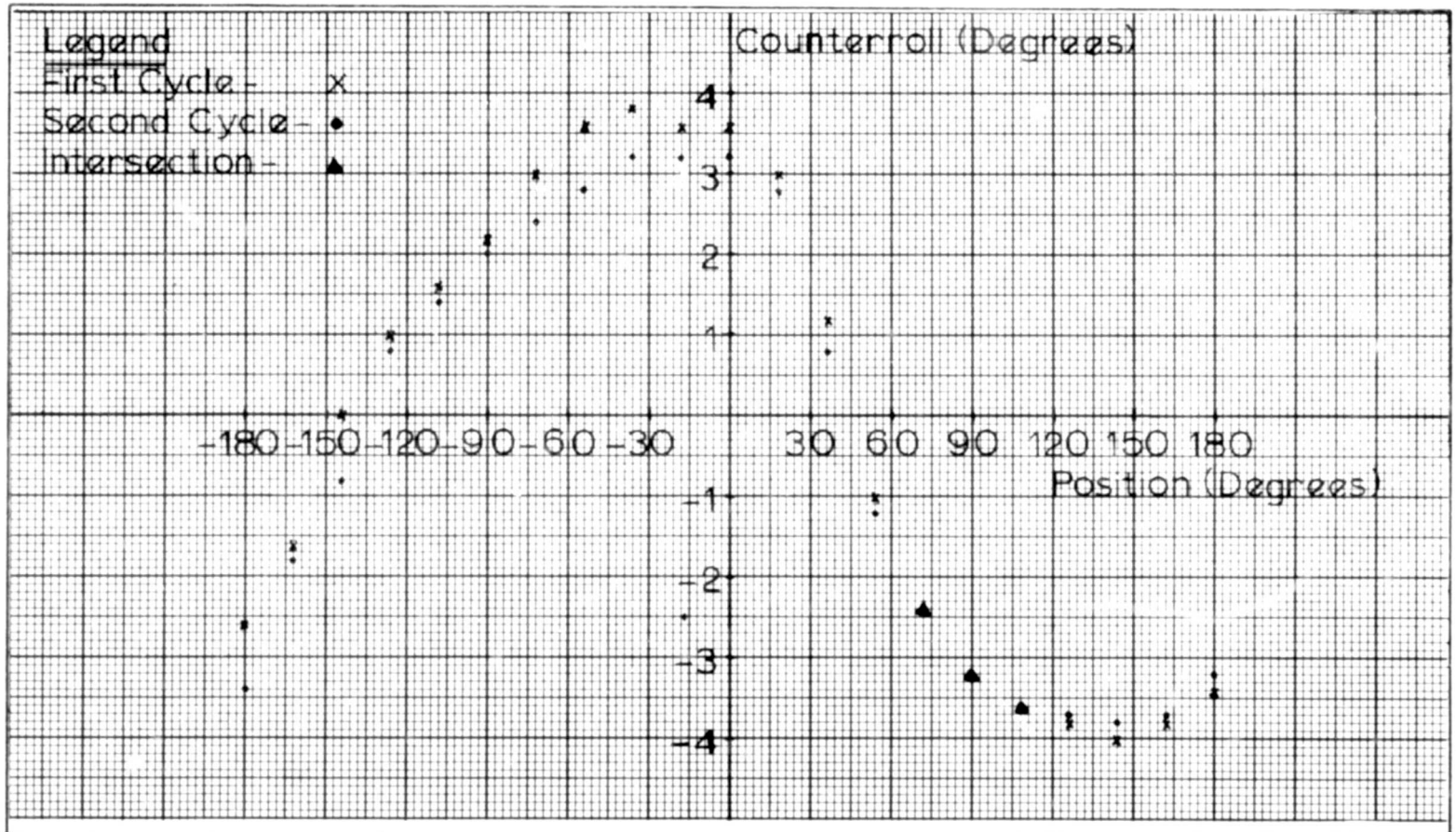

Counterroll versus Position (Constant Speed 30 rpm Clockwise)
Fig. 6-5

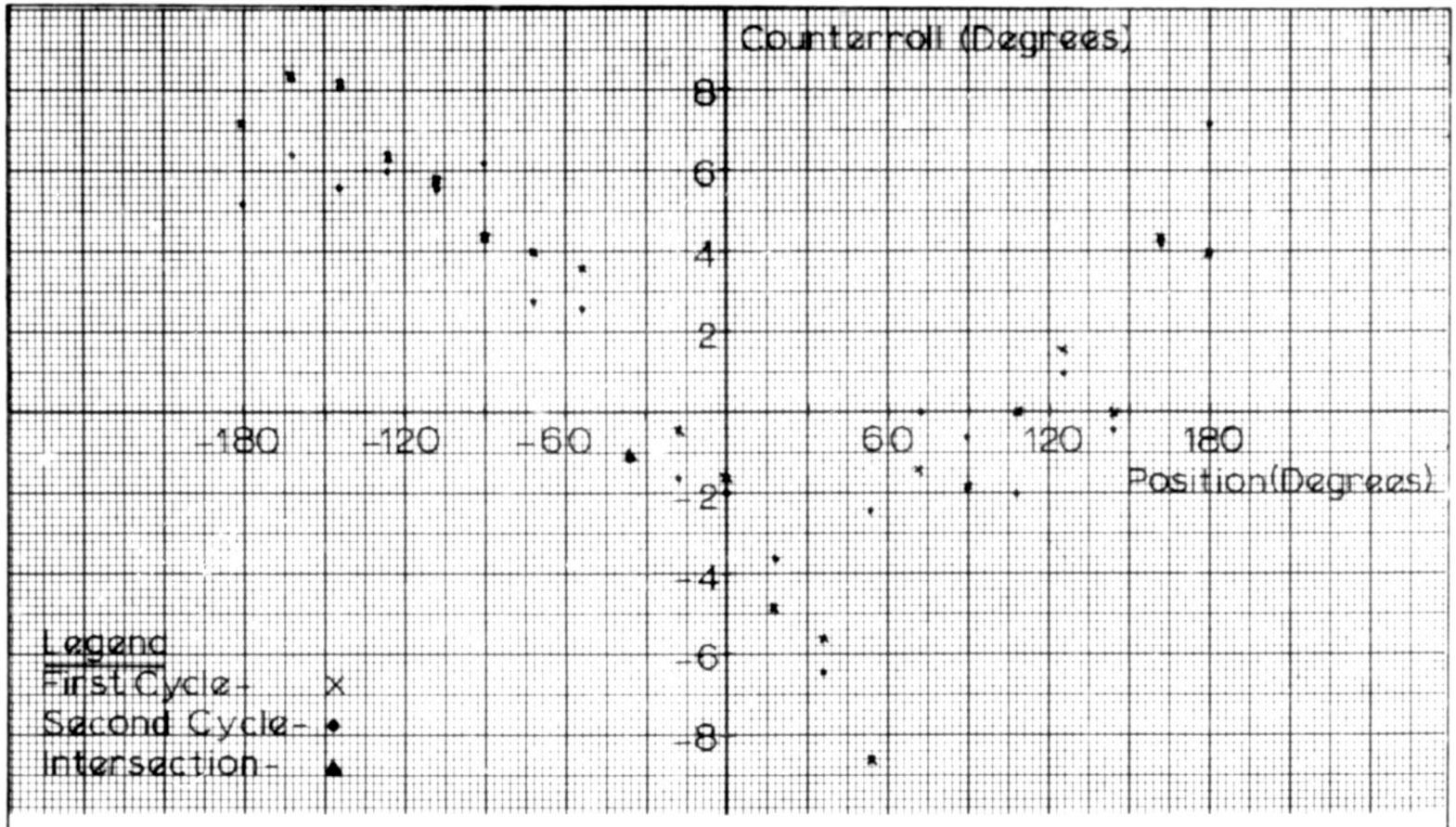

Counterroll versus Position (Constant Speed 5rpm Counterclockwise)
Fig. 6-6

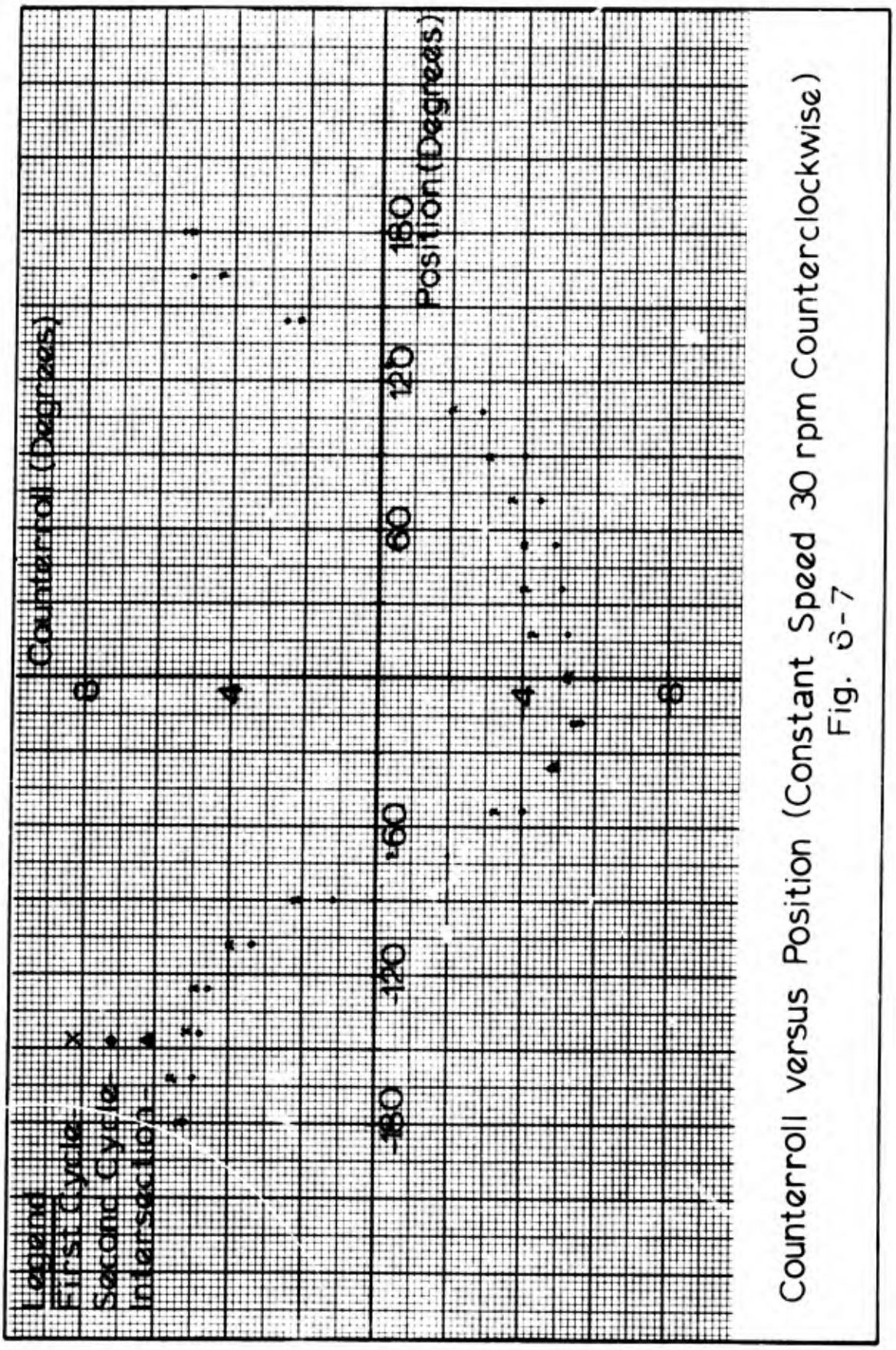

Counterroll versus Position (Constant Speed 30 rpm Counterclockwise)
Fig. 3-7

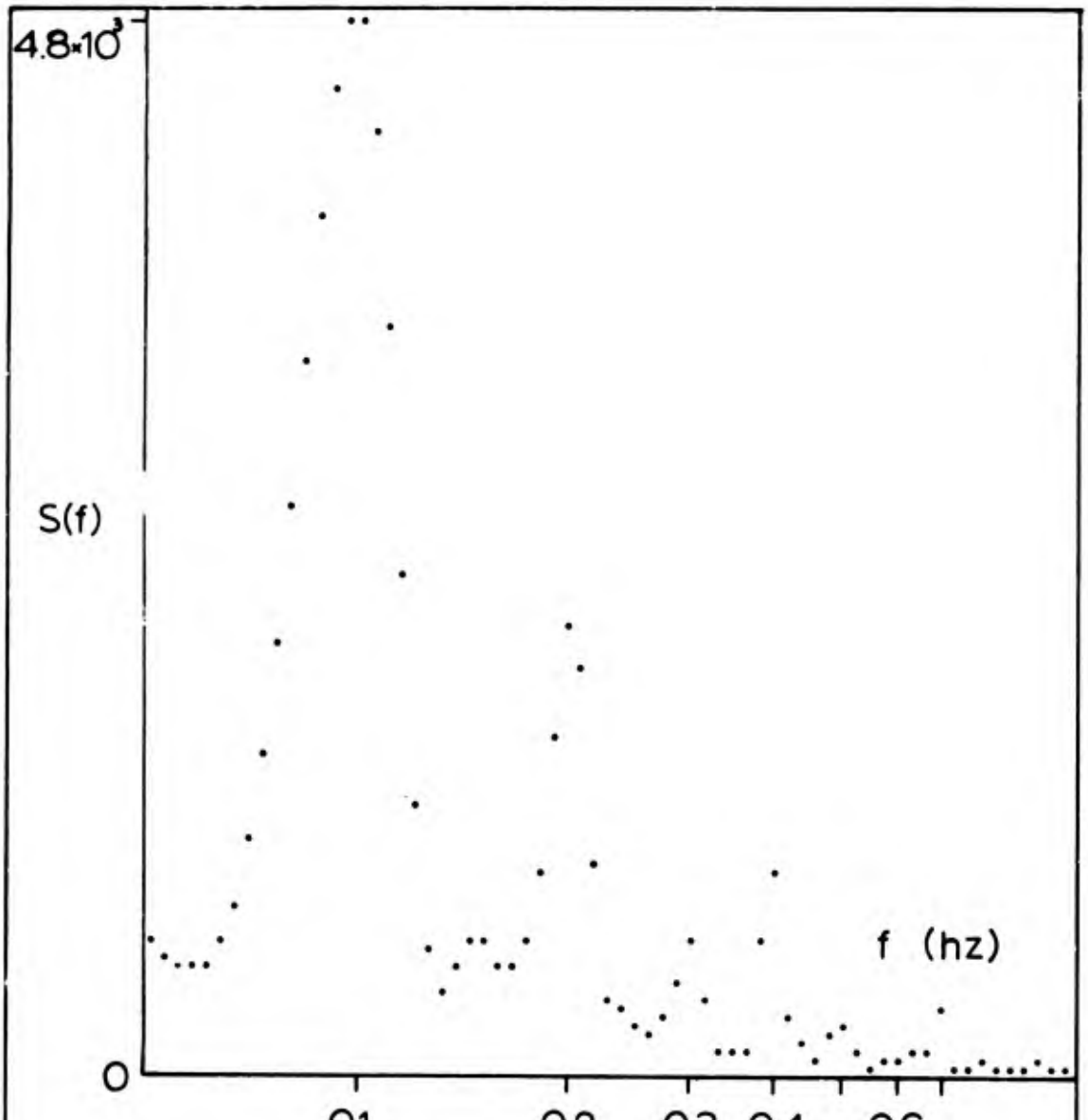

Power Spectral Density of the Counterroll Response to a 5 rpm Counterclockwise Constant-Speed Rotation
Fig. 6-8

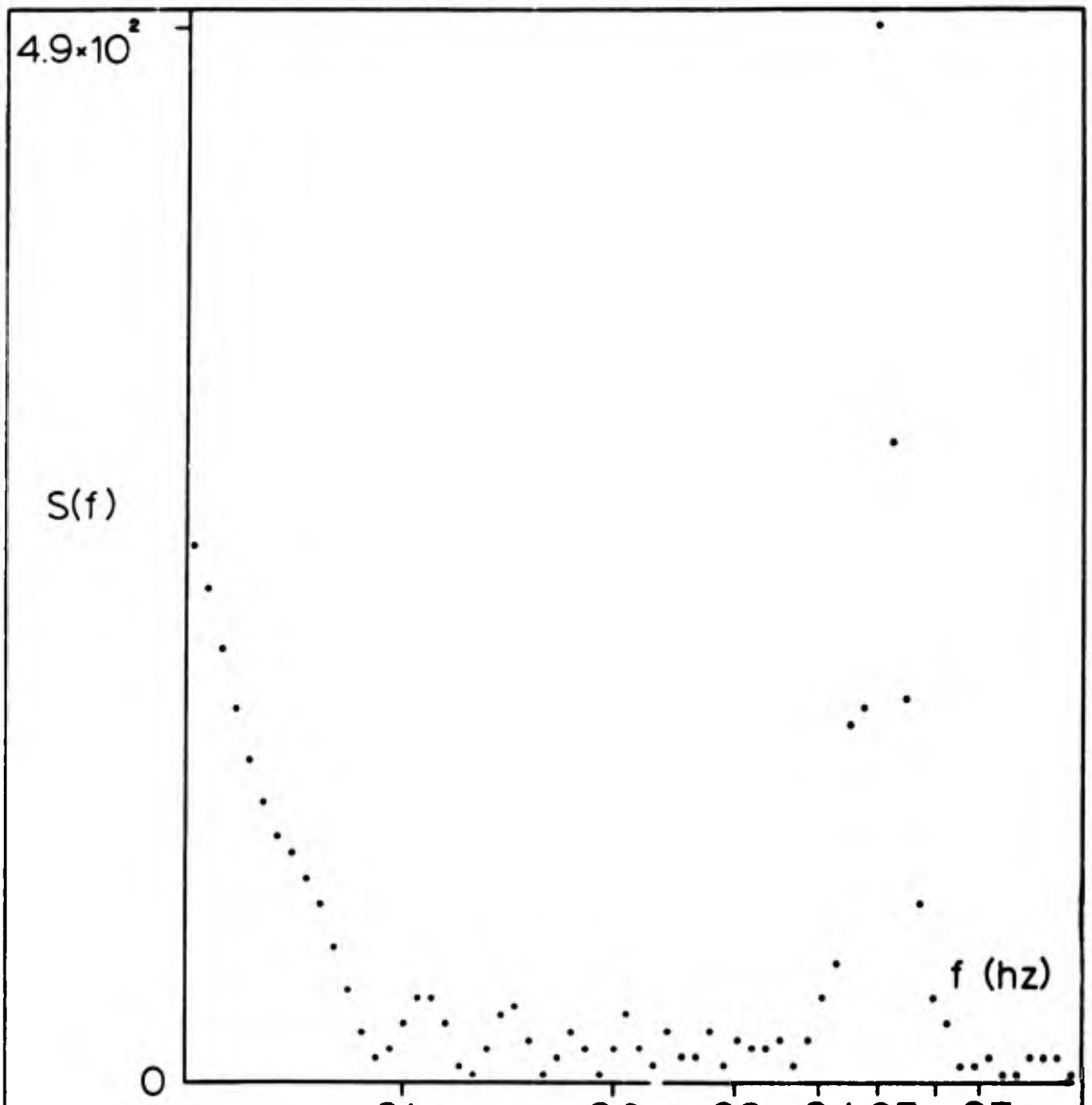

Power Spectral Density of the Counterroll Response to a 30 rpm Clockwise Constant-Speed Rotation

Fig. 6-9

these organs point toward the median sagittal plane. Since the subject's head was positioned so that the otolith organs were centered about the axis of rotation, there is a radially directed acceleration on the otoliths due to centripetal force. With a constant angular velocity, the resultant radial acceleration will displace the otoliths away from the median sagittal plane because their specific gravity is greater than that of the gelatinous mass upon which they rest. If Dr. Miller's theory is assumed to be correct, this displacement would tend to decrease the otolith response.

The data obtained by previous investigators using human subjects exhibited less variability than that from the Rhesus monkeys under static conditions and low rates of rotation. This is because human subjects can be instructed to fixate during the tests. Lessard and Gnuse, who were the only investigators to use Rhesus monkeys as subjects before this study, reported that no useful data could be obtained for rotations below 5 rpm because of the continual bias drifts. The spectral analysis done in this study proved useful in separating the bias drifts from the response in the frequency domain for low rates of rotation. However, the bias drifts could not be separated from the response to static tests since both occur in the same frequency range.

The large peak-to-peak transient of the counterroll response is attributed to the angular acceleration which is present when the rotating chair starts from rest and accelerates to a constant angular velocity. The effects of angular acceleration on the counterroll will be discussed in the next section.

Pendular-Motion Tests

Seven pendular motion tests were performed on each subject. In these tests, each subject's counterroll response was recorded for various frequencies of rotational oscillation. The axis of rotation was the same used in the constant angular velocity tests, and the equilibrium position was the position in which the subject's body was in line with the vertical. The frequencies of oscillation ranged from 0.2 hz to 0.5 hz. The amplitudes of oscillation ranged from 60°

to 80°; however, the amplitudes were held constant while testing any one subject.

Result. The counterroll responses obtained in the pendular motion tests increased with increasing frequencies of pendular oscillation. Time records of counterroll response to pendular input frequencies of 0.2 hz and 0.4 hz are given in Figures 6-10 and 6-11. The approximate steady-state peak-to-peak counterroll for the 0.4 hz pendular input is 14° as compared to 12.5° for the 0.2 hz response. The counterroll responses obtained in the 0.25 hz, 0.3 hz, 0.35 hz, 0.45 hz, and 0.5 hz tests are consistent with the above result.

The power spectral densities of the counterroll responses shown in Figures 6-10 and 6-11 are given in Figures 6-12 and 6-13. Both power spectra have peaks at the frequency of the pendular input; however, the magnitude of the 0.4 hz peak is greater than the 0.2 hz peak. This further indicates that the counterroll response increases for increasing frequencies of pendular input. The power spectra also show that the responses have components which occur at the harmonics of the input frequency. The power spectral density of the 0.2 hz pendular input (Fig. 6-14) shows that the input position also had harmonics present. This indicates that the pendular oscillations of the rotating chair were not completely sinusoidal. Harmonic components were found in all pendular inputs below 0.3 hz.

Discussion of Result. The constant angular velocity tests showed that the peak-to-peak counterroll response decreases with increasing angular velocities. In the pendular tests, the peak angular velocity increases with increasing input frequencies, but the peak-to-peak counterroll response also increases. This increase in peak-to-peak counterroll response is attributed to stimulation of the semicircular canals. Unlike the constant angular velocity tests, the pendular tests provide a continuous angular acceleration input. The semicircular canals are known to be stimulated by angular acceleration; however, the magnitude of their effect on counterroll is not known.

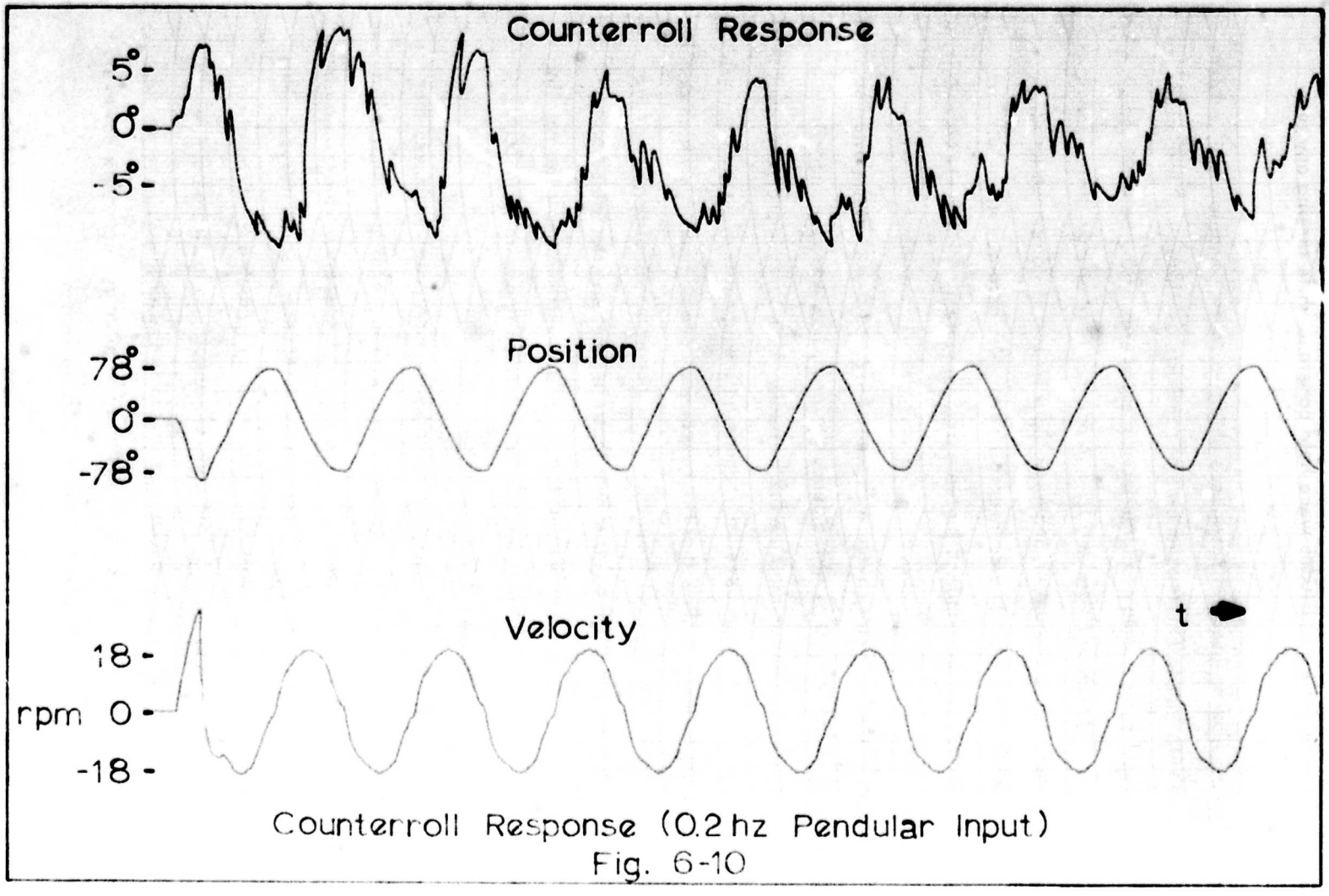

Counterroll Response (0.2 hz Pendular Input)
Fig. 6-10

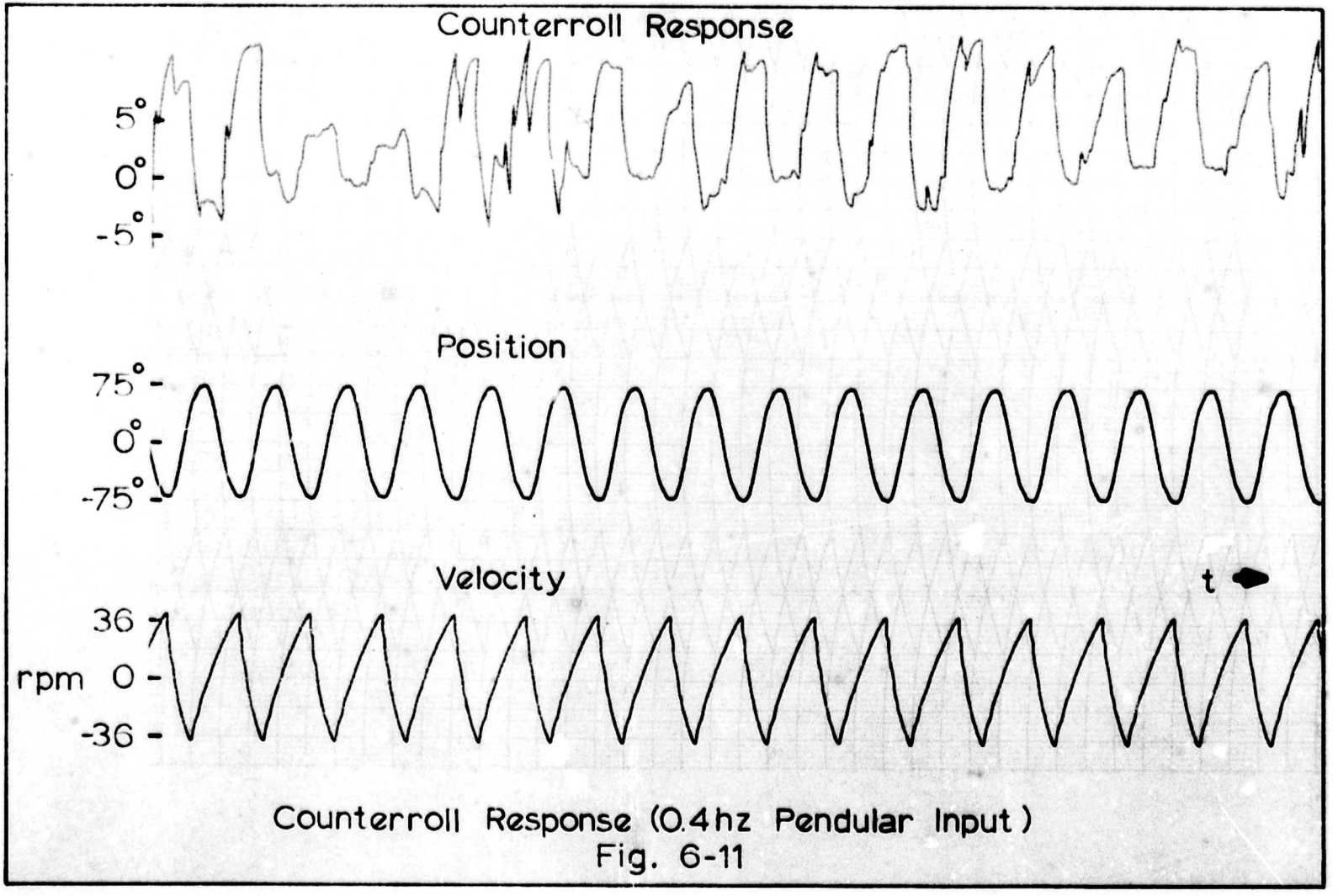

Counterroll Response (0.4hz Pendular Input)
Fig. 6-11

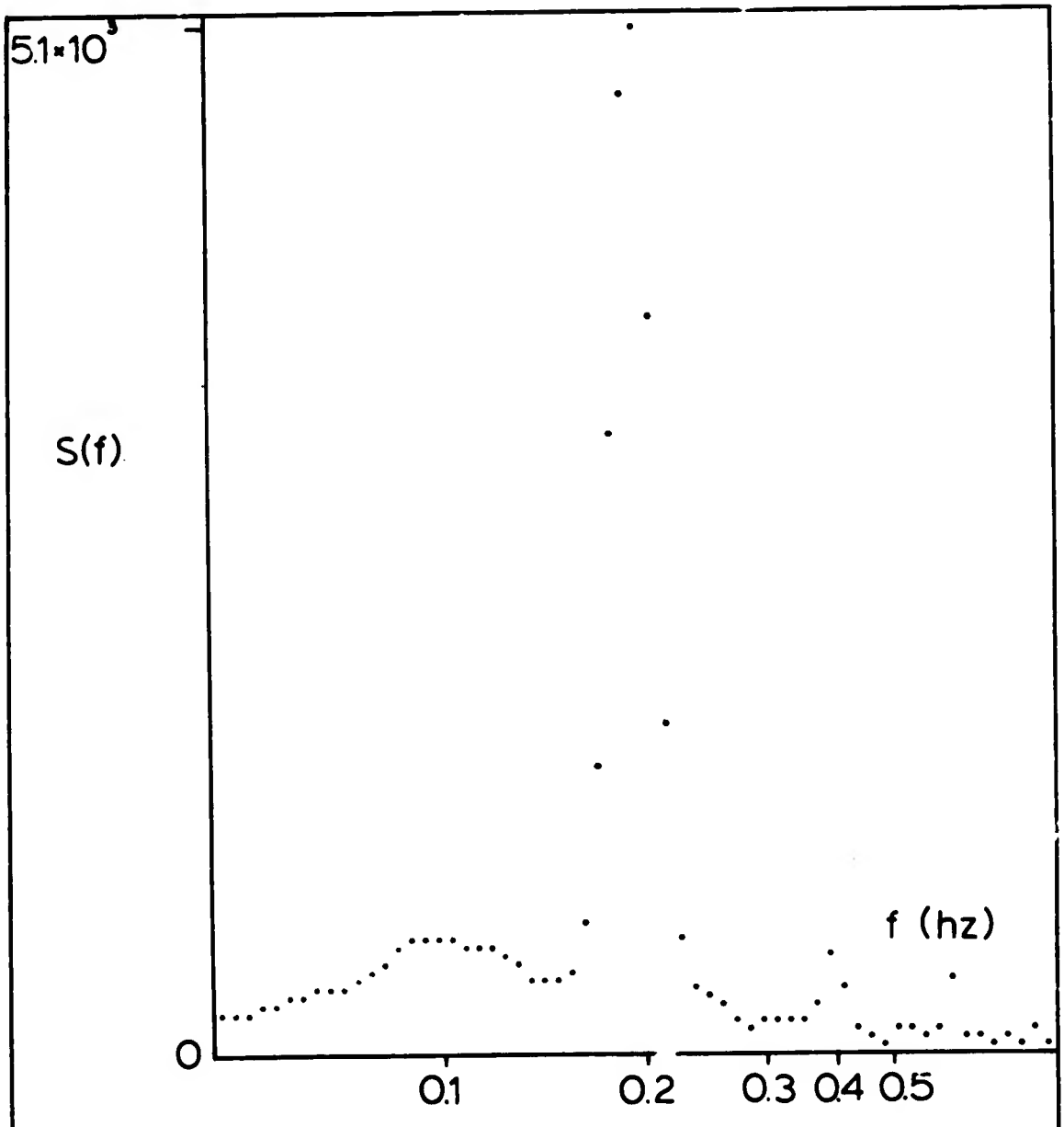

Power Spectral Density of the
Counterroll Response to a 0.2 hz Pendular Input
Fig. 6-12

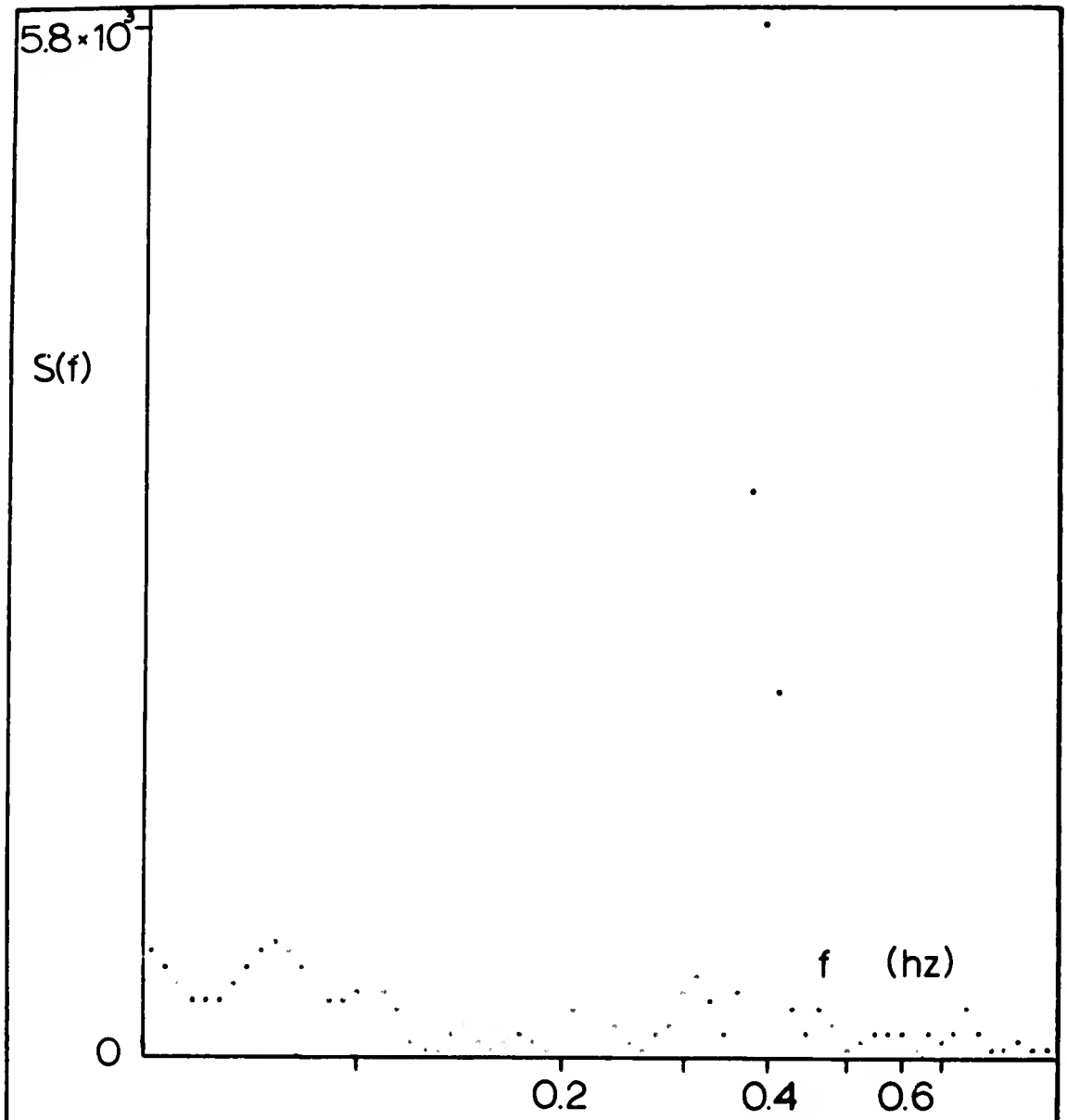

Power Spectral Density of the
Counterroll Response to a 0.4 hz Pendular Input
Fig. 6-13

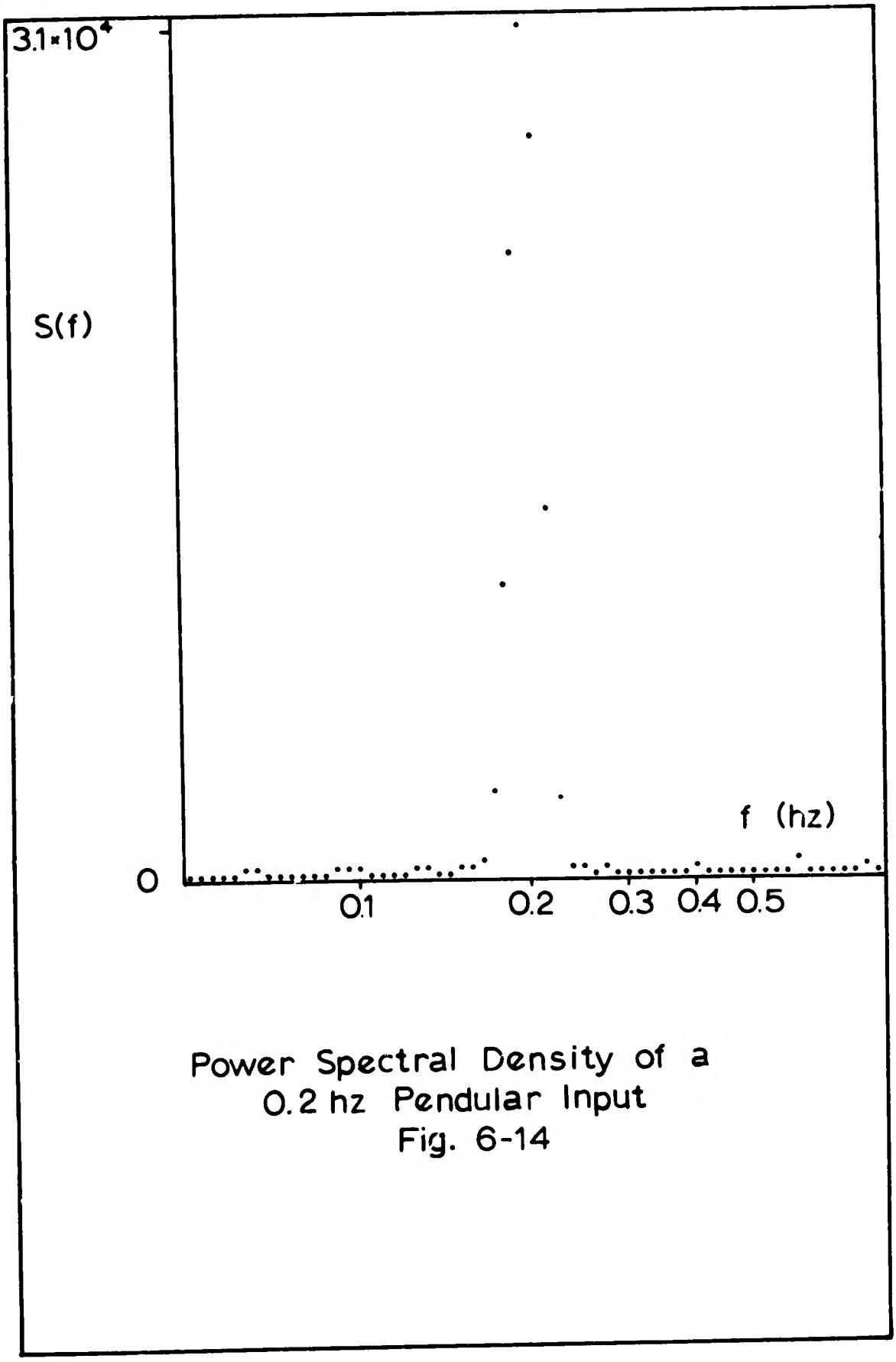

Power Spectral Density of a
0.2 hz Pendular Input
Fig. 6-14

At no time, during the pendular input tests, was the subject oscillated beyond 80° from the vertical in either direction. According to Dr. Miller's theory, the saccules will not be stimulated unless the subject is rotated beyond ±44°, and they respond maximally at ±134° (Ref 9:27 and Appendix A). In most tests, the subject was not oscillated beyond 75° in either direction. Thus assuming Dr. Miller's theory is correct, the saccules were not stimulated to their full output. Therefore, they could not contribute as much to the counterroll as in the constant-speed tests where complete 360° rotations were made. A report of the work of D. A. Ross on the frog's labyrinth indicates that the saccules do not affect counterroll at all, but are low frequency vibration sensors (Ref 12). Until further analysis is made and specific experiments are conducted on saccule response, the increase in peak-to-peak counterroll in the pendular tests is not attributed to the saccules. Therefore, the increase is attributed to the effects of the semicircular canals on counterroll. These effects make it impossible to investigate only the otolith organ response (through measurement of counterroll) when angular acceleration inputs are present.

Gaussian Random Noise Tests

A Gaussian random noise test was performed on each subject. In these tests, each subject's counterroll response was recorded while the subject was oscillated in his frontal plane. The amplitudes of the oscillations were normally distributed with zero mean and a standard deviation of 20 degrees. Figure 6-15 is a time record of the response to a Gaussian noise input.

Results. One of the reasons for using Gaussian noise as a position input to the rotating chair was to attempt to eliminate the suppression of counterroll reported by previous investigators (Ref 8). It was hypothesized that the suppression might be due to the subject's anticipation of the input. It was found that the subjects could suppress counterroll with a random noise input. Figure 6-16 is a section of a time record which illustrates this sup-

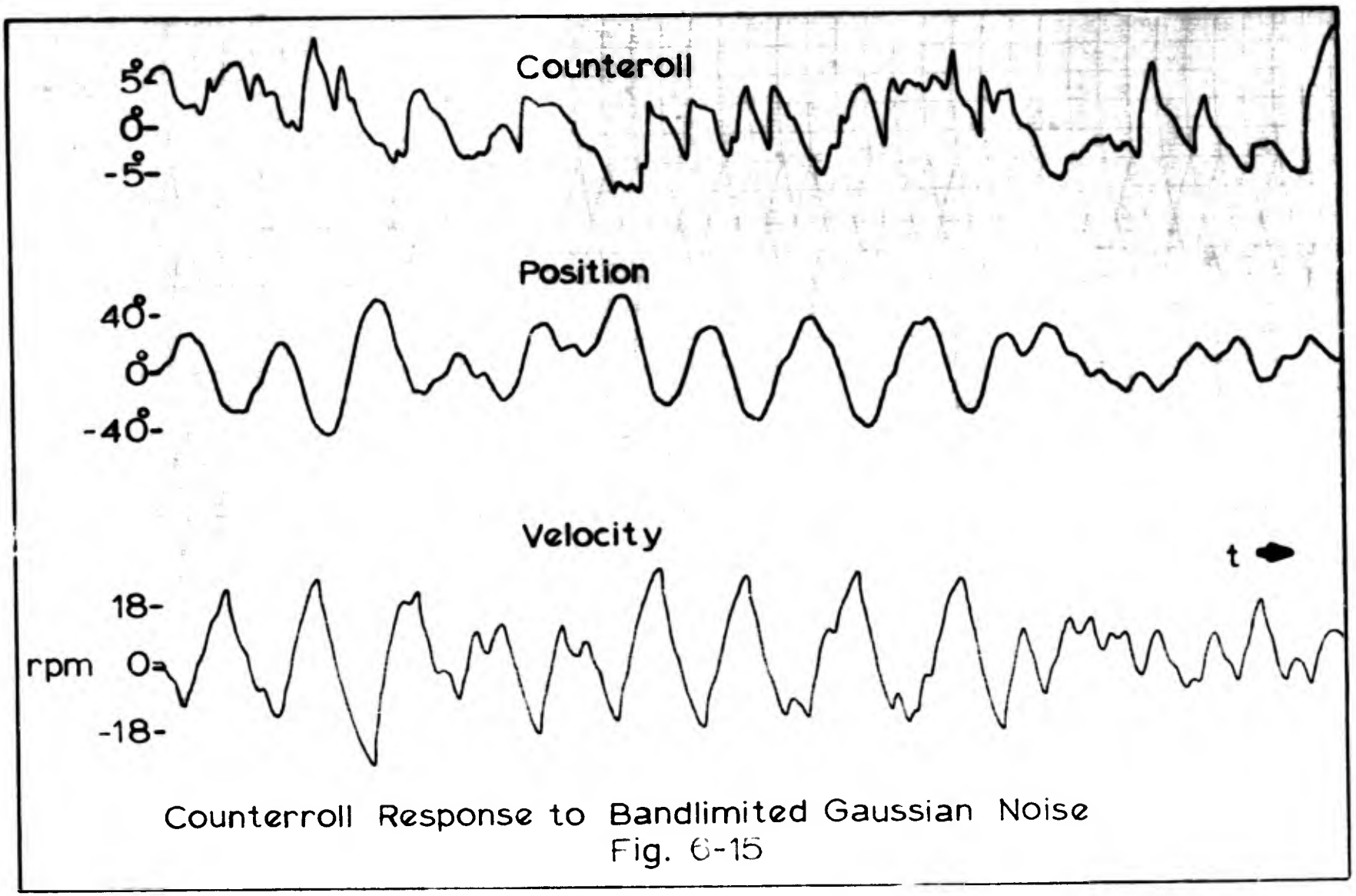

Counterroll Response to Bandlimited Gaussian Noise
Fig. 6-15

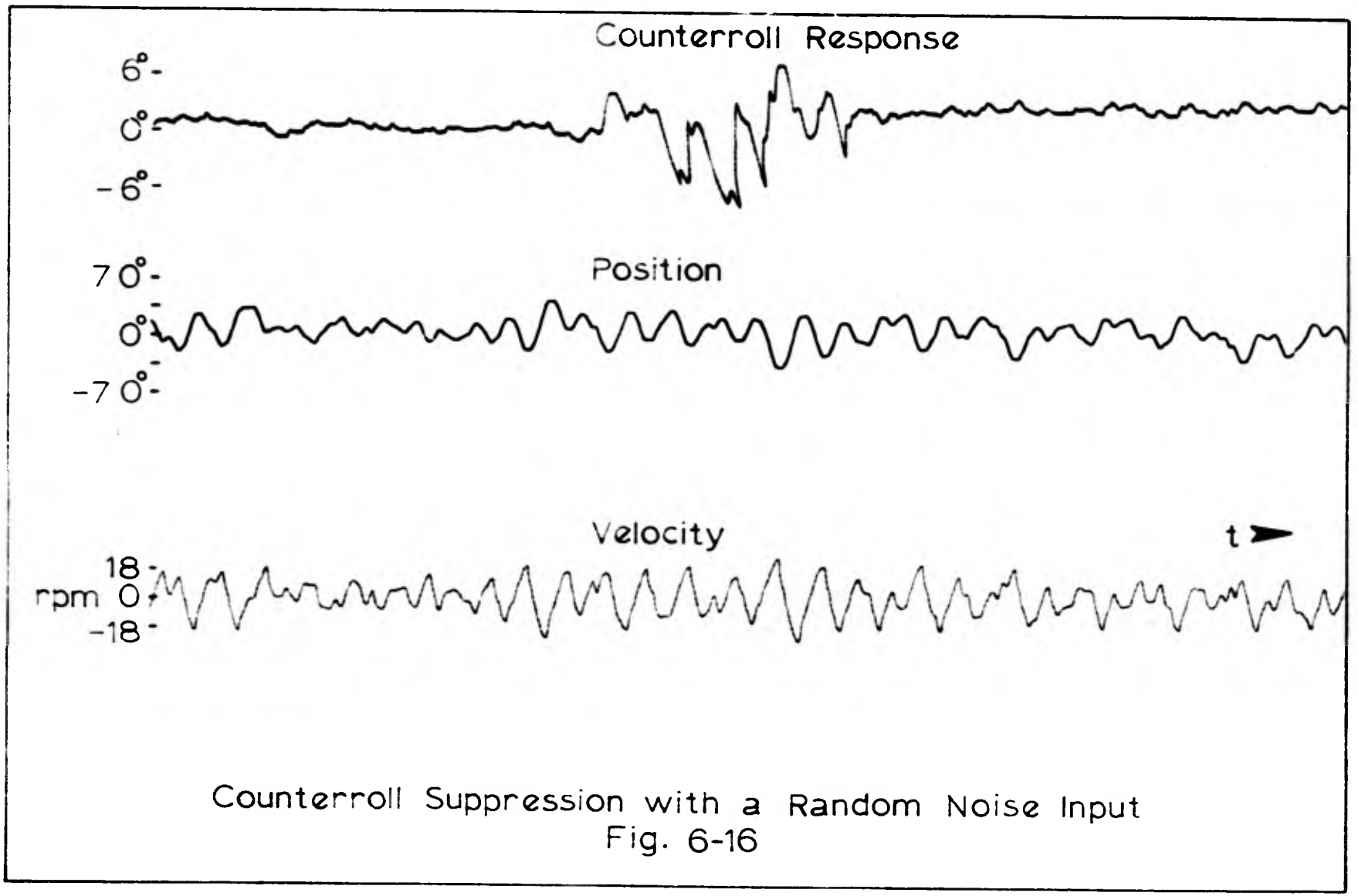

Counterroll Suppression with a Random Noise Input
Fig. 6-16

pression. The random noise input failed to eliminate the suppression; however, it did demonstrate that the subjects can suppress counterroll even though they cannot predict the input.

Figures 6-17 and 6-18 are autocorrelation functions of a Gaussian noise input and corresponding counterroll response. The autocorrelation of the input has the shape of an autocorrelation function of narrow-band random noise, but it does not decay to zero for large τ (as it should). This is assumed to be a result of the number of τ shifts used in calculating the autocorrelation functions. The digital computer program used allows a maximum of 100 τ shifts. Each shift is equal to the sampling period, or 0.1 seconds. The lowest frequency data which will be recovered in the autocorrelation function is given by

$$\frac{1}{2LF} = N\tau \qquad \text{(Ref 2)} \qquad (6\text{-}1)$$

Where,

LF = lowest frequency data recovered

N = number of shifts

τ = length of a τ shift

With 100 shifts each 0.1 seconds in length, equation (6-1) becomes

$$LF > \frac{1}{2N\tau} = 0.05\text{hz} \qquad (6\text{-}2)$$

Therefore, any components of the input below 0.05 hz are not recovered in the autocorrelation function.

The power spectral densities of a Gaussian noise input and the corresponding counterroll response are shown in Figures 6-19 and 6-20. Assuming the system is linear, the frequency response function, H(f), may be calculated by use of equation 5-18. The cross-spectral density function, used in the computation of H(f), is shown in Figure 6-21. The resulting frequency response function is given in Figure 6-22. It must be emphasized that this analysis only applies to linear systems.

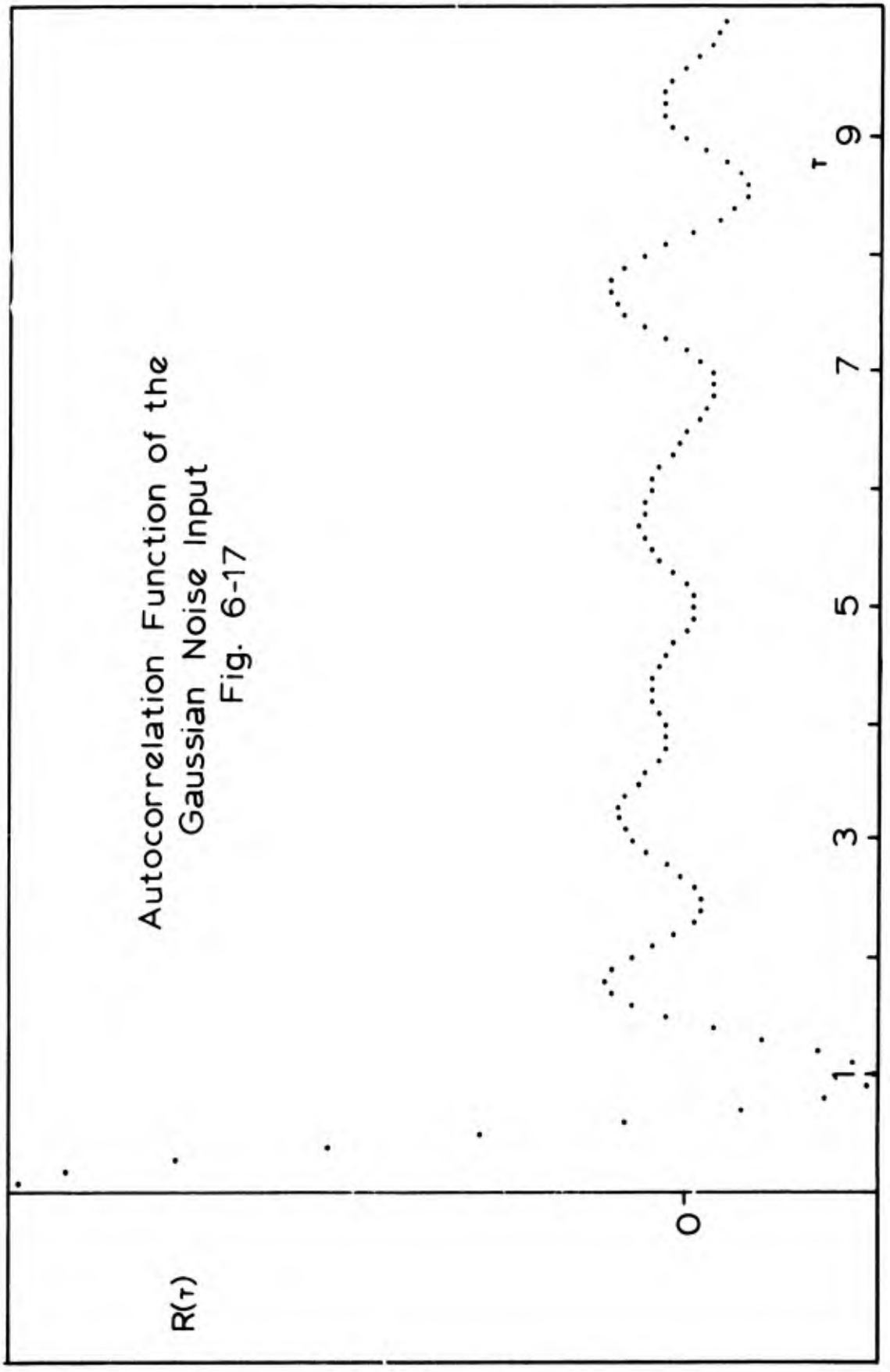

Autocorrelation Function of the
Gaussian Noise Input
Fig. 6-17

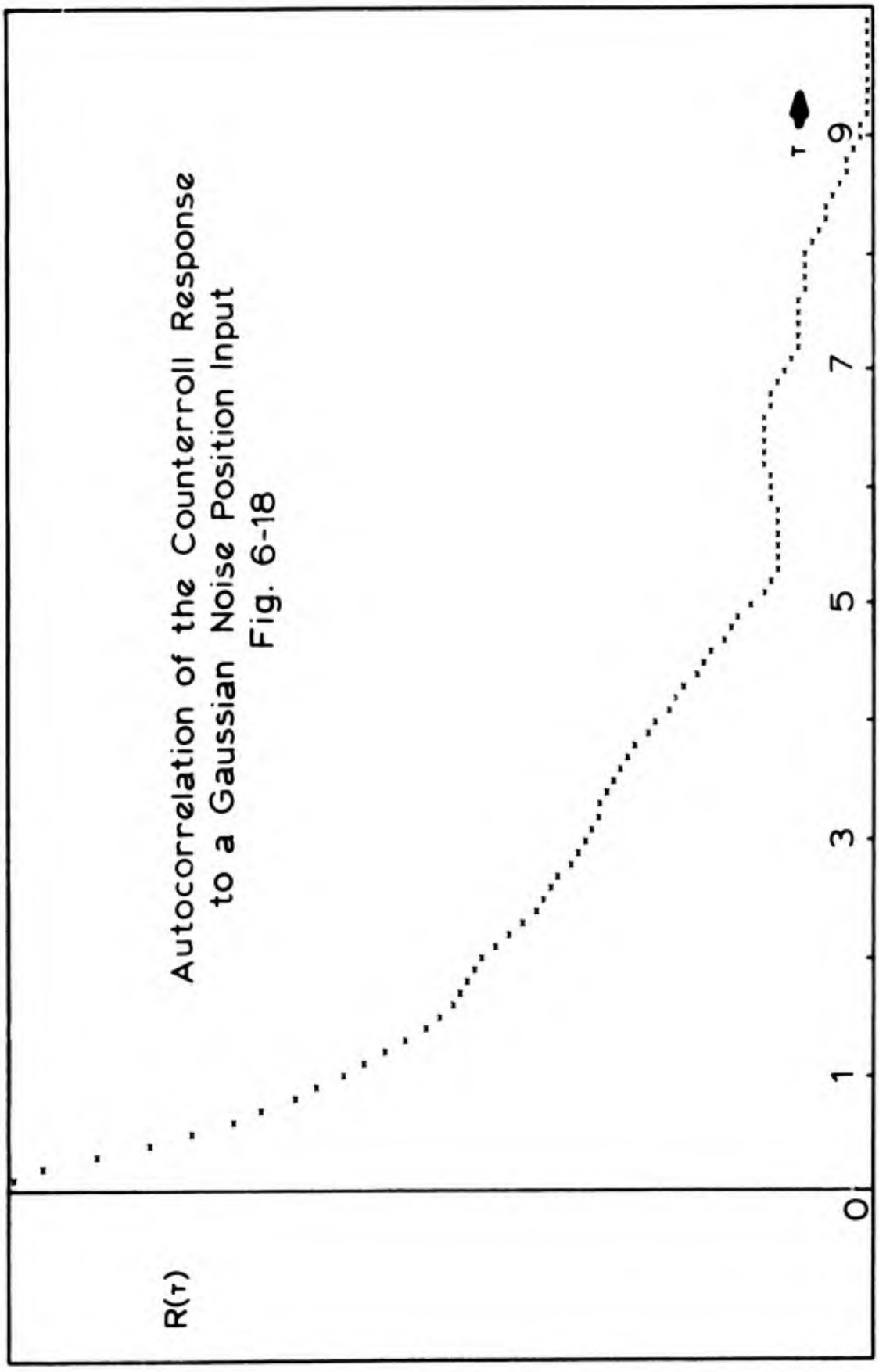

Autocorrelation of the Counterroll Response to a Gaussian Noise Position Input
Fig. 6-18

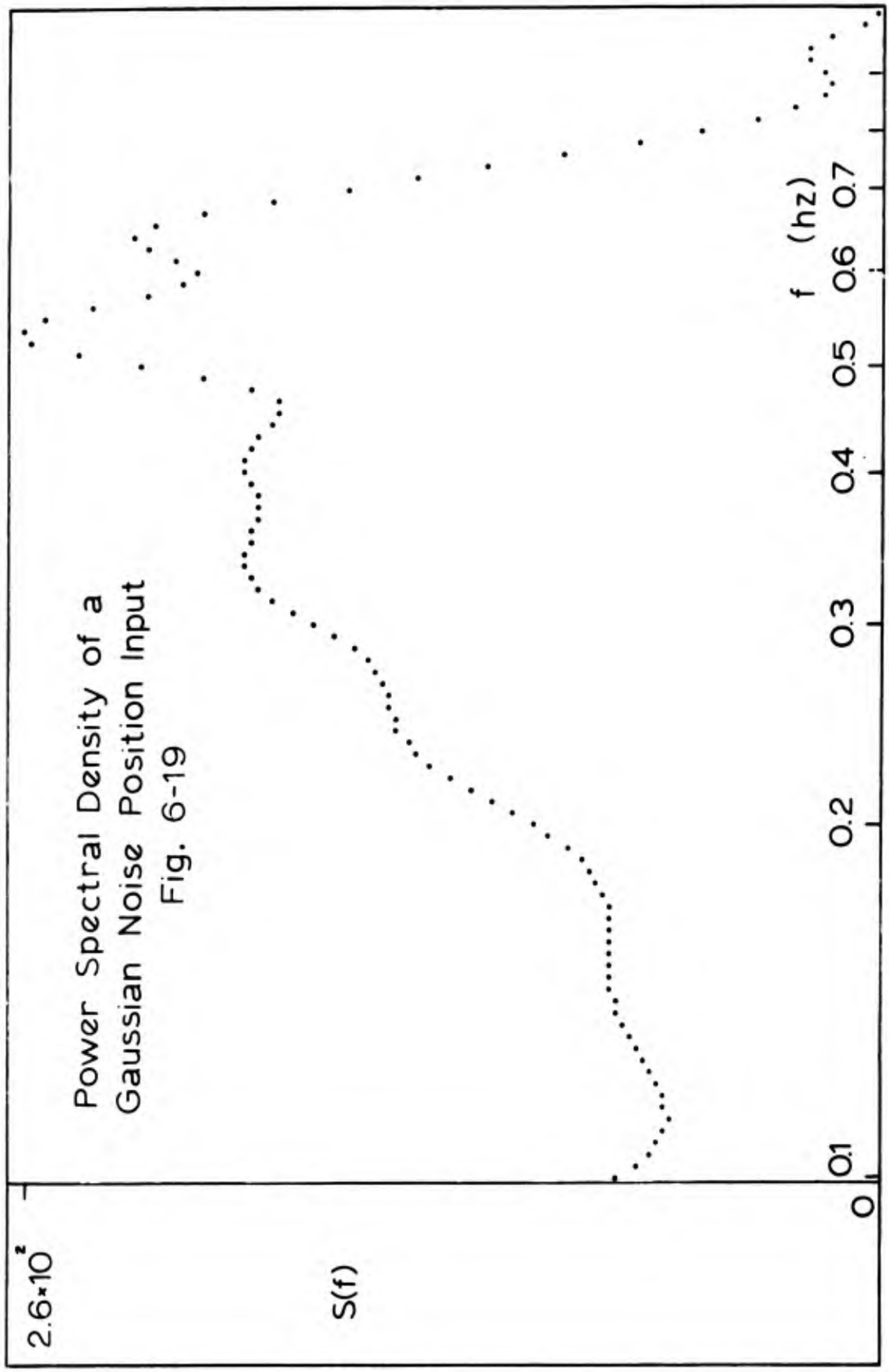
Power Spectral Density of a
Gaussian Noise Position Input
Fig. 6-19
S(f)
2.6×10²
0
0.1
0.2
0.3
0.4
0.5
0.6
0.7
f (hz)

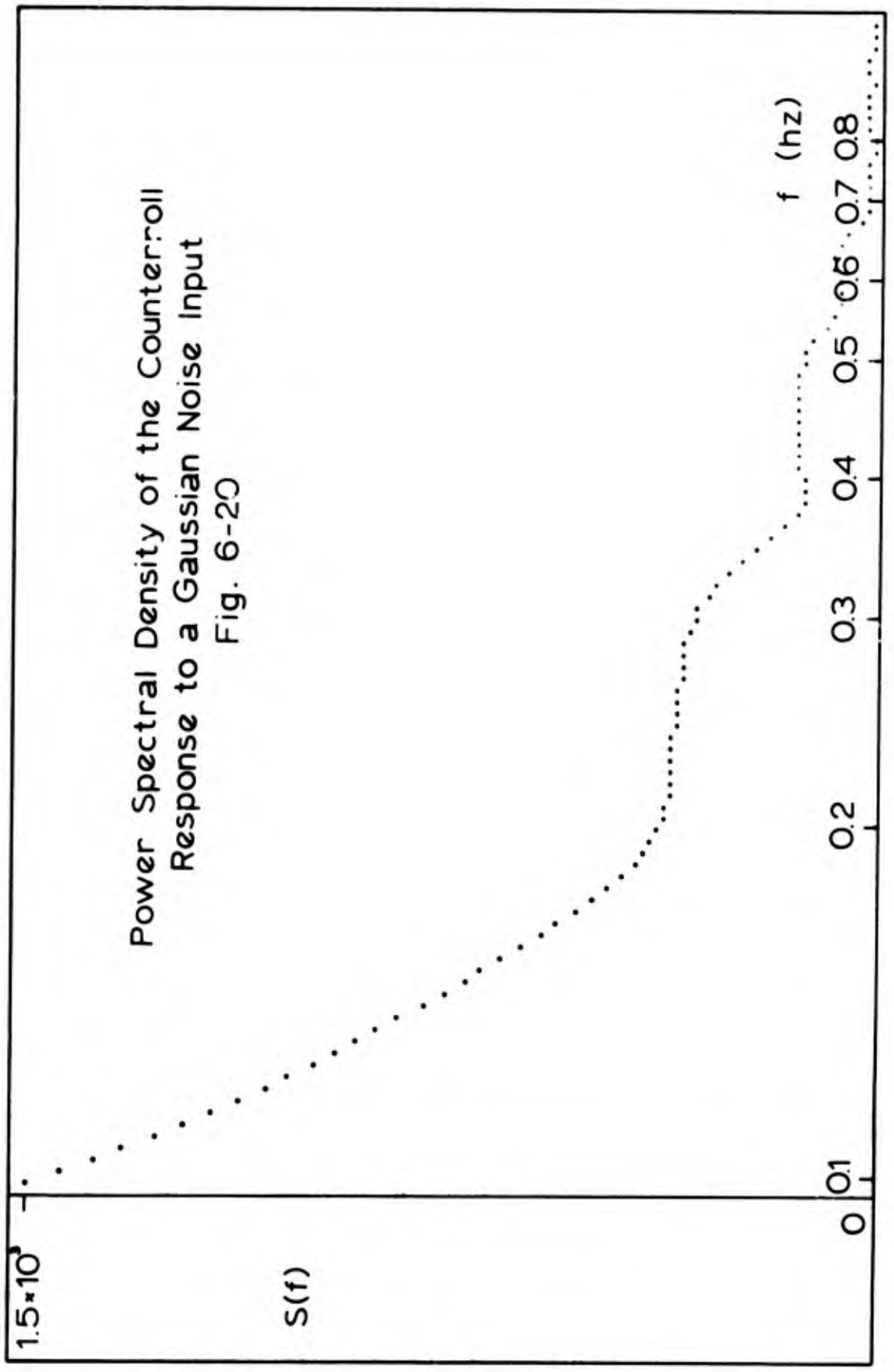
Power Spectral Density of the Counterroll
Response to a Gaussian Noise Input
Fig. 6-20
S(f)
1.5×10³
0
0.1
0.2
0.3
0.4
0.5
0.6
0.7
0.8
f (hz)

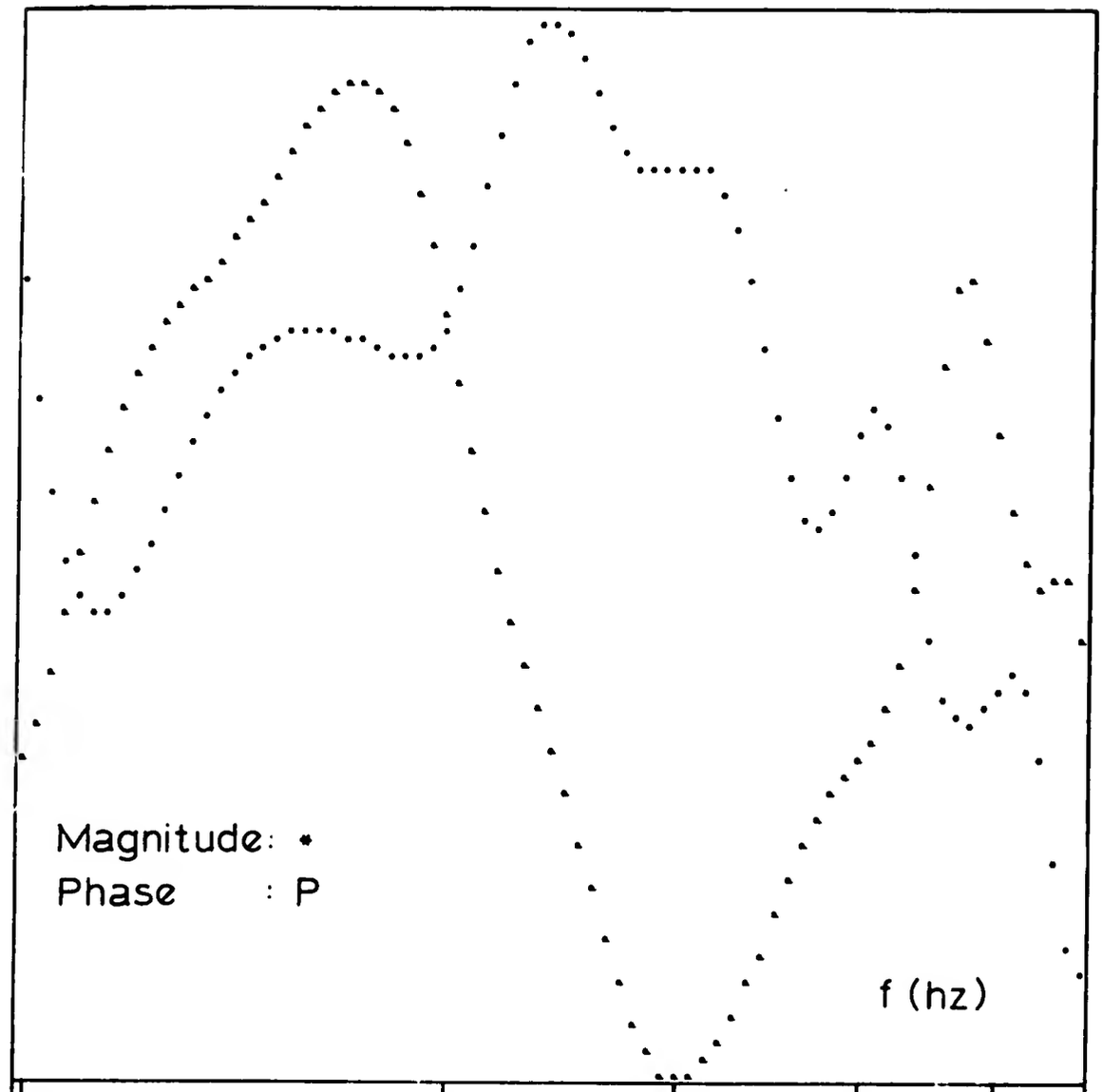

Cross-Spectral Density Between the Input and Output for a Gaussian Noise Position Input
Fig. 6-21

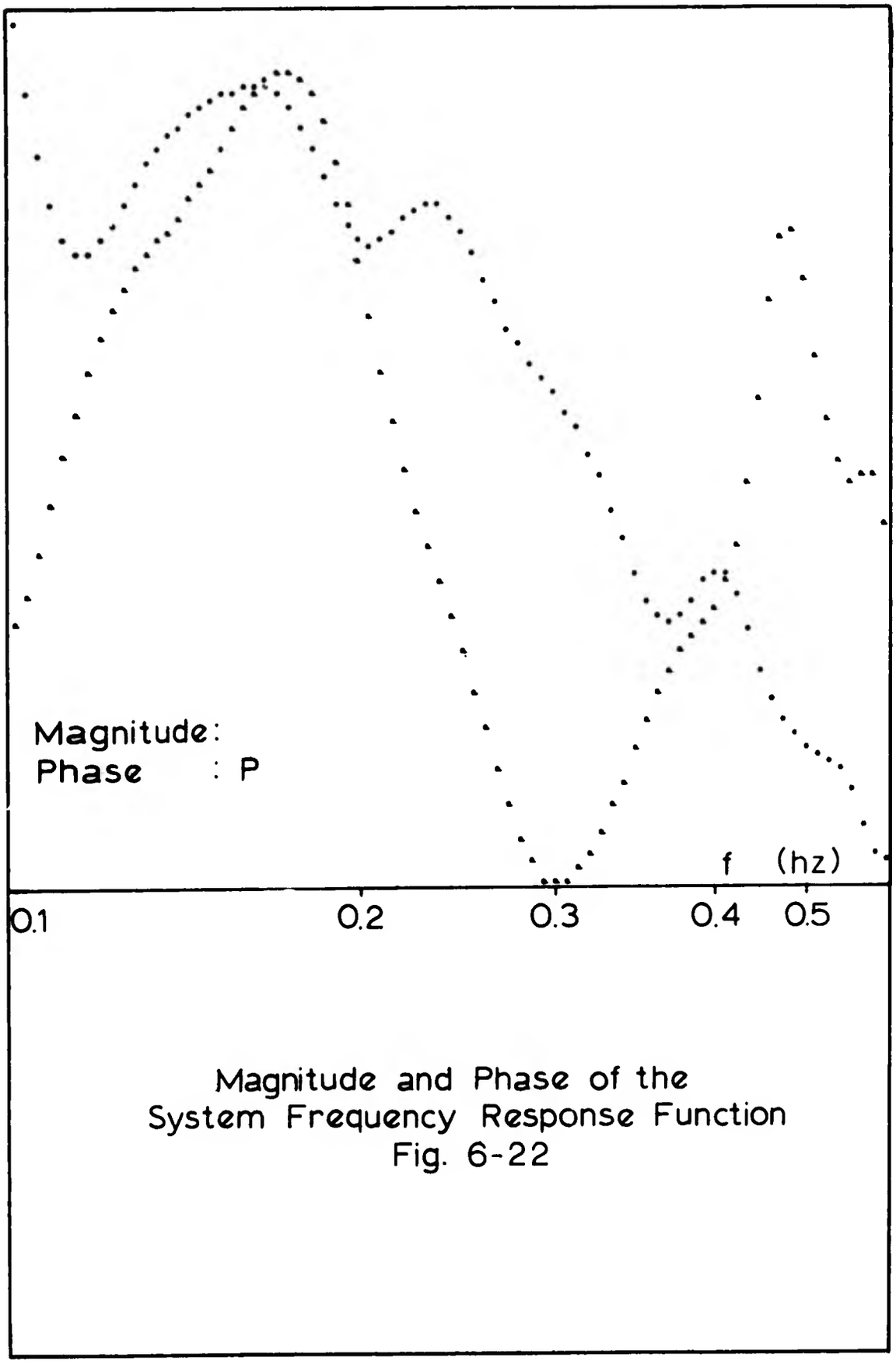

Magnitude and Phase of the
System Frequency Response Function
Fig. 6-22

A Gaussian noise position input to the system provides a means to test for linearity. A fundamental theorem from the theory of transformations of stochastic processes is that a linear system with a Gaussian input will produce a Gaussian output. Figure 6-23 is a histogram of the counterroll response to a Gaussian distributed input. The histogram was tested for normality using the Kolmogorov-Smirnov test (given in Appendix E) and was determined not to be normally distributed. This result was obtained for all the subjects tested.

Discussion of Results. The fact that a normally distributed position input did not produce a normally distributed counterroll response appears to be evidence that the system is not linear. It was mentioned that the angular acceleration and the rectilinear acceleration in the radial direction appear to produce effects on the counterroll response. Therefore, counterroll becomes a function of three random variables rather than one. The angular acceleration will also be normally distributed since it is formed by a linear operation on the position variable. The radially directed acceleration will not be normally distributed. The random variable, $\overline{a}_r$, representing the radially directed acceleration, is given by the following expression:

$$\overline{a_r} = R\overline{\omega}^2 \qquad (6\text{-}3)$$

where,

R = radius

$\overline{\omega}$ = angular velocity random variable.

The angular velocity, $\overline{\omega}$, will be normally distributed since it results from a linear operation on the position. It can be shown that the probability density function of $\overline{a}_r$ is given by:

$$p(a_r) = \frac{1}{\sqrt{2\pi R a_r}} e^{-a_r/2R\sigma^2} U(a_r) \qquad \text{(Ref 11)} \qquad (6\text{-}4)$$

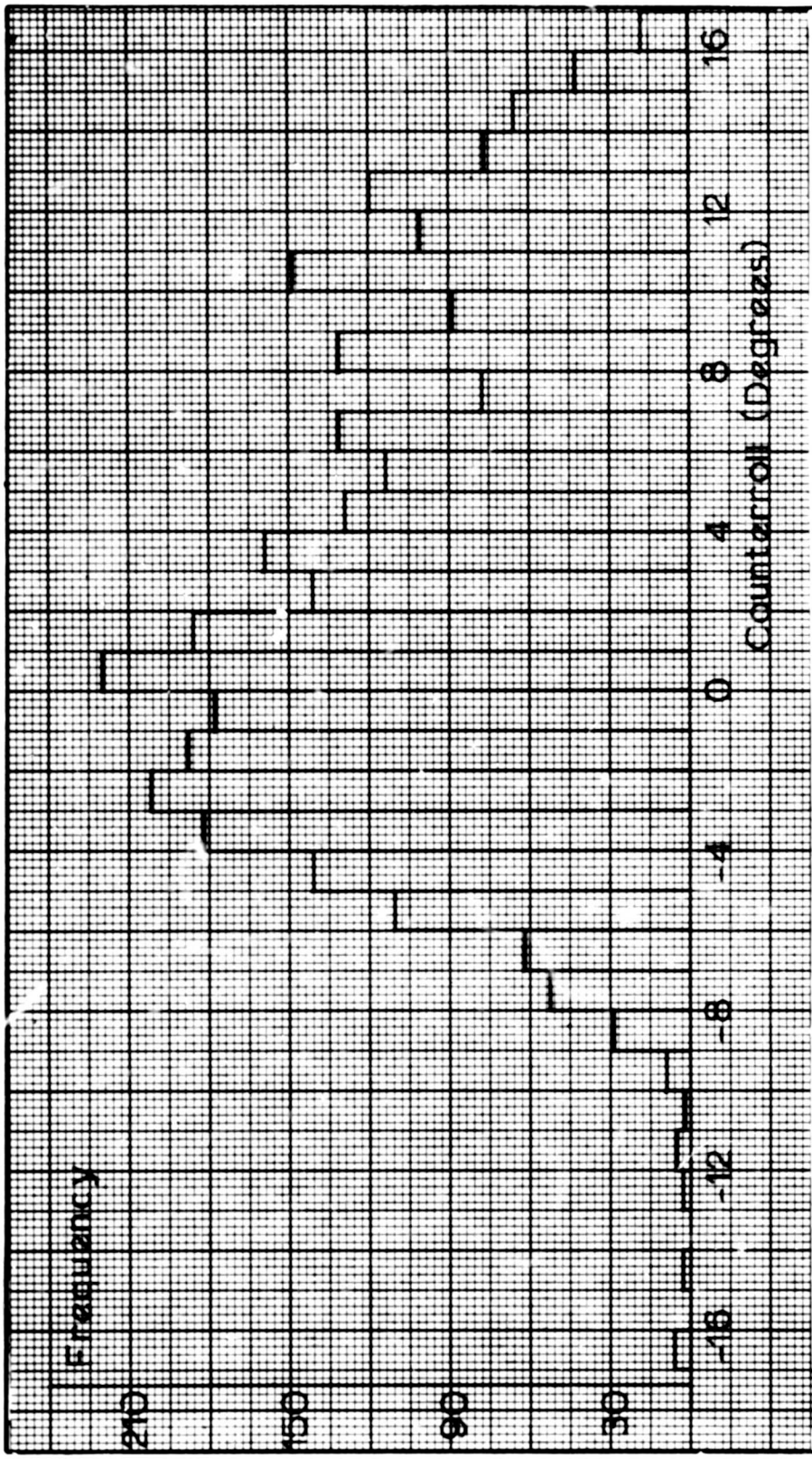

Histogram of Counterroll Response to a Gaussian Noise Position Input
Fig. 6-23

where,

σ^2 = variance of ω

$u(a_r)$ = unit step function

R = radius.

Therefore, if the two accelerations are assumed to be system inputs, the counterroll response becomes a function of three inputs (the position and angular acceleration which are normally distributed and the radial acceleration which is not normally distributed). With these inputs, the response, in general, would not be Gaussian. Therefore, the fact that the output is not normally distributed is not conclusive evidence that the system is nonlinear.

VII. Summary

A summary of the conclusions reached in Section VI are given below:

(1) Peak-to-peak counterroll response decreases with increasing rates of rotation for constant angular velocity inputs

(2) Bias drifts can be separated from the counterroll response by the use of power spectral density functions

(3) Counterroll suppression can occur even though the subject cannot predict the input

(4) Peak-to-peak counterroll response increases for increasing pendular motion frequencies between 0.2 hz and 0.5 hz

(5) Angular acceleration and radial acceleration appear to affect counterroll response.

VIII. Recommendations

This study is primarily concerned with developing equipment and techniques for extending the available input stimuli to the vestibular system. The results of the experiments indicate that additional investigations need to be conducted before a model of the vestibular system can be formulated.

It is recommended that investigations be conducted to determine the effect of the semicircular canals on counterroll. This investigation would involve testing subjects with defective otolith organs. A study of this type could provide information concerning the threshold level of the semicircular canals.

It is further recommended that subjects be tested which have been rendered bilaterally labyrinth defective. This investigation would yield information on the effects of proprioceptors on counterroll. Tests on bilaterally labyrinth defective humans (Ref 6) have resulted in small counterroll responses or none at all. Tests of this nature on Rhesus monkeys could help to justify the use of the data collected from them to model the human vestibular system.

A third recommendation is to further investigate the effects of angular acceleration on subjects with intact labyrinths. This investigation would require input stimuli with controlled acceleration profiles. A particular input stimuli which would be useful in this investigation is a ramp angular velocity input (constant angular acceleration). It is recommended that the instrumentation system be modified for this investigation to include the measurement of angular acceleration.

Bibliography

1. Alley, C. L. and K. W. Atwood. Electronic Engineering. New York: John Wiley and Sons, Inc., 1962.

2. Bendat, J. S. and A. G. Piersol. Measurement and Analysis of Random Data. New York: John Wiley and Sons, Inc., 1966.

3. Beyer, W. H. Handbook of Tables for Probability and Statistics. Cleveland, Ohio: Chemical Rubber Company, 1966.

4. Flaherty, R. J. and G. K. Pritchard. "Counterrolling of the Human Eye." Master's Thesis, Air Force Institute of Technology, WPAFB, Ohio, 1964.

5. Hannen, R. A., et al. "Experimental Determination of a Portion of the Human Vestibular System Response Through Measurement of Eyeball Counterroll." Bio-Medical Engineering, 13: 65-70 (April 1966).

6. Hartzler, V. L. and P. A. Roccaforte. "Experimental Determination of Human Vestibular System Response Through Measurement of Eyeball Counterroll." Master's Thesis, Air Force Institute of Technology, WPAFB, Ohio, 1965.

7. LaJeunesse, D. J., et al. SYSTRAN (Systems Analysis Translator): A Digital Computer Program. AMRL-TR-65-133. WPAFB, Ohio: Aerospace Medical Research Laboratories, Aerospace Medical Division, Air Force Systems Command, July 1965.

8. Lessard, C. S. and J. R. Gnuse. "A Study of the Primate Vestibular System." Master's Thesis, Air Force Institute of Technology, WPAFB, Ohio, 1966.

9. Miller, E. F. II. Counterrolling of the Human Eyes Produced by Head Tilt with Respect to Gravity. Research Report. Pensacola, Fla.: U. S. Naval Aviation Medical Center, 1962.

10. Netter, F. H. Nervous System: I. The Ciba Collection of Medical Illustrations. Summit, New Jersey: CIBA Pharmaceutical Co., 1964.

11. Papoulis, A. Probability, Random Variables, and Stochastic Processes. New York: McGraw-Hill Book Co., 1965.

12. Ruch, T. C. and H. D. Patton. Physiology and Biophysics (Nineteenth Edition). Philadelphia, Penn.: W. B. Saunders Co., 1965.

13. Taber, C. W. Cyclopedic Medical Dictionary (Tenth Edition). Philadelphia, Penn.: F. A. Davis Co., 1965.

14. Weis, E. B. and D. J. LaJeunesse. SYSTRAN (Systems Analysis Translator): A Digital Computer Program, Supplement One. AMRL-TR-65-133 (Sup 1). WPAFB, Ohio: Aerospace Medical Research Laboratories, Aerospace Medical Division, Air Force Systems Command, March 1966.

Appendix A

Summary of Results of Previous Investigations

Dr. Earl F. Miller. Dr. Miller has proposed a theory to explain the function of the otolith organs. He contends that the utricles and saccules are gravity detectors that are stimulated only when a force tends to shear the macular plane across the sensor hair cells in a direction toward the median sagittal plane. This has been supported by reports that counterrolling in unilaterally defective labyrinths occurs only when the head is tilted toward the defective side. Figure A-1 is a schematic of the topography of the utricular and succular maculae. Analysis of this diagram shows that six possible inputs to the system can occur in various combinations dependent upon the angle at which the head is tilted with respect to the vertical. Dr. Miller obtained data to verify his theory by static tests on human subjects. He pointed out that other investigators contend that the sensors of the otolith system are bidirectional rather than unidirectional and the system actually operates in a differential mode. A complete discussion of the theory including the mathematics to support the theory based upon the static test data obtained can be found in Reference 9.

Flaherty and Pritchard. The following results were reported by Flaherty and Pritchard based upon data obtained from human subjects under static and dynamic conditions:

(a) The counterrolling index (one half the peak-to-peak counterrolling amplitude in minutes of arc) decreases with increasing rates of rotation.

(b) The maximum slope (counterrolling in degrees versus head tilt in degrees near the upright body position) decreases with increasing rates of rotation.

(c) There is an increasing positive phase shift in the clockwise direction associated with the response for increasing rates of rotation.

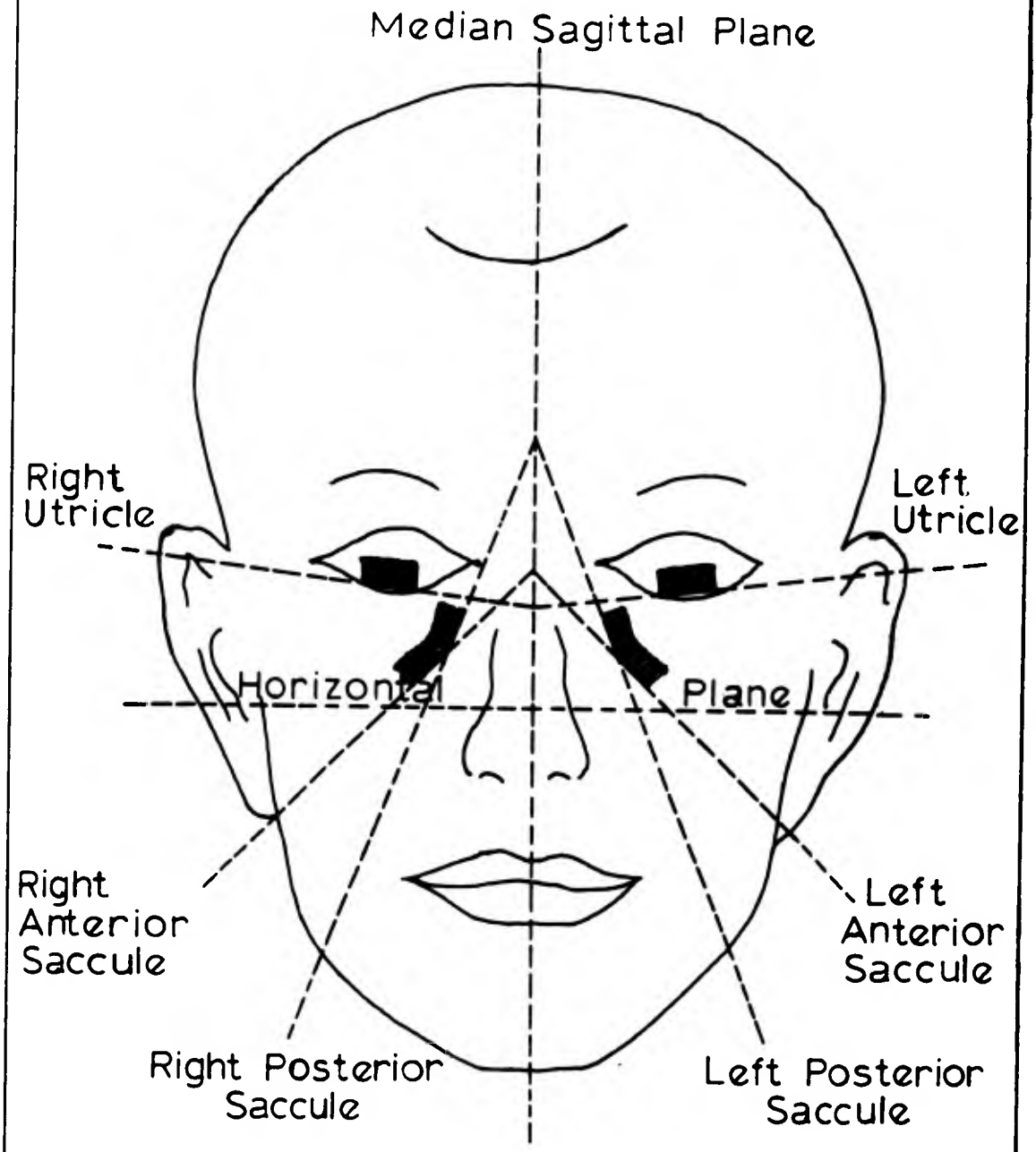

Schematic Drawing (Frontal Section) of the Topography of the Utricular and Saccular Macula (From Ref 9) Fig. A-1

(d) There is an increasing negative phase shift in the counterclockwise direction associated with the response for increasing rates of rotation.

(e) There is generally a small, one to two degree, amplitude shift associated with the dynamic counterrolling response.

(f) The measured counterrolling response for static positions of lateral head (body) tilt were similar to responses obtained by other investigators.

A detailed discussion of the above results can be found in Reference 4.

Hartzler and Roccaforte. The following results were reported by Hartzler and Roccaforte based upon data obtained from human subjects under static and dynamic conditions:

(a) The peaks of the static response occurred when the subject was tilted at an angle of 60°-70° from the vertical in either direction.

(b) The static counterroll response was an approximate linear function of head tilt in the range of 320°-040° and in the range of 140°-220°.

(c) As the angular velocity was increased, the response tended to approach an approximate sinusoid. For most subjects, this occurred around 20 rpm.

(d) The peak-to-peak magnitude of the dynamic response was approximately constant in the range ±15 rpm and was attenuated markedly at higher velocities.

(e) The mean value of the dynamic response was generally not zero. The magnitude of deviation from zero (bias) varied considerably between subjects and between subsequent runs with the same subject. The bias was variable in magnitude and appeared to vary directly with velocity.

A detailed discussion of the above results can be found in Reference 6.

Lessard and Gnuse. The following results were reported by Lessard and Gnuse based upon data obtained from Rhesus monkeys and a direct readout scheme to obtain counterroll:

(a) Transient responses to step angular velocities decrease after the rotating apparatus attains constant speed.

(b) Two consecutive cycles of dynamic counterrolling responses of the Rhesus monkey are qualitatively similar to the results from human subjects.

(c) The amplitude of the counterrolling response and the maximum slope decreased for increases in rates of rotation.

(d) Amplitude shifts, bias drifts, and variations in the magnitude of counterrolling response were observed for consecutive revolutions after more than 30 seconds duration at constant rates of rotation.

(e) Adaptation to consecutive stimuli and suppression of the vestibular response were observed.

(f) Sedated subjects demonstrated a reduced counterrolling approximating a square wave form.

A detailed discussion of the above results can be found in Reference 8.

Appendix B

Equipment List

Rotation System

Gear Assembly:	General Railway Signal Company Model W8258225-G5 Reduction Gear Ratio of 66:1
Motor:	US Army Air Force Direct Current Turret Drive Motor Electric Vacuum Cleaner Co., Inc. 1/2 hp 4,000 rpm Field 27v, 2.3 amps Armature 60v, 8.3 amps Model 5BA50LJ2A
Bearings:	Dodge Company Type E, Pillow Block, 1-1/2 in. diameter
Sliprings:	EE Lab Made Eight Pairs
Low Frequency Function Generator:	Wavetek Inc. Voltage Controlled Generator Model 111 Frequency Range 0.003 to 1 MHz
Band Pass Filter:	Krohn-Hite Instrument Co. Ultra-Low Frequency Band Pass Filter Model 330-A
Gaussian Noise Generator:	Elgenco Incorporated Gaussian Noise Generator Model 311A
Direct Coupled Amplifier	Electro Instruments, Inc. DC Amplifier Model A20B-3
SCR Power Amplifier	Designed and constructed as a part of this study; see Appendix C.

Instrumentation

Linear Transformer:	Clifton Precision Products Co., Inc. Linear Transformer Input 26v, 400 Hz, Single Phase Output 0.4 volts per degree Type LTC-10-AS-4
D-C Power Supply:	Electronic Research Associates, Inc. Transistor Power Supply Model 210 A-C to D-C Voltage Regulated Power Input 110v, 60 Hz Rated Output 0-100v, 100 ma d-c
Tachometer:	Electric Indicator Company, Inc. Elinco D-C Generator Permanent Magnet 4.5 volts per 100 rpm Type 55 Style FB
Shaft Position:	Fairchild Potentiometer 30,000 ohm, one turn (360°)
Restraining Chair:	Lab Made Fiberglass
Plastic Contact Lens:	Medical Contact Lens Service 52.0 Dioptics Plano Power
Recorders:	Dynagraph Six Channels Type MC Recorder Magnetic Tape Recorder Reproducer Seven Channels Ampex Model SP-300

Exterior Power Sources

120 volts; 400 Hz

115 volts; 60 Hz

26 volts (regulated); 400 Hz

28 volts; Direct Current

Appendix C

Wiring Diagram

A wiring diagram of the position/velocity control system is given in Figure C-1.

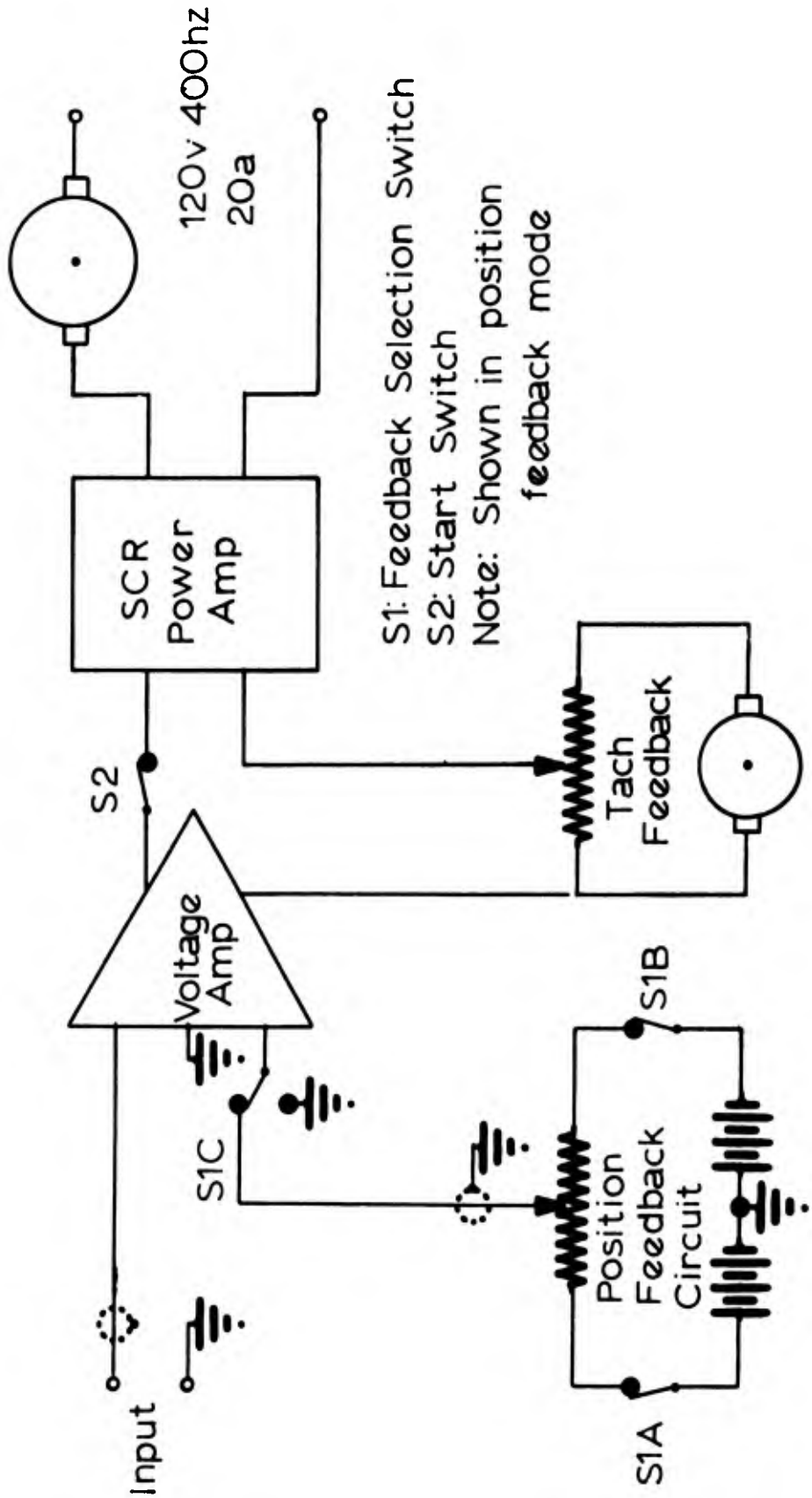

Control System Wiring Diagram
Fig. C-1

Appendix D

Silicon Controlled Rectifier Power Amplifier

A schematic diagram and a list of components of the silicon controlled rectifier power amplifier is shown in Figure D-1. The circuit converts a 400 hz power input voltage to a d-c output voltage. The magnitude and polarity of the d-c output voltage is controlled by the magnitude and polarity of the signal input voltage to the amplifier. The circuit may be divided into five subassemblies, as indicated by the block diagram shown in Figure D-2.

Phase-Control Subassembly

The phase-control subassembly consists of two silicon controlled rectifiers (CR1, CR2) and two power diodes (D1, D2). If a pulse is applied to the trigger terminal of CR1 during the positive half cycle of the 400 hz input voltage, CR1 will go into conduction allowing positive current to flow through the path consisting of the load, CR1, and diode D1. For the purpose of this discussion, positive current is defined as indicated by the arrow in Figure D-1. When the positive half cycle of the input voltage reaches zero, CR1 will turn off, and the load current will become zero. Unless another pulse is applied to the trigger of CR1 during subsequent positive half cycles of the input voltage, CR1 will remain in the non-conducting state, and the load current will remain zero. The magnitude of the average load current is a function of the conduction angle of CR1. For example, if the trigger pulse is applied at the beginning of the positive half cycle of the 400 hz input voltage, the conduction angle will be 180° and the average d-c load current, I_L, is given by:

$$I_L = \left[\frac{1}{R_L}\right] \frac{E_M}{\pi} \int_0^{\pi} \sin\theta \, d\theta$$

$$= 0.637 \frac{E_M}{\pi} \qquad \text{(D-1)}$$

R_L = load resistance

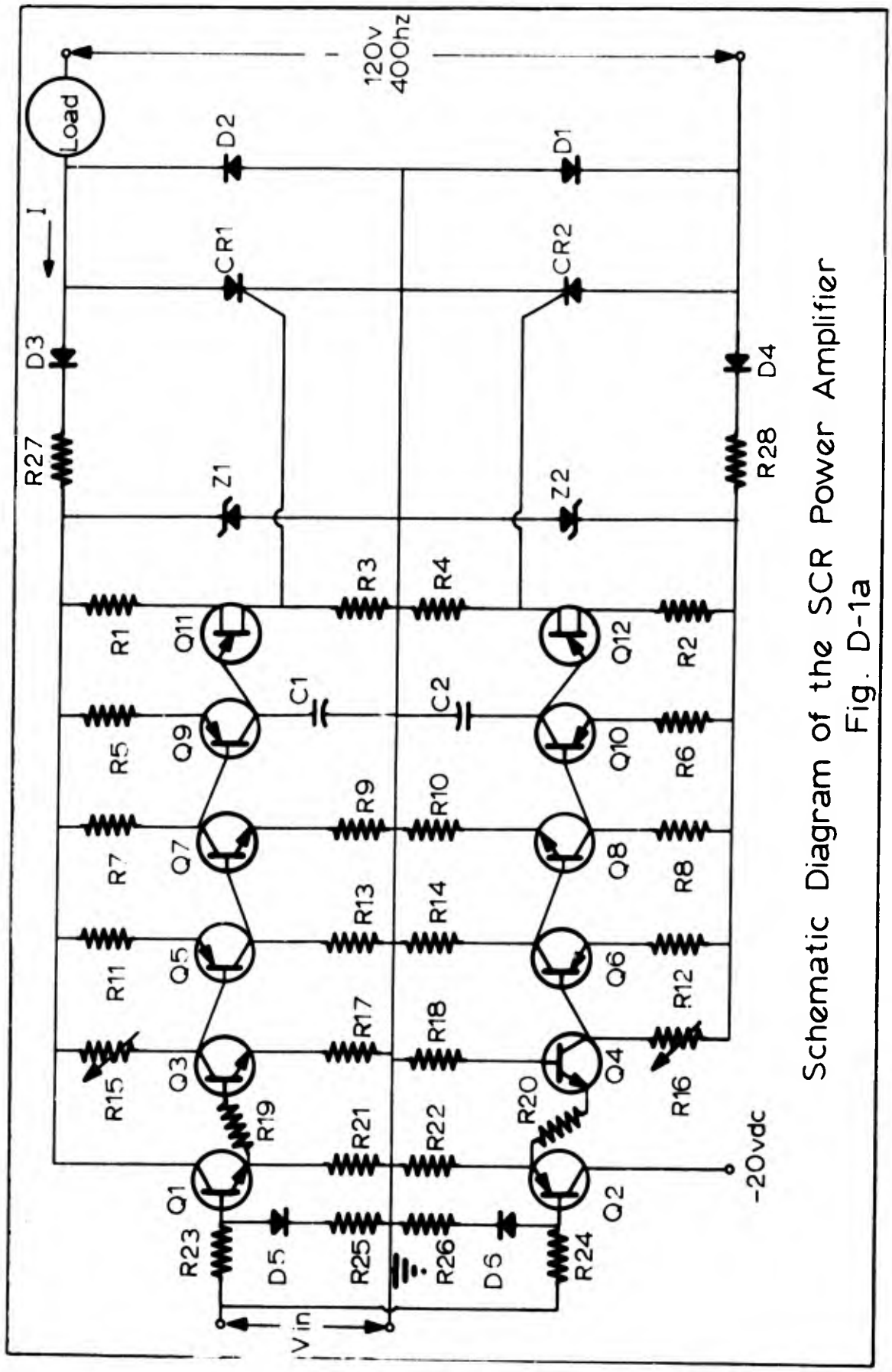

Schematic Diagram of the SCR Power Amplifier
Fig. D-1a

Identification	Element
Q1, Q3, Q4, Q7, Q8	2N167
Q2, Q5, Q6, Q9, Q10	SK3004
Q11, Q22	2N1671
D1, D2	1N1194
D3, D4	1N315
D5, D6	122358A
Z1, Z2	1N3027B
CR1, CR2	2N685
R1, R2, R11, R12, R17, R18, R19, R20	100 ohm 1/2 watt
R3, R4	51 ohm 1/2 watt
R7, R8	510 ohm 1/2 watt
R5, R6, R9, R10, R13, R14	1 kilohm 1/2 watt
R27, R28	3 kilohm 5 watt
R23, R24	4.7 kilohm 1/2 watt
R21, R22	10 kilohm 1/2 watt
R15, R16	10 kilohm Pots
R25	510 ohm 1/2 watt
R26	100 ohm 1/2 watt
C1, C2	0.1 uf

List of Components
Fig. D-1b

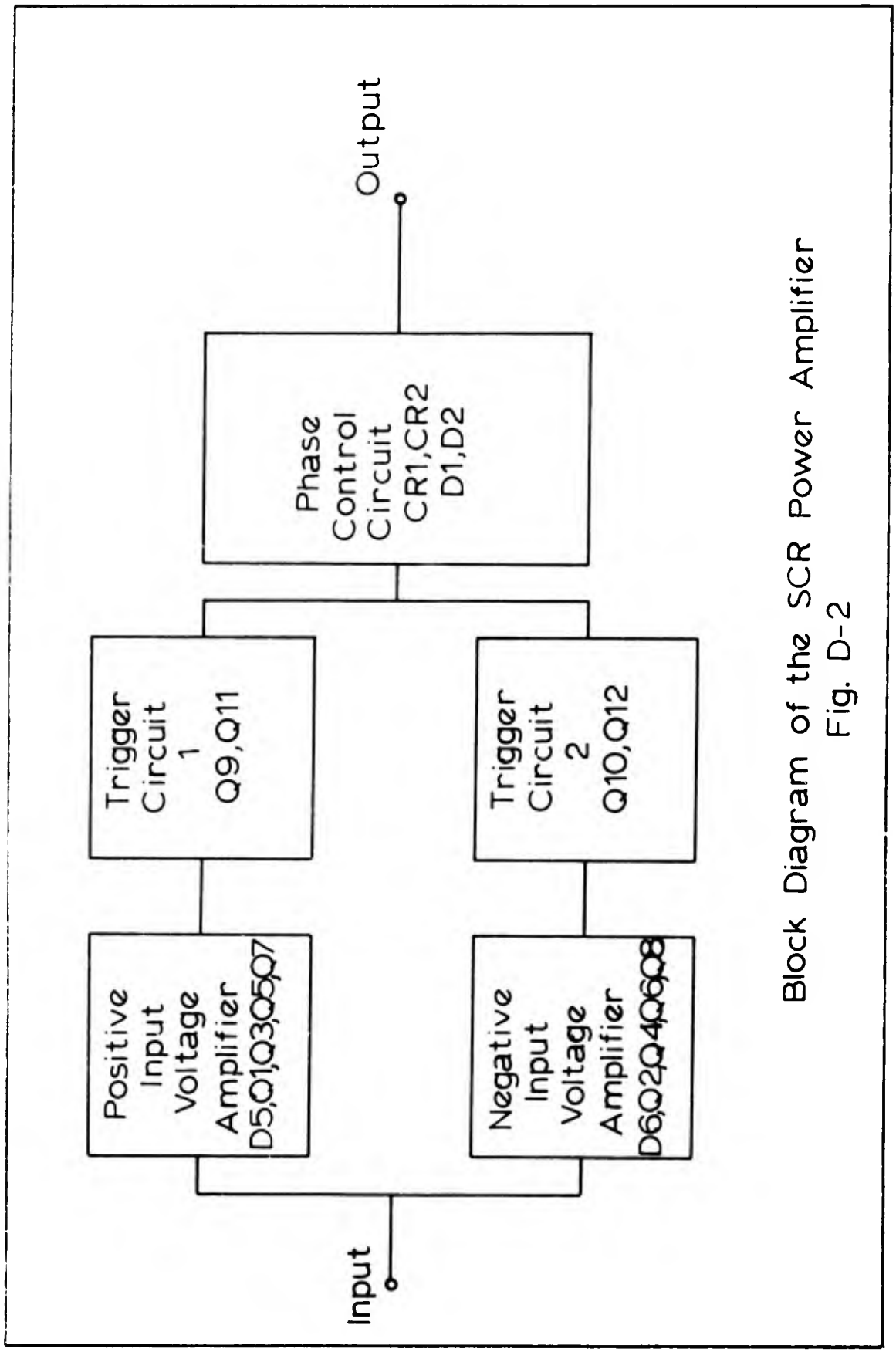

Block Diagram of the SCR Power Amplifier
Fig. D-2

E_M = peak value of the 400 hz input voltage.

In general, the average d-c load current depends on the angle the a-c input voltage has reached when the trigger pulse is applied. A general expression for the load current is given by:

$$I_L = \left[\frac{1}{R_L}\right] \frac{E_M}{\Pi} \int_{\theta_o}^{\Pi} \sin\theta \, d\theta \qquad \text{(D-2)}$$

θ_o = angle of 400 hz input voltage when trigger pulse is applied.

Therefore, the positive load current can be varied by varying the point that the trigger occurs during the positive half cycle of the a-c input voltage. Figure D-3 illustrates the relationship between the input voltage, the trigger pulse, and the load current.

If a pulse is applied to the trigger terminal of CR2 during a negative half cycle of the a-c input voltage, a negative load current will flow through the path consisting of the load, CR2, and diode D2. The magnitude of the negative load current is controlled in exactly the same way as the positive load current.

The Trigger-Circuit Subassemblies

The circuit configuration and the operation of the two circuits (1 and 2) are identical. The only difference in the two circuits is that trigger circuit 1 provides trigger pulses to CR1, and trigger circuit 2 provides trigger pulses to CR2. Therefore, only the operation of trigger circuit 1 will be discussed.

The basis for the trigger circuit is the unijunction transistor Q11. The operation of a unijunction transistor (shown schematically in Figure D-4) is such that when the emmitter voltage is less than a certain voltage, called the peak point voltage, the emitter to base 1 resistance is high, and therefore the emitter current is approximately zero. When the emitter voltage reaches the peak point voltage, the emitter to base resistance drops to a low value and the emitter base current increases. The peak point voltage is a function of the device characteristics and the base to base voltage V_{BB}. The emitter voltage

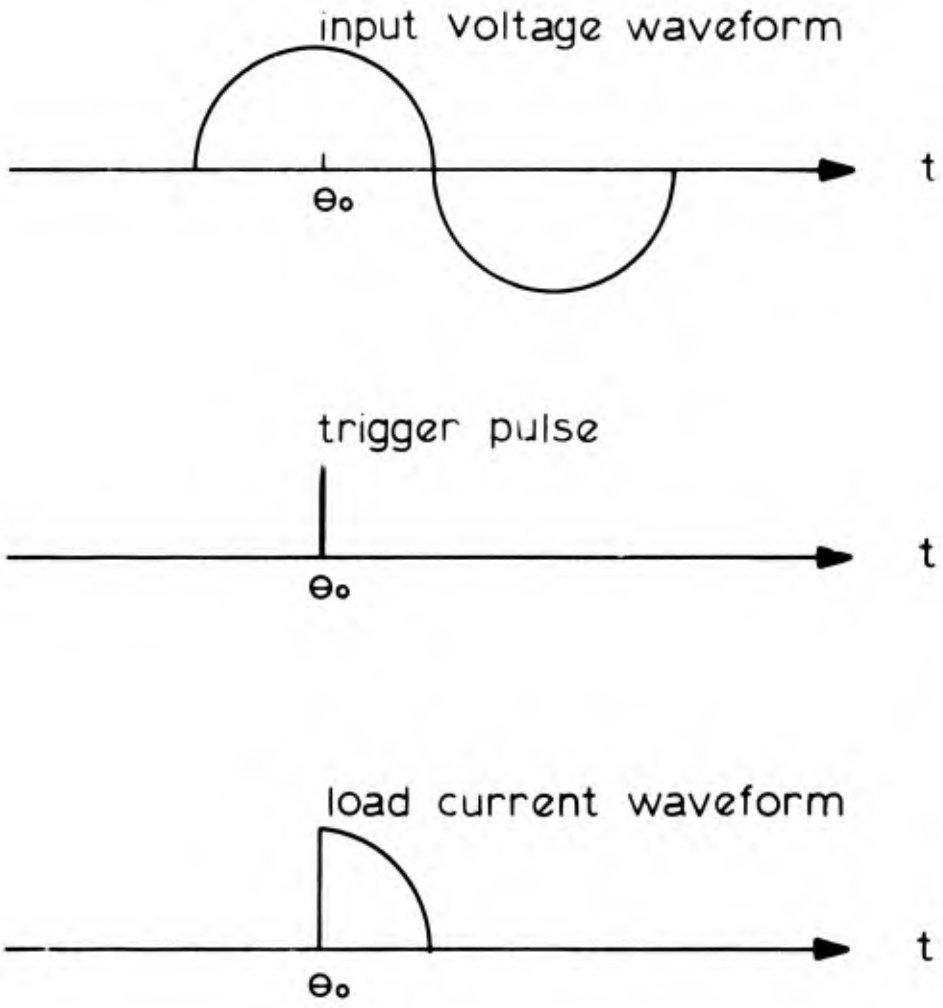

Relationship Between the Input Voltage, Trigger Pulse and Load Current
Fig. D-3

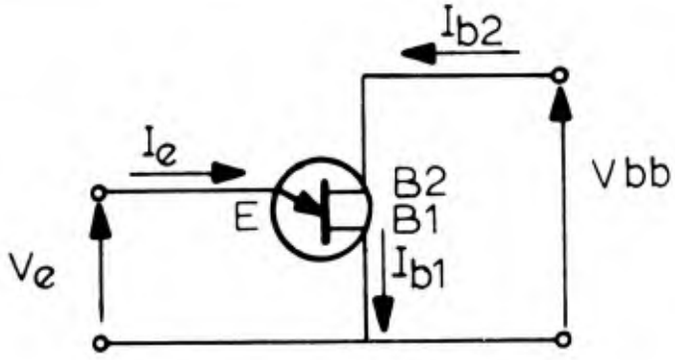

Unijunction Transistor
Fig. D-4

in the trigger circuit is equal to the voltage across the capacitor C1. When the voltage across C1 is less than the peak point voltage of Q11, the emitter to base 1 current is low (on the order of microamps); therefore the voltage across the base 1 resistor, R3, is low. When the capacitor charges to a voltage equal to the peak point voltage, the emitter to base 1 resistance drops and the capacitor quickly discharges through the emitter-base junction of the unijunction and the resistor R3. The discharge current produces a pulse of voltage across R3 which is the trigger voltage to the silicon controlled rectifier, CR1. Transistor Q9 is used as a constant current generator to supply charging current to C1. If Q9 is turned on, C1 charges linearly toward the supply voltage until the peak point voltage of the unijunction is reached, then is quickly discharged. The rate at which C1 is charged depends on the input voltage to Q9. The supply voltage to the trigger circuit (and to the other stages as well) is provided by the 400 hz input which is rectified by diode D3 and regulated by zener diode Z1. This configuration provides synchronization of the trigger circuit to the 400 hz input voltage. For example, as the positive half cycle of the 400 hz input voltage begins, the supply voltage to the trigger circuit is zero as shown in Figure D-5.

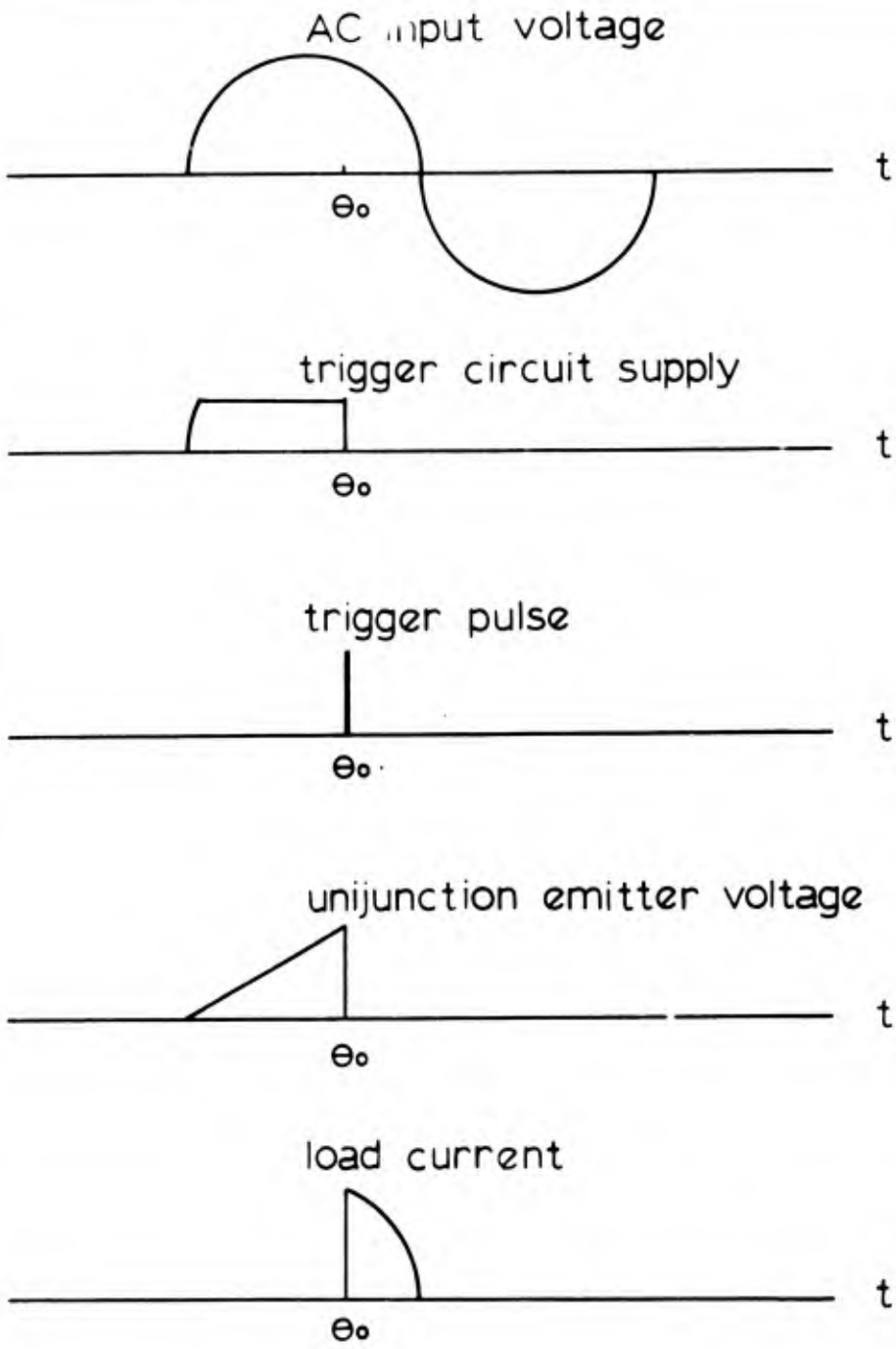

Trigger Circuit Operation
Fig. D-5

As the a-c input increases, the supply voltage increases to the zener voltage of Z1. If Q9 is turned on, capacitor C1 charges toward the supply voltage. If the charging rate is fast enough (determined by the forward bias on Q9), the capacitor voltage will reach the peak point voltage of Q11 before the end of the positive half cycle of the a-c input. A trigger pulse will be produced, CR1 will turn on, and load current will flow. When CR1 turns on it shorts the trigger circuit supply voltage which prevents any further trigger pulses from developing during that particular positive half cycle of the a-c input. By varying the forward bias on Q9 the trigger pulse can be made to occur early or late during the positive half cycle of the a-c input; thus varying the conduction angle of CR1. In the particular circuit which was constructed, the conduction angle could be varied from 0^{o} to approximately 120^{o}. The amplitude of the trigger voltage which is developed across R3 is approximately 4 volts, which is sufficient to turn on the silicon controlled rectifier CR1.

Voltage Amplifier Subassemblies

The two voltage amplifier subassemblies are identical in operation with one exception. The positive input voltage amplifier only amplifies positive signal inputs and ignores negative inputs as opposed to the negative input voltage which amplifies negative signal inputs and ignores positive inputs. The output from the positive input amplifier is the input to trigger circuit 1 which provides the trigger pulses to control the positive load current. Likewise, the negative input amplifier provides the input to trigger circuit 2 which controls the negative load current.

The positive input voltage amplifier consisting of Q1, Q3, Q5, and Q7 is simply a conventional direct-coupled amplifier. The circuit was designed such that no bias voltages other than the supply voltage are needed. This fact eliminates the problems associated with bias drifts which are normally encountered with direct coupled amplifiers. The circuitry which was used in the amplifiers is common and, therefore, a detailed analysis of the design will

not be given. Reference 1 contains a complete discussion of solid state direct coupled amplifiers. The input stages to the amplifiers are the only critical stages. Since no bias voltages are used, it is necessary that the input stages have high gain for small inputs. The transistors which were used had current bains of approximately 30 for inputs as low as 10 microamps. The input stage to the positive input amplifier is a NPN transistor, and therefore only amplifies positive inputs since there is no bias voltage used. Likewise, the input stage to the negative input amplifier is a PNP transistor, and therefore only amplifies negative input signals.

One of the undesirable qualities of phase control circuits is that the output current does not vary linearly as a function of the conduction angle of the silicon controlled rectifier. This is because the output current varies in accordance to the integral given in equation D-2. To compensate for the nonlinearity, the two diode-resistance networks consisting of D5, R23, R25, and D6, R24, R26 were placed in the two input voltage amplifiers as shown in Figure D-1. The operation of the compensation circuits is based on the facts that practical diodes do not go into conduction until a small forward bias is applied (approximately 0.6 volts for silicon diodes) and that the forward resistance of practical diodes does not equal zero. The voltage-current transfer curve of an uncompensated power amplifier, the voltage transfer curve of a compensation circuit, and the resulting voltage-current transfer curve of the compensated circuit are illustrated in Figure D-6.

Complete Circuit Operation

Figure D-7 is an oscilloscope photograph of the output voltage waveforms of the complete circuit with a 100 ohm resistive load. The upper photograph shows the output voltage for both a positive and negative signal input of Q5 volts d-c. The lower photograph shows the output voltage for both a positive and negative signal input of 2 volts d-c. With a low frequency a-c input the operation of the circuit is exactly as with a d-c input except that the magnitude

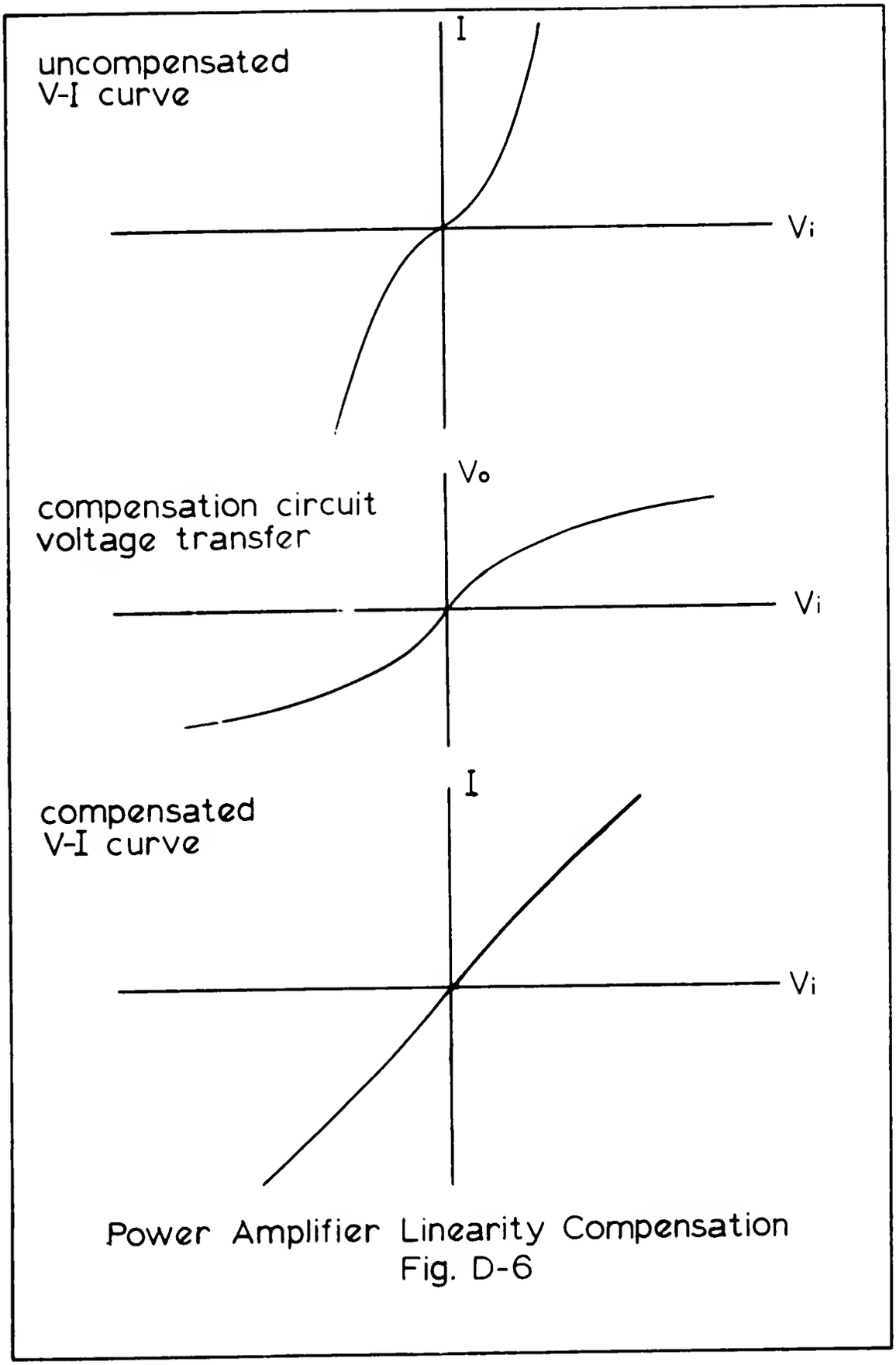

Power Amplifier Linearity Compensation
Fig. D-6

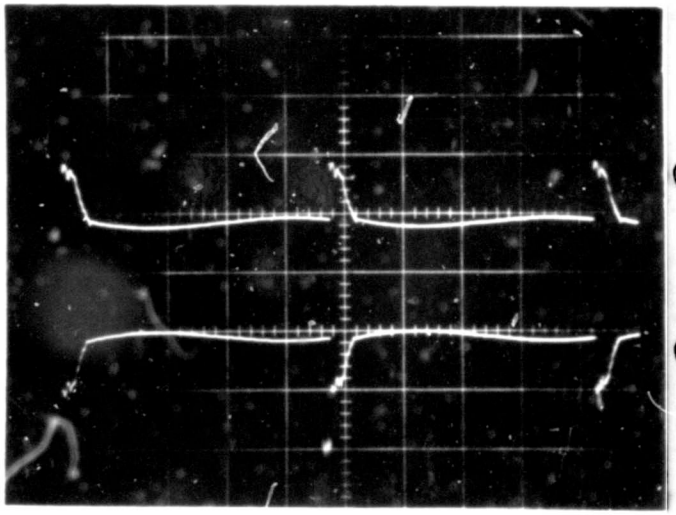

response to a 0.5 volt positive input

response to a 0.5 volt negative input

response to a 2 volt positive input

response to a 2 volt negative input

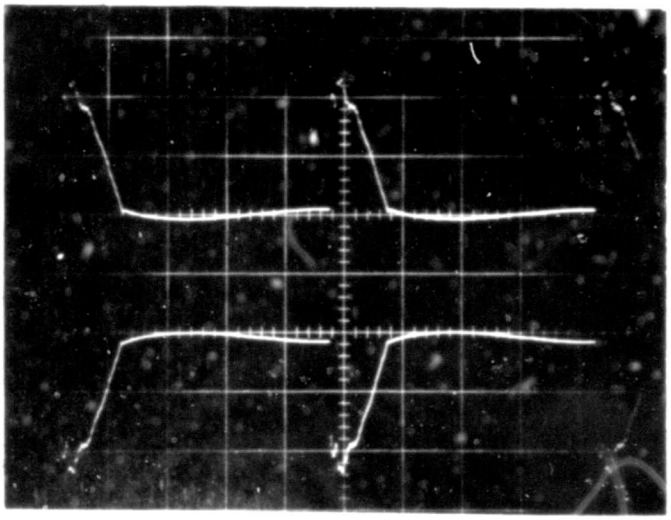

Power Amplifier Output Waveforms
Fig. D-7

and polarity of the output voltage varies as the magnitude and polarity of the input.

A summary of the circuit specifications is as follows:

Voltage Gain	20
Power Gain (into 100 ohm resistive load)	20,000
Input Impedance	5,000 ohms
Output Impedance	< 1 ohm
Maximum Output Current	20 amps
Maximum Output Voltage	50 volts

Figure D-8 illustrates the construction of the completed circuit.

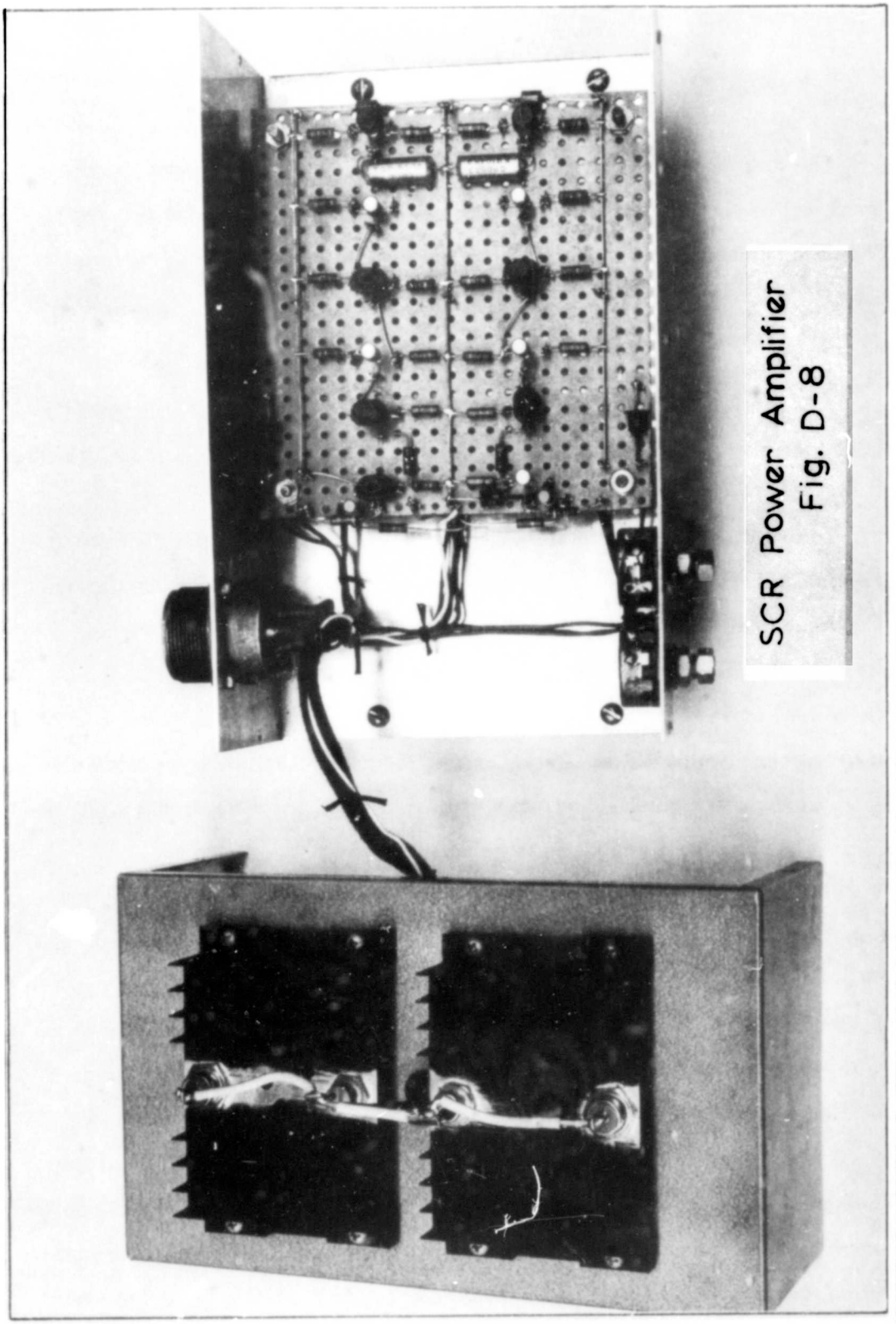

SCR Power Amplifier
Fig. D-8

Appendix E

Kolmogorov-Smirnov Test

The Kolmogorov-Smirnov statistic (Ref 3: 176-178) is a means of testing an experimentally determined probability distribution function for "goodness of fit" to an assumed distribution function. The test is based on the statistic:

$$Dn = \max [F_n(x) - F(x)] \qquad (E-1)$$

where

$F_n(x)$ = the distribution function being tested

$F(x)$ = the assumed distribution function

To use the test, it is necessary to graph both the distribution function being tested and the assumed distribution on the same piece of graph paper. The value of D_n is then found from the graph (D_n = the largest discrepancy in the ordinate values of the tested distribution and the assumed distribution). The value obtained for D_n can then be compared with the values given in a table of acceptance limits for the Kolmogorov-Smirnov test. If the computed value of D_n exceeds that given in the table, the hypothesis that the tested distribution equals the assumed distribution is rejected.

The hypothesis that the density function shown in Figure 3-8 (chair position with a Gaussian input) was a normal density function with zero mean and variance equal to one was tested using the Kolmogorov-Smirnov test. The resulting graph is shown in Figure E-1. The value found for D_n was determined to be less than the 20% acceptance limit; therefore, the hypothesis that the density function was normal was accepted at the 20% significance level.

The probability density function of counterroll with a normally distributed chair position input (Fig. 6-28) was also tested for normality. The distribution function of the counterroll is plotted in Figure E-2 along with a normal distribution function whose mean is two and variance is 64. The value determined

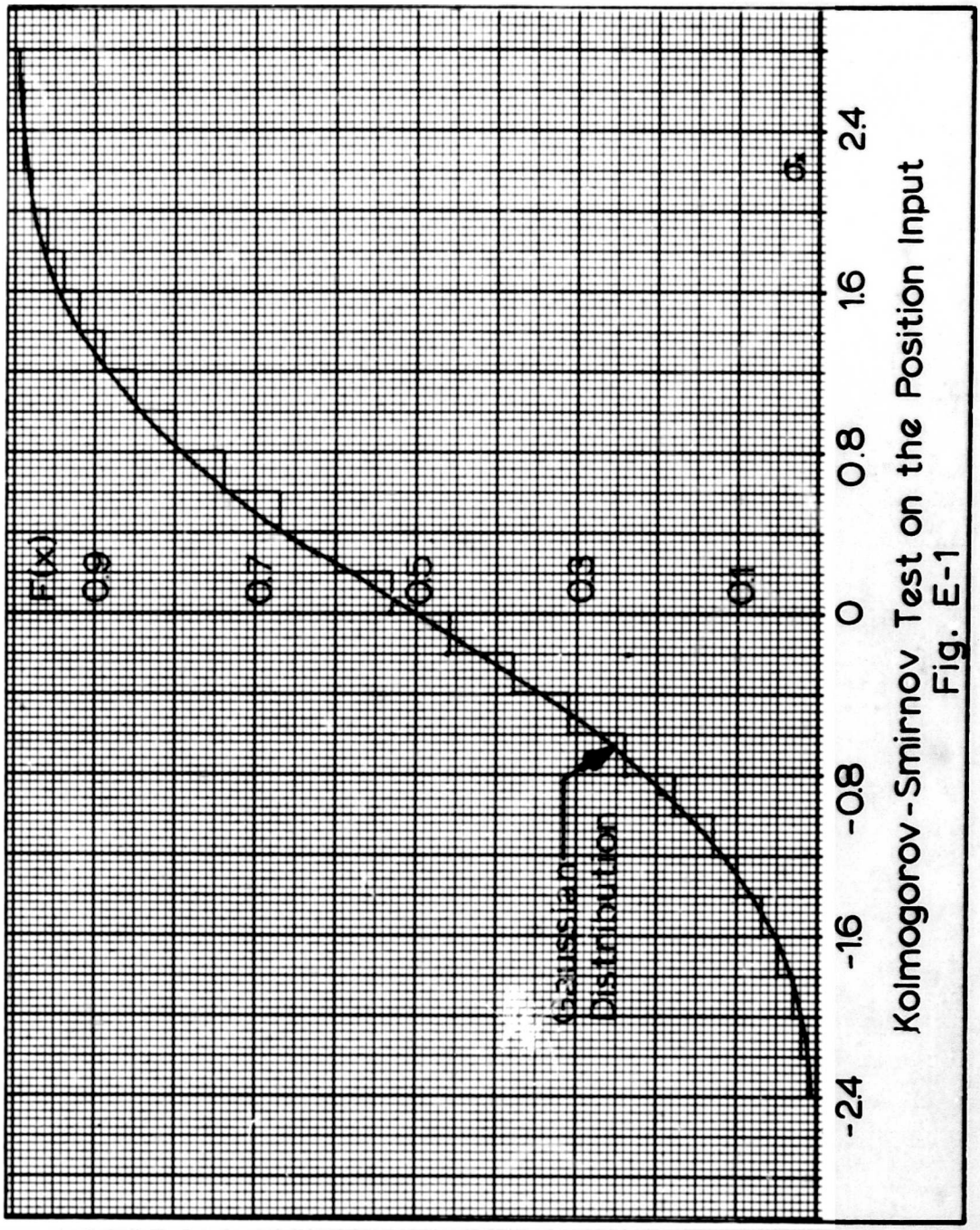

Kolmogorov-Smirnov Test on the Position Input
Fig. E-1

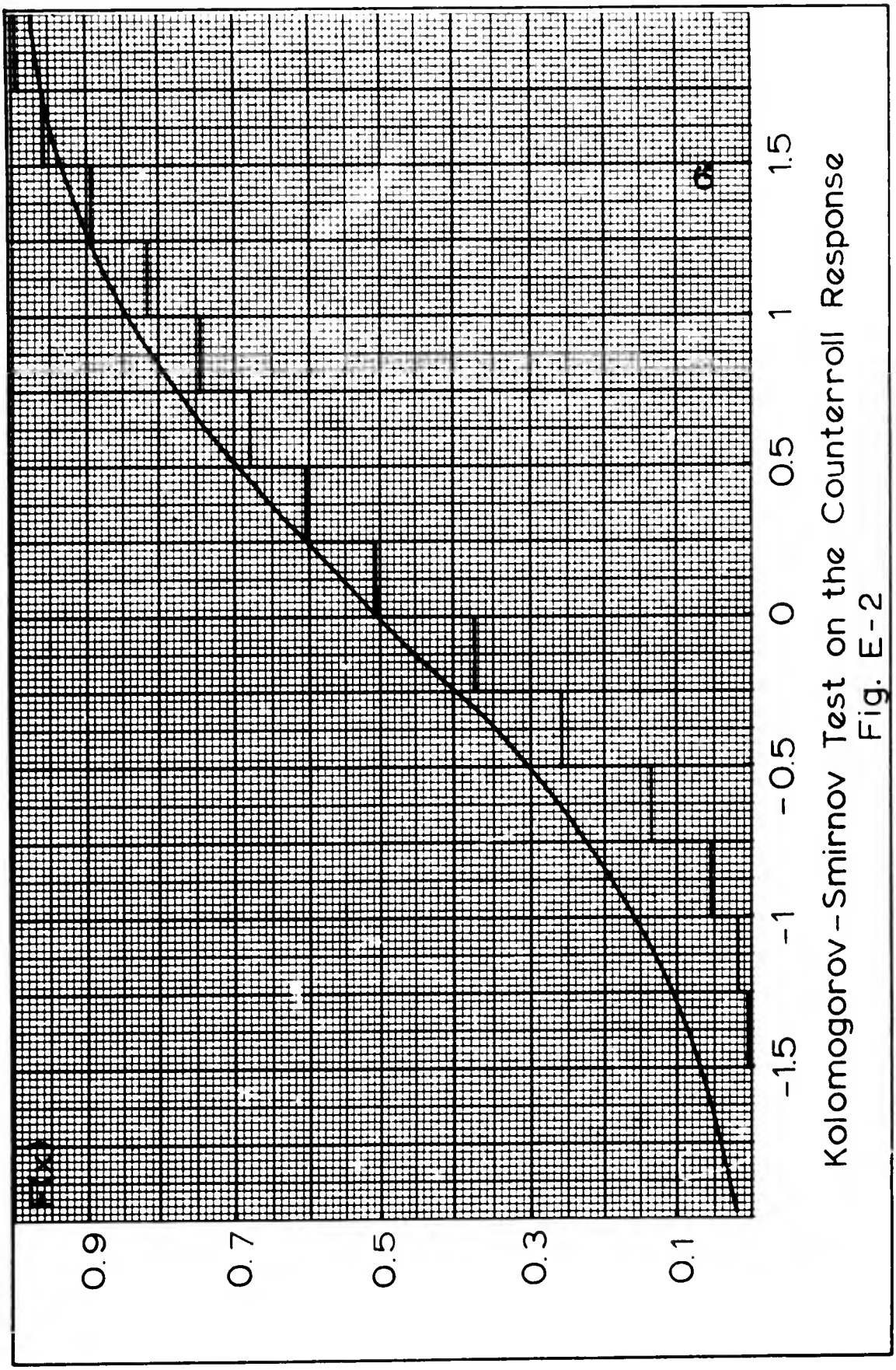

Kolomogorov-Smirnov Test on the Counterroll Response
Fig. E-2

for D_n was found to exceed the acceptance limit. Therefore, the hypothesis that the distribution function is equal to the assumed distribution was rejected at the 1% level of significance (i.e. the probability that the tested distribution is normal even though the test failed equals 0.01).

Appendix F

Control Decks for the Systems Analysis Translator Program

Examples of control decks to provide the necessary instructions to the Systems Analysis Translator Program for calculation of correlation functions, power spectral density functions, and probability density functions are given in this appendix.

```
*       JOB BIO SYSTEM ANALYSIS CHASEN GUTHRIE THESIS DATA
*       BEGIN TIME SYSTEM
*       DELTAT, 0.1,,SAMPLING RATE
*       FREQUENCY,COMPUTE/3,BASE/0.1,NFREQ/100,ENDFREQ/1
C       TIME DOMAIN CORRELATION
*       BEGIN CORRELATION SYSTEM
*       CRLOAD,TEST/1, CHANNELS/(2,3),CALS/(1,1),NORMS/(0,0),SAMPLE/1,IZERO/1,
        TMAX/500 ,TAUZERO/0,NTAU/100,DELTATAU/3
*       COMPUTE,ID/1
*       CORRELATION FUNCTIONS,TAU(1),
        PHI(2,2),OUTPUT(2),LABELED$AUTOCOR OF INPUT$,
        PHI(2,3),OUTPUT(4),LABELED$CROSSCOR OF IN OUT$,
        PHI(3,2),OUTPUT(1),LABELED$CROSSCOR OF OUT IN$,
        TPHI(2,2),OPTION(5),OUTPUT(5),
        TPHI(2,3),OPTION(5),OUTPUT(7),
        TPHI(3,2),OPTION(5),OUTPUT(8)
*       PRINT,PHI(2,2),PHI(3,3),PHI(2,3)
*       PLOT,PHI(2,2),SCALED/DYNAMIC,USE/*,END
*       PLOT,PHI(3,3),SCALED/DYNAMIC,USE/X,END
*       PLOT,PHI(2,3),SCALED/DYNAMIC,USE/A,END
*       END
```

Correlation Functions Control Program

Fig. F-1

```
C       PWR SPECTRUM
*       BEGIN FREQUENCY SYSTEM
*       FOURIERTRAN
*       FUNCTION DEFINITIONS
*       NAME,F/5,AS/$PWR SPECTRUM INPUT$
*       NAME,F/6,AS/$PWR SPEC OUTPUT$
*       NAME,F/7,AS/$CROSS SPEC IN OUT$
*       NAME,F/8,AS/$CROSS SPEC OUT IN$
*       LOAD,TEST/1
*       DEFINE,F/5,CH/5,CAL/1
*       DEFINE,F/6,CH/6,CAL/1
*       DEFINE,F/7,CH/7,CAL/1
*       DEFINE,F/8,CH/8,CAL/1
*       TRANSLATE
        F5=F5+CONJ(F5)
        F6=F6+CONJ(F6)
        F8=F7+CONJ(F8)
        F9=F8/F5
        END
*       PRINT,F/5
*       PRINT,F/6
*       PRINT,F/8
*       PRINT,F/9
*       PLOT,N/5,RF/5,SCALE/DYNAMIC,USE/*
*       PLOT,N/6,RF/6,SCALE/DYNAMIC,USE/*
*       PLOT,N/1,MF/9,SCALE/DYNAMIC,USE/*
*       PLOT,N/1,AF/9,SCALE/DYNAMIC,USE/P
*       PLOT,N/2,MF/8,SCALE/DYNAMIC,USE/*
*       PLOT,N/2,AF/8,SCALE/DYNAMIC,USE/P
*       END
```

Power Spectral Densities Control Program
Fig. F-2

```
*       BEGIN PROBABILITY SYSTEM
*       COPY,TESTS/1
*       PROBABILITY,
        TEST/( 1,31),CH/(2,2),CAL/0.94488,PD/1,LIMITS/200(-120,120),
        TZERO/1,TMAX/ 550,DISTRIBUTION/1,SAMPLE/1,NORM/(0)
*       END
```

A Probability Density Control Program

Fig. F-3

Vita

Marvin H. Chasen, son of Max M. Chasen and Rose Chasen, was born on [redacted] After graduating in 1958 from Brooklyn Technical High School, he enrolled in the School of Technology of the City College of New York. He was awarded the Bachelor of Electrical Engineering degree in June 1963, and was then employed as an engineer with the Consolidated Edison Company of New York. In February 1964 he entered Officer Training School at Lackland Air Force Base, Texas, and upon graduation and commissioning as a 2nd Lieutenant was assigned to the Manned Orbiting Laboratory System Program Office of the Air Force Systems Command, Los Angeles, California. He was project officer for electrical power until his selection to attend the Air Force Institute of Technology in June 1966.

Permanent address: [redacted]

Vita

James W. Guthrie was born on [redacted], the son of George W. Guthrie and Gladys Guthrie. He attended Woodrow Wilson High School, Dallas, Texas. In 1959 he enlisted in the U. S. Naval Reserve and served as an electronics technician. He received the degree of Bachelor of Science in Electrical Engineering from Texas Technological College, Lubbock, Texas in August 1964. In September 1964 he entered the U. S. Air Force Officer Training School and was commissioned a Second Lieutenant in the USAF Reserve in December 1964. He was then assigned as a project engineer to the San Antonio Air Material Area, San Antonio, Texas. In June 1966 he received a regular commission in the U. S. Air Force. He is a member of Eta Kappa Nu and Tau Beta Pi engineering honorary societies.

Permanent address: [redacted]

This thesis was typed by Mrs. Gloria S. McNally.

Security Classification

DOCUMENT CONTROL DATA - R & D

(Security classification of title, body of abstract and indexing annotation must be entered when the overall report is classified)

ORIGINATING ACTIVITY (Corporate author)

Air Force Institute of Technology (AFIT-SE)
Wright-Patterson AFB, Ohio 45433

2a. REPORT SECURITY CLASSIFICATION

Unclassified

2b. GROUP

3 REPORT TITLE

INVESTIGATION OF THE PRIMATE VESTIBULAR SYSTEM FUNCTION THROUGH ANALYSIS OF THE VESTIBULO-OCULAR REFLEX RESPONSE TO VARIOUS INPUT STIMULI

4 DESCRIPTIVE NOTES (Type of report and inclusive dates)

AFIT Thesis

5 AUTHOR(S) (First name, middle initial, last name)

Chasen, Marvin H, Captain, USAF Guthrie, James W., 1st Lt., USAF

6 REPORT DATE	7a. TOTAL NO OF PAGES	7b. NO OF REFS
December 1967	113	14

8a. CONTRACT OR GRANT NO	9a. ORIGINATOR'S REPORT NUMBER(S)
N/A	AFIT Thesis GE/EE/67S-7
b. PROJECT NO: N/A	
c.	9b. OTHER REPORT NO(S) (Any other numbers that may be assigned this report): N/A
d.	

10 DISTRIBUTION STATEMENT

This document has been approved for public release and sale; its distribution is unlimited.

11 SUPPLEMENTARY NOTES	12. SPONSORING MILITARY ACTIVITY
	Air Force Institute of Technology Wright-Patterson AFB, Ohio 45433

13 ABSTRACT

An indirect measurement of dynamic responses of the primate vestibular system was obtained through the measurement of eyeball counterroll from six Rhesus monkeys. A control system was developed to provide three types of input stimuli. These stimuli consisted of constant speed rotations, pendular oscillations, and Gaussian random noise. The experimental data was analyzed by use of correlation functions, power spectral density functions, and probability densities. Results show that angular acceleration and the acceleration resulting from centripetal force affect the counterroll response. Gaussian noise position inputs failed to produce counterroll distributions that are Gaussian. Suppression of response to random inputs was observed, indicating that suppression does not necessarily result from anticipation of the input.

DD FORM 1 NOV 65 1473

Security Classification

14 KEY WORDS	LINK A		LINK B		LINK C	
	ROLE	WT	ROLE	WT	ROLE	WT
labyrinth						
counterroll						
vestibulo-ocular reflex						
inner ear						
otolith organs						
semicircular canals						